On the Decay of Strong Concentrated Columnar Vortices

Yasser Aboelkassem

A Thesis

In

The Department

of

Mechanical and Industrial Engineering

Faculty of Engineering and Computer Science

Presented in Partial Fulfillment of Requirements
for the Degree of Master of Applied Science at
Concordia University
Montreal, Quebec, Canada

April 2003

ABSTRACT

On the Decay of Strong Concentrated Columnar Vortices

Yasser Aboelkassem

Being able to predict the properties of a decaying vortex is of value to various technological and scientific problems. The hazards presented by the vortices shed by large, heavily loaded, aircraft to an incoming plane are well known. A safe separation distance makes sure that the vortices shed by the first aircraft have been decayed to a level that is safe for the following aircraft. The decay of geophysical vortices is a highly complex phenomenon. Nevertheless, simplified time-dependent vortex models, like the one presented in this thesis, do elaborate on the basic processes involved during the energy dissipative phase. The general approach also provides a method that enables us to study the transient flow development in a plethora of swirling flow problems that evolve by starting or halting a pair of circular cylinders.

In the present thesis, a novel analytical method is developed to study the decay of a strong, concentrated vortex. Based on the equations representing the transient fluid motion and using a standard solution formulation via Fourier-Bessel expansions will show that different initial profiles of the velocity produce distinct velocity time distributions. Three initial velocity shapes will be explored

here. The first deals with the decay of a potential vortex. This type presents the known theoretical discrepancy of infinite velocity and vorticity in the center at the start. The second case considers an initial velocity distribution of a Rankine's vortex. The latter although posses a continuous velocity and static pressure distributions, it is also theoretically dubious since in this situation the vorticity presents a jump discontinuity at the core radius. The final distribution will assume the Vatistas' n = 2 vortex. The last kind of approximation does not suffer from the previously mentioned theoretical contradictions. It will be seen that all the relevant fluid properties are indeed continuous and bounded, and all their derivatives preserve the same mathematical qualities as well. The methodology is kept general as to accommodate formulation of any initial steady-state initial vortex profile.

Although, there were found no appreciable differences among the three near the asymptotic condition regions i.e. near the center of rotation (forced-vortex) and far away (free-vortex), they do produce substantial disparities in the mixed-vortex region (near the core). Finally, it is shown that the time history profiles of the velocity, and thus the pressure, exhibit a distinct self-similarity characteristic. The last made possible the collapse of the various time distributions into a single curve that is solely a function of the space coordinate.

Acknowledgements

The author expresses a deep appreciation to his supervisors, Professor Georgios H. Vatistas and Professor Nabil Esmail for their guidance and valuable advice throughout the course research work.

Sincere appreciation also goes to Professor Alex Povitsky, for his valuable and useful discussions. The support provided by staff members of the Mechanical and Industrial Engineering Department at Concordia University is appreciated. The author is very grateful to his parents for their advice, encouragement, moral and financial support.

Yasser Aboelkassem

Table of Contents

List of Figures

Figure **Page**

List of Tables

Table **Page**

Nomenclature

Listed below the main symbols used in this thesis. Note that more than one meaning maybe assigned to a symbol. Other symbols are defined internally within each chapter.

Symbol	Description
A_n	Bessel function arbitrary constant
$a,b,c\ \&\ d$	Arbitrary constants
J	Bessel function of 1st kind
J_0	Bessel function of 1st kind and zero order
J_1	Bessel function of 1st kind and 1st order
J_2	Bessel function of 1st kind and 2nd order
m	Arbitrary constant
P	Static pressure.
$\overline{P}$	Normalized pressure
R_e	Reynolds number
$\overline{r}$	Normalized vortex radial distance
$\overline{r}_m$	Normalized maximum viscous core radius
R_c	Vortex core radius
R_o	Outer vortex radius
t	Time
$\overline{t}$	Normalized time parameter based on the outer vortex radius
$\overline{t}_c$	Normalized time parameter based on the vortex core radius
$\vec{V}$	Total velocity vector
V_r, V_θ, V_z	Radial, tangential and axial velocity components
$\overline{V}$	Normalized velocity
$\overline{V}_{\theta)\max}$	Maximum normalized tangential velocity
$\tilde{V}$	Transformed swirl velocity

Y	Bessel function of 2nd kind
x, y, z	Cartesian coordinates

Greek Letters

β	Normalized vortex radii parameter
Γ	Vortex circulation
Π	Normalized pressure
$\Pi_{) \max}$	Maximum normalized pressure
μ	Dynamical viscosity
λ_n	Zeros of the 1st kind 1st order Bessel function
ρ	Density
υ	Kinematical viscosity
$\vec{\Omega}$	Total vorticity vector
$\overline{\Omega}$	Normalized vorticity
$\overline{\Omega}_{z) \max}$	Maximum normalized axial vorticity

Subscripts

c	Quantities at the vortex core radius
n	Vatistas'n=2 vortex model parameter
o	Quantities at the outer vortex radius
r, θ, z	Radial, tangential and axial

Superscripts

$\sim$	Initial quantities
$\_$	Non-dimensional quantities

Chapter 1

Introduction

1.1. Historical –General

Vortex motion is generally regarded as one of the most complicated and yet very important of the natural mechanisms to efficiently transport mass, momentum and energy. Consequently, their study has sustained a considerable degree of interest throughout the past one and a half centuries. The theory was first mathematically modeled by Helmholtz [1858], considering the irrotational motion of a perfect fluid. Helmholtz' formulation was later adapted by Kelvin [1880] in an attempt to develop an atomic theory [1]. It was natural for scientists to ponder of how fast the vortex - like atoms would decay if they were immersed in a nearly inviscid fluid. Although this model has long been abandoned, the ensued research impetus has considerably advanced knowledge in this area.

The considerable mathematical difficulties associated with the subject matter have prevented the development of a universal theoretical vortex model. Instead, investigators have used a variety of simplified models to study aspects of swirling flows. The decay of an initial potential vortex including the viscous effects was derived by, Ossen[22] [1911] and Hamel [1916]. The model was later on known as Ossen-Lamb vortex. Burger [4] [1948] obtained simplified steady

flow solution by balancing the outward swirl velocity momentum diffusion by an equivalent amount carried by the radial velocity of the traveling from the extreme periphery towards the vortex center.

Burger's vortex time development was formulated later by Rott[1] [1958]. The two-cell vortex was derived by Sullivan[30] [1959]. His formulation exhibited an axial reversal flow near the axis of rotation, which was absent in Burger's model.

1.2 Wakes Due to Tip Vortices

Bi-product of lift generation by fixed and rotating wings is the evolution of the wing-tip-vortices. The latter is due to the pressure difference between the suction and the pressure sides of the wing. Vortex decay within the far field domain is very important phenomenon to reduce the hazards and noise created by the aircraft wake. Current investigations are focusing on predicting, monitoring and controlling the vortex decay. The approach is to minimize the vortex strength and thus moderating the potential hazards that emerge from large heavily loaded aircrafts.

The generation of hazardous wakes is one of the main factors of the Airport limiting capacity problems. To overcome this problem, knowledge of the flow behavior under various metrological conditions must be predicted with confidence. This can only be achieved by understanding well the vortex decay phase. Vortices shed by an aircraft are natural consequence of its lift. The wake

flow behind the aircraft can be described by near field and far field characteristics. Behind the trailing edge of the wing a strong down ward motion (downwash) exists while beyond the wing tip a weak upward motion (up wash) is formed [34]. The separation of the boundary layer causes small vortices to emerge from the wing tip in the area of near field. Meanwhile the roll-up process of the vortex sheet consists of counter-rotating vortices that initiate vortex instability, see figure [1.1]. This process defines the aircraft induced wakes during the severe phase of its development in the far field.

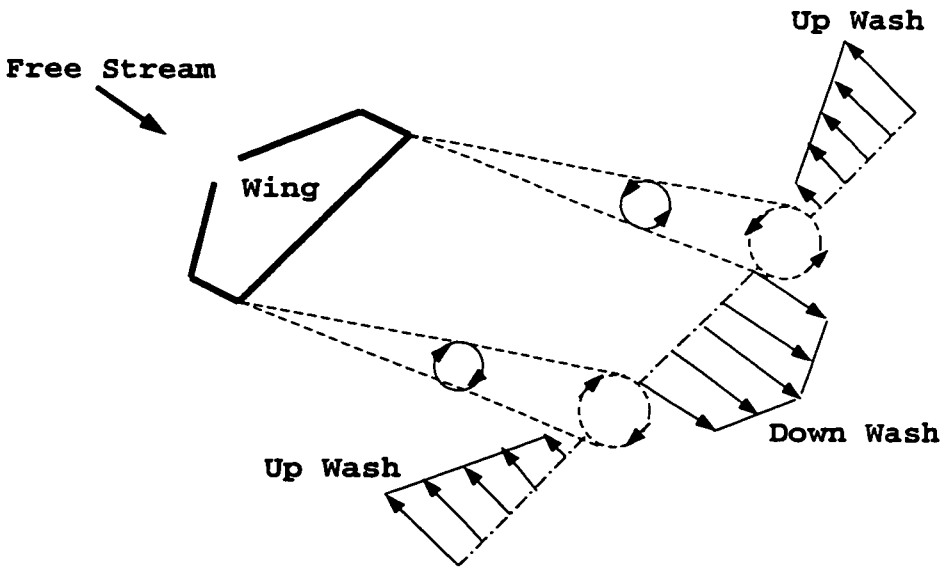

Fig. 1-1 Schematic Figure Shows the Wing Tip Vortices

A similar phenomenon can be encountered in horizontal tornadoes where two vortices of almost equal strength posses a strong potentially hazardous

circulation $\Gamma(r)$. The potentially dangerous conditions depend on the geometrical characteristics of the wing such as its shape span and length as well as the aircraft takes off weight.

The far field domain is defined as the region where the impact of the atmosphere on the wake vortices becomes important. The vortex circulation $\Gamma(r)$ is one of the reliable parameters that can be used to express the degree of vortex hazard. Recent research is dedicated towards finding ways to control and produce a less harmful wakes by means of wing constructive techniques, which called [Low Vorticity Approach][34]. Another approach is related to the fast decay of the sheet vortices called [Quickly Decaying Vortex Approach][34]. The assessment of the potential hazards requires a reliable estimation of the induced aerodynamic forces and moments, which consecutively requires the employment of an accurate vortex model. Advances in this area can increase the airport capacity. Predicting the vortex flow field parameters and the decay of concentrated vortices in both confined and unconfined domains is very difficult. However, a simplified time dependent vortex model can capture most of the main physical features involved during the energy dissipative phase. The previously reported steady state vortex formulations can then serve as initial conditions.

1.3 Problem and Contributions

Vortex motion appears in liquids, gases and plasmas. Their size can vary from the extremely small (quantized vortices of super fluid helium) to enormously large (galactic vortex). Depending on their aspect ratio (core size/height) these can be categorized as columnar or disk-like. Furthermore, if they exist in a limited domain, they are called confined, otherwise are unconfined vortices. Concentrated vortices are those where most of its vorticity is clustered within a tubular region close the center of rotation and rapidly decaying outward along the radial direction. Intense or strong vortices are those who have a swirl velocity that is orders of magnitude larger than the other two components.

This analytical study presents a new formulation, which describes the vortex decaying process of intense, isolated, concentrated and columnar vortices that is more realistic than those previously reported in the technical literature. As an initial condition it assumes Vatistas [38] n = 2 vortex model which is known to be more accurate in simulating real vortices and which does not suffer from the mathematical or physical contradictions that are inherent in the other formulations. Both the confined and unconfined types are addressed. The results of the present model are compared with those having as initial conditions the potential and Rankine's swirl velocity and pressure distributions.

Chapter 2

Literature Review

Steady Formulation of Vortex Flows

2.1 Preface

One of the important properties of vortex flows is to determine velocity fields, especially the radial distribution of the induced tangential velocity, which is used frequently to model the vortex roll-up wake behind heavily loaded aircraft. Based on experimental measurements, the induced swirl velocity is seen to exhibits a strong self-similarity when the core radius is used as a reference scale length. There are several generalized vortex models, that can describe the tangential, radial and axial velocity components induced by the viscous core. These models are derived by solving a simplified form of Navier-Stokes's equations.

A complete formulation of viscous and turbulent vortex flow requires a solution of Navier-Stokes's equations, which is indeed challenging due to difficulties associated with boundary condition implementation. The fitted algebraic vortex models are commonly used in the engineering due to their simplicity and computational efficiency. There are common techniques used to represent the induced velocity profile. One approach involves using the well-fitted algebraic

profile by assuming a constant viscous core size, while another uses the time dependent core growth diffusion such as Lamb Ossen's model. One of the most over utilized models is Scully [29] & Sullivan [known as Kaufmann's model], which predicts qualitatively the overall velocity distribution. However, a result compared with measurements in both rotating and fixed wings indicates that this model underestimates the peak swirl velocity [14]. Vatistas et al [1991] proposed a family of algebraic vortex induced velocity models. The results of the tangential velocity and static pressure for the n = 2 member along with experimental data are shown in Figure [2.1][40]. It is evident that the two correlate well. Because the latter quality and the fact that the model is mathematically manageable it has become the basis of several studies involving vortices shed by wings. It was successfully used to investigate the periodic wake of a hovering rotor, Leishman [13] (1998), in the visualization of the compressible vortex flow structure Bagai [2] and Leishman (1993), and the numerical characterization of wakes produced by wings, Bagai [3] and Leishman (1998), Tauszig [33] (1998) Nilay [21] (2001), and Coton [5] et al (1998) and others.

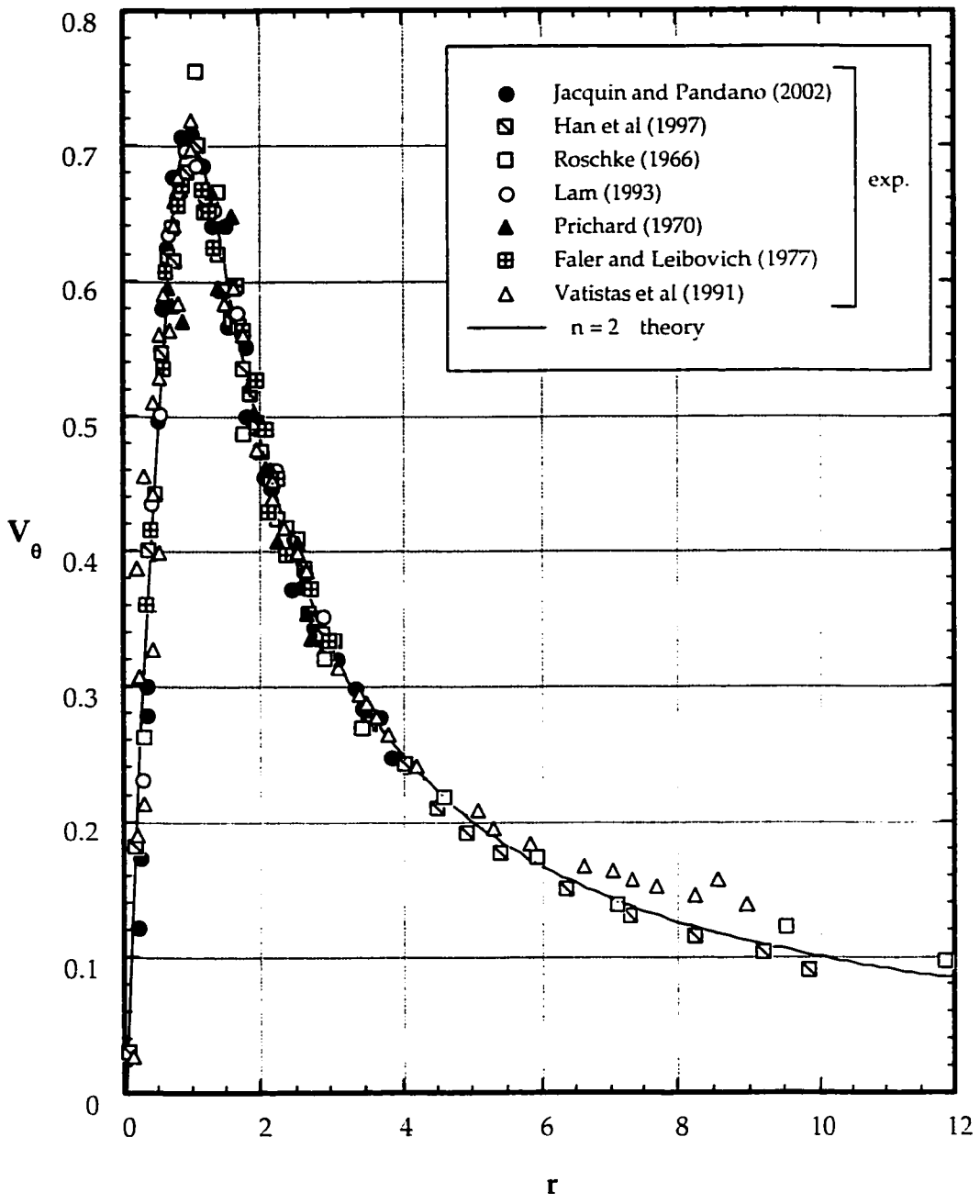

Fig.2.1- Tangential velocity based on experimental results and Vatistas [40] n=2

2.2 Axisymmetric Vortex Flow Equations

The vortex motion in laminar flows can be described as axisymmetric flow problem. Therefore the general equation of motion can be derives in cylindrical coordinates shown in figure [2.2].

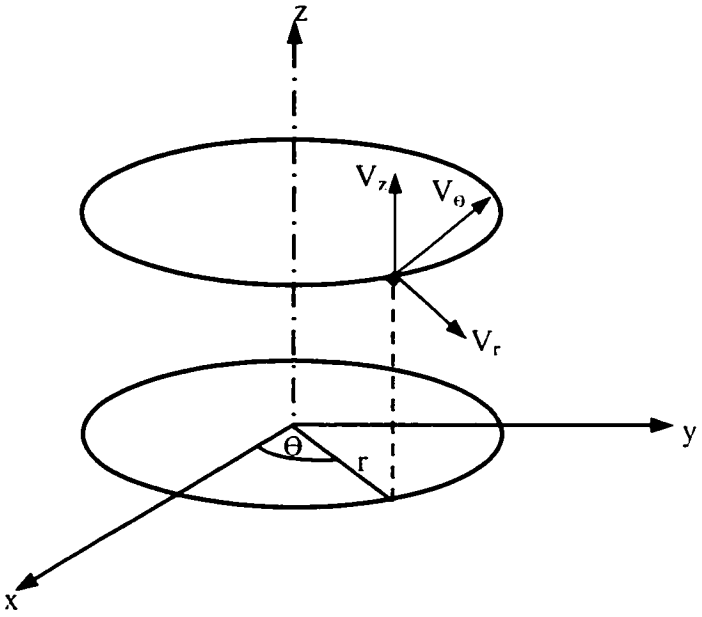

Fig. 2-2 Velocity vector in cylindrical system of axes.

Logical assumptions such as, the flow is considered to be incompressible, body free forces and laminar. Hence under these assumptions, the governing equations are:

Mass Conservation

$$\frac{\partial[V_r]}{\partial r}+\frac{\partial[V_z]}{\partial z}+\frac{[V_r]}{r}=0 \tag{2.1}$$

Radial Momentum

$$\frac{\partial V_r}{\partial t}+V_r\frac{\partial V_r}{\partial r}+V_z\frac{\partial V_r}{\partial z}-\frac{V_\theta^2}{r}=-\frac{1}{\rho}\frac{\partial P}{\partial r}+\upsilon[\nabla^2 V_r-\frac{V_r}{r^2}] \tag{2.2}$$

Where $\nabla^2 = \frac{\partial^2}{\partial r^2} + \frac{1}{r}\frac{\partial}{\partial r} + \frac{1}{r^2}\frac{\partial^2}{\partial \theta^2} + \frac{\partial^2}{\partial z^2}$ & $\frac{D}{Dt} = \frac{\partial}{\partial t} + V_r\frac{\partial}{\partial r} + \frac{V_\theta}{r}\frac{\partial}{\partial \theta} + V_z\frac{\partial}{\partial z}$

Tangential Momentum

$$\frac{\partial V_\theta}{\partial t} + V_r\frac{\partial V_\theta}{\partial r} + V_z\frac{\partial V_\theta}{\partial z} + \frac{V_r V_\theta}{r} = \upsilon[\nabla^2 V_\theta - \frac{V_\theta}{r^2}] \tag{2.3}$$

Axial Momentum

$$\frac{\partial V_z}{\partial t} + V_r\frac{\partial V_z}{\partial r} + V_z\frac{\partial V_z}{\partial z} = -\frac{1}{\rho}\frac{\partial P}{\partial z} + \upsilon[\nabla^2 V_z] \tag{2.4}$$

2.3 Previous Steady Vortex Flows

In this section, we introduce the simple steady state solutions of self-similar vortex flows such as the potential, Rankine and Vatistas's model. These are used as initial conditions for the simplified decay analysis via Bessel solution. Both confined and unconfined solutions are addresses based on these steady models.

2.3.1 Potential Vortex Model [1]

Consider a flow where all the streamlines are concentric circles about a given point 0, see Figure [2.2.], The velocity along any given circular streamline is constant but it varies from one streamline to another inversely with the distance r, such as the free vortex flow.

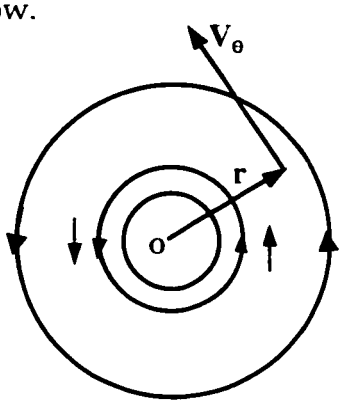

Fig. 2-3- Schematic illustrates the Viscous Potential Vortex flow.

Let the velocity take the form of:

$\vec{V} = \vec{V_\theta} = \frac{C}{r}\vec{e_\theta}$ where, C= constant depends on the vortex hazard.

It is easy to show that, the potential vortex flow is kinetically physically possible flow at each point in the flow field because it satisfies the mass conservation i.e. $\vec{\nabla} \bullet \vec{V} = 0$. This elementary vortex flow is irrotational at each point except at the origin, which posses a singularity. To evaluate the constant C, one can take the circulation around a given circular streamline and integrate over a closed path to obtain: $\Gamma = -\oint_c V \bullet ds = -V_\theta[2\pi]$

The above integration shows that, the tangential velocity depends mainly on the radial parameter. Therefore,

$V_\theta = [-\frac{\Gamma}{2\pi}]\frac{1}{r}$ And $C = [-\frac{\Gamma}{2\pi}]$,

The potential vortex model in the normalized form is then:

$$V_\theta = \frac{\Gamma}{2\pi r} = \frac{\Gamma}{2\pi r_c \frac{r}{r_c}}$$

$\frac{V_\theta}{\Gamma/2\pi r_c} = \frac{1}{r/r_c}$ If we let $\overline{V_\theta} = \frac{V_\theta}{\Gamma/2\pi r_c}, \bar{r} = \frac{1}{r/r_c}$

$$\overline{V_\theta}(\bar{r}) = \frac{1}{\bar{r}}, \qquad 0 < \bar{r} < \infty \tag{2.5}$$

where, $\Gamma = 2\pi C$ is the vortex strength

Based on the tangential and radial momentum equations, the radial and axial velocity components must vanish. From experimental observations we can

assume that the pressure is only a function of the radius r. Since the axial and the radial velocity components are zeros, the radial momentum equation simplifies into:

$$\frac{V_\theta^2}{r} = \frac{1}{\rho}\frac{\partial P}{\partial r},$$

or in normalized form

$$2\frac{(\bar{V}_\theta)^2}{\bar{r}} = \frac{\partial \bar{P}}{\partial \bar{r}} \quad , \bar{P} = \frac{P}{0.5\rho(\Gamma/2\pi r_c)^2}$$

Hence we can integrate directly to obtain

$$\bar{P}(\bar{r}) = \int 2\frac{(\bar{V}_\theta)^2}{\bar{r}}d\bar{r} = \int 2\frac{1}{\bar{r}^3}d\bar{r} = \frac{-1}{\bar{r}^2} \tag{2.6}$$

The axial vorticity is

$$\vec{\Omega} = \vec{\nabla}\times\vec{V} = \frac{1}{r}\begin{vmatrix} \vec{e}_r & \vec{e}_\theta & \vec{e}_z \\ \frac{\partial[-]}{\partial r} & \frac{\partial[-]}{\partial \theta} & \frac{\partial[-]}{\partial z} \\ V_r & rV_\theta & V_z \end{vmatrix} \text{ Therefore, } \Omega = \frac{1}{r}\frac{\partial[rV_\theta]}{\partial r}$$

$$\Omega = 0.0 \tag{2.7}$$

The velocity, pressure and vorticity is plotted along the radial direction, see figures [2.4], [2.5] and [2.6] respectively. It is clear that the tangential velocity, axial vorticity and static pressure are singular at the vortex center. The potential formulation has no information about the radial and axial velocity components. This model is considered as single scale model, therefore it dose not give any information around the viscous core radius.

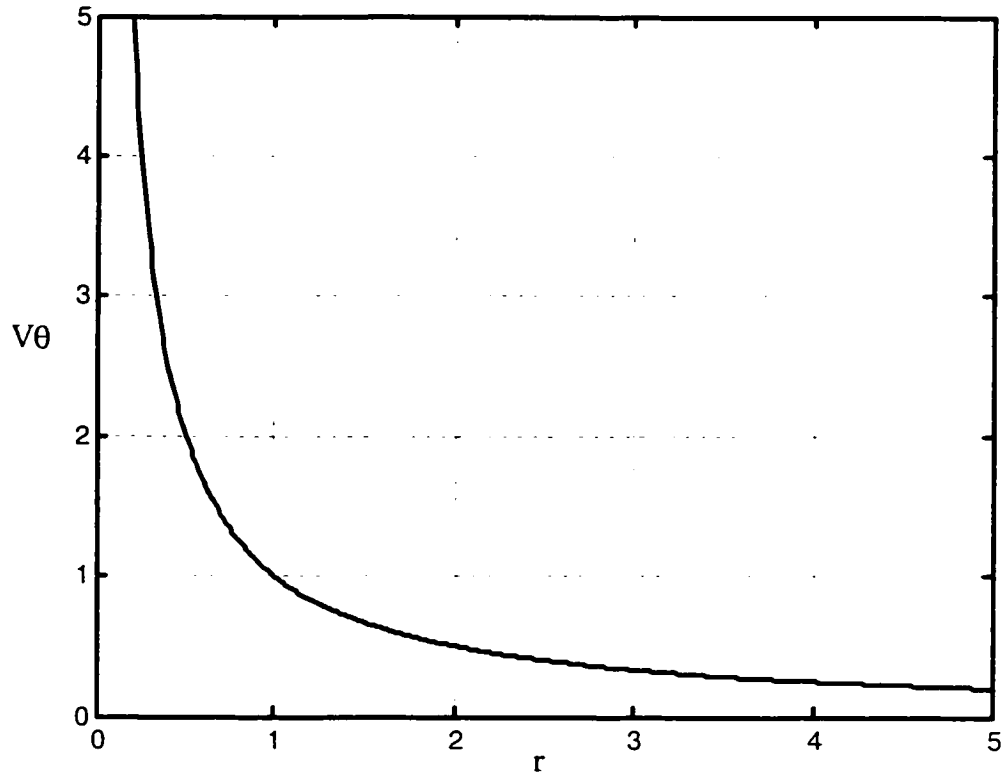

Fig. 2-4. Tangential velocity distribution of the potential vortex model

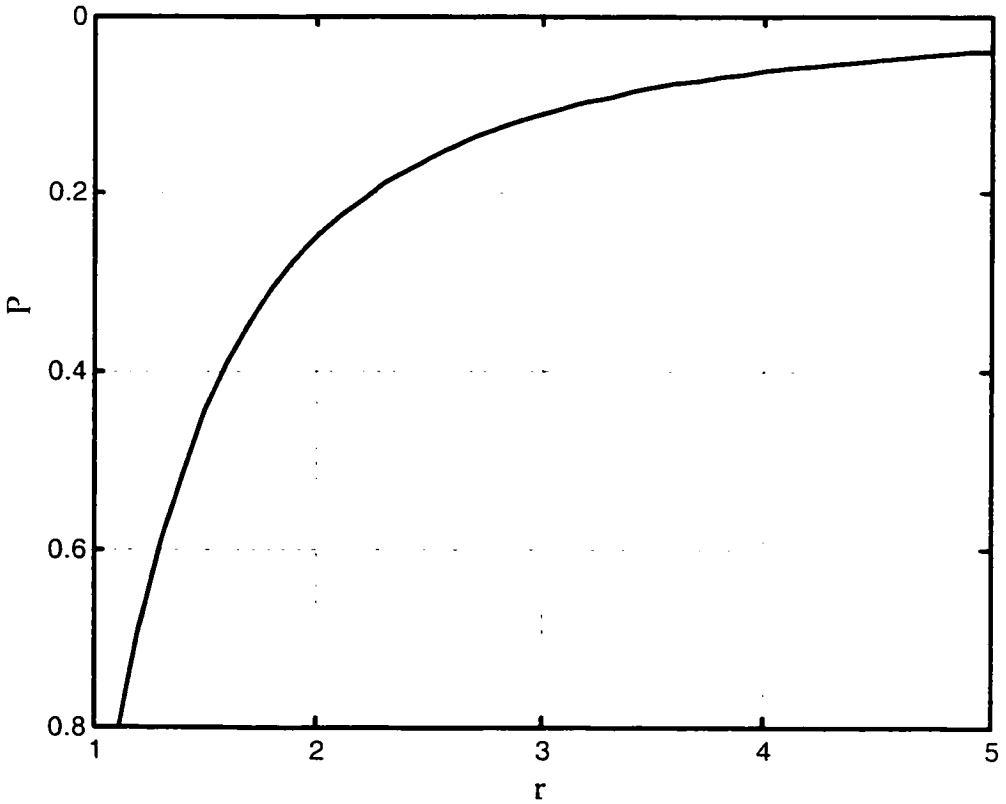

Fig. 2-5. -Pressure distribution of the potential vortex model

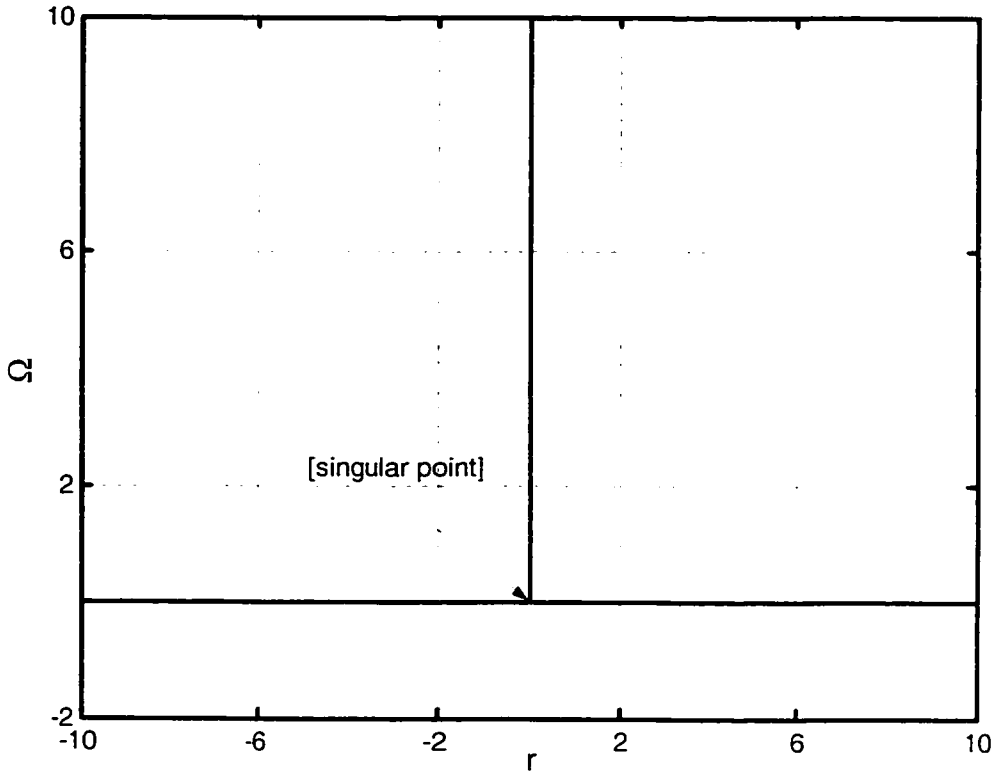

Fig. 2-6. -Vorticity distribution of the potential vortex model

2.3.2 Rankine Vortex Model [1]

Due to the need for reliable models that can describe the nature of the vortex flow around and away from the viscous core radius, Rankine developed a simple model for the tangential velocity. This model represented a two-scale formulation that can predict the most salient features of the viscous core. Rankine's model exhibits a solid body rotational motion [forced vortex] inside the core and free vortex [potential] outside the core. The tangential velocity is given by:

$$V_\theta(r) = \begin{cases} \dfrac{\Gamma}{2\pi r_c}\dfrac{r}{r_c} & 0 \le r \le r_c \\ \dfrac{\Gamma}{2\pi r} & r_c < r < \infty \end{cases}$$

or in normalized form

$$\bar{V}_\theta(\bar{r}) = \frac{V_\theta(\bar{r})}{\Gamma/2\pi r_c} = \begin{cases} \bar{r} & 0 \le r \le 1 \\ \dfrac{1}{\bar{r}} & 1 < r < \infty \end{cases} \tag{2.8}$$

where $\bar{r} = \dfrac{r}{r_c}$, r_c represents the vortex core radius, the radial and axial velocity are null everywhere. The radial momentum equation provides the static pressure distribution

$$\bar{P}(\bar{r}) = \begin{cases} \int \frac{\bar{V}_\theta^2}{\bar{r}} d\bar{r} = \int \bar{r} d\bar{r} & 0 \le \bar{r} \le 1 \\ \int \frac{\bar{V}_\theta^2}{\bar{r}} d\bar{r} = \int \frac{1}{\bar{r}^3} d\bar{r} & 1 < \bar{r} < \infty \end{cases}$$

Integrating along the radius yields

$$\bar{P}(\bar{r}) = \begin{cases} \frac{1}{2}\bar{r}^2 & 0 \le \bar{r} \le 1 \\ 1 - \frac{1}{2\bar{r}^2} & 1 < \bar{r} < \infty \end{cases} \tag{2.9}$$

Similarly, the axial vorticity is given by

$$\Omega = \frac{1}{r}\frac{\partial [r V_\theta]}{\partial r}$$

$$\Omega = \frac{1}{r}\frac{\partial}{\partial r}\begin{cases} r^2 \frac{\Gamma}{2\pi r_c} & 0 \le r \le r_c \\ \frac{\Gamma}{2\pi} & r_c < r < \infty \end{cases}$$

$$\bar{\Omega} = \frac{\Omega}{\Gamma / r_c^2} = \begin{cases} \frac{1}{\pi} & 0 \le r \le r_c \\ 0 & r_c < r < \infty \end{cases} \tag{2.10}$$

The velocity, pressure and vorticity are plotted along the radial direction, see figures [2.7], [2.8] and [2.9]. The results show that for this case the singularity at the vortex center is removed. However, generating a discontinuity of the vorticity at the core radius. One can notice that this model is overestimating the tangential velocity. This formulation also does not predict the other velocity components.

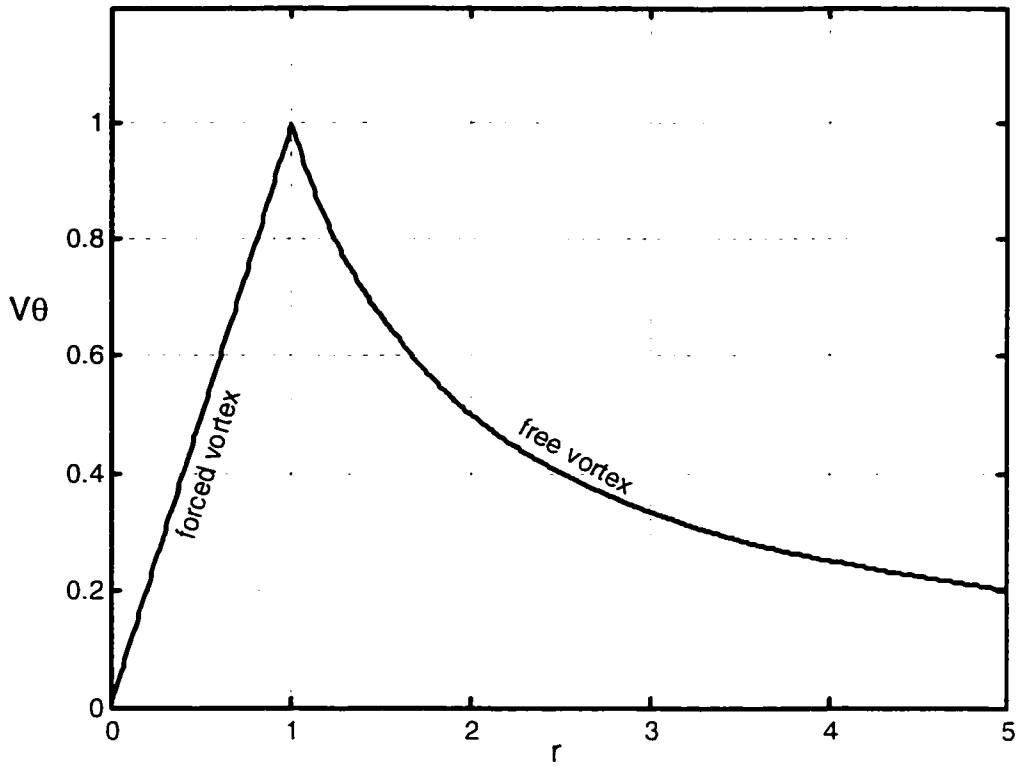

Fig. 2-7. Tangential velocity distribution of Rankine vortex model

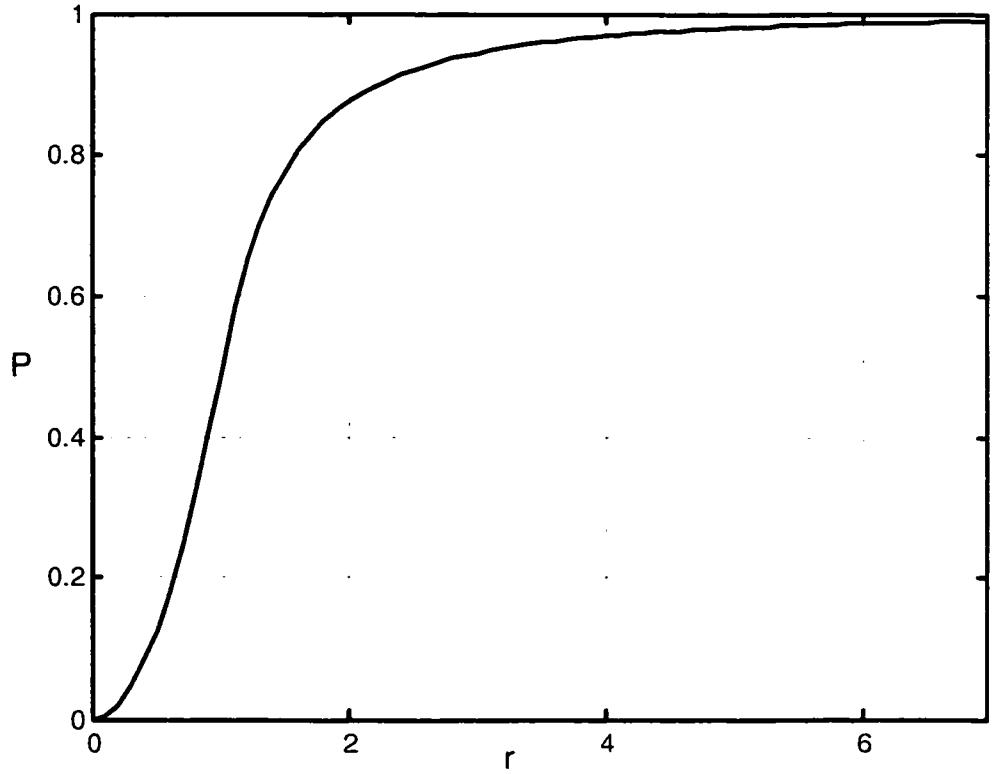

Fig. 2-8. Pressure distribution of Rankine vortex model

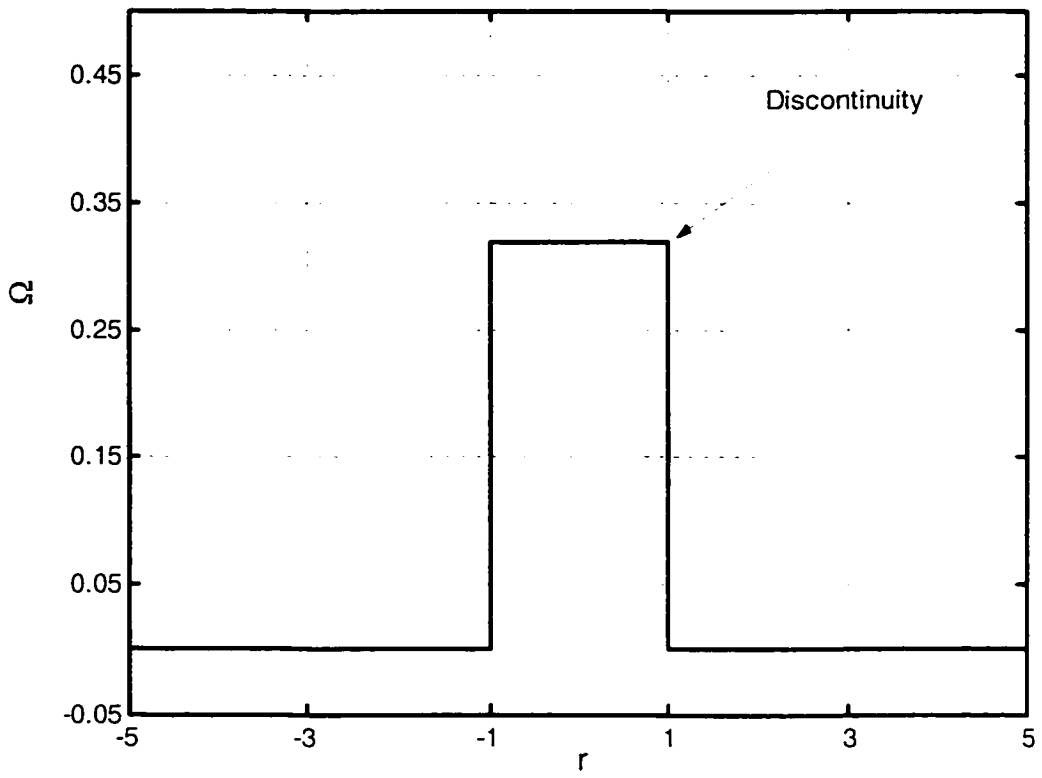

Fig. 2-9- Vorticity distribution of Rankine vortex model

2.3.3 Scully Vortex Model [29]

A singularity point is found at the vortex center in case of the potential model, while a discontinuity of axial vorticity at the viscous core radius exist in case of Rankine's model. As a result scientists were seeking to develop a new vortex model that is free of the last two inconsistencies. Scully's model was successful in achieving this. He developed a continuous tangential velocity component around the core radius and far way from the core radius as well. His model also estimates continuous axial and radial velocity components.

The tangential velocity in this case is given by

$$V_\theta(r) = \frac{\Gamma}{2\pi}\left[\frac{r}{r_c^2 + r^2}\right] \qquad 0 \le r \le \infty$$

The normalized form is

$$V_\theta(\bar{r}) = \frac{\Gamma}{2\pi r_c}\left[\frac{\bar{r}}{1+\bar{r}^2}\right] \qquad ,\bar{r} = \frac{r}{r_c}$$

$$\bar{V}_\theta(\bar{r}) = \frac{V_\theta(\bar{r})}{\Gamma/2\pi r_c} = \left[\frac{\bar{r}}{1+\bar{r}^2}\right] \qquad ,0 \le \bar{r} \le \infty \tag{2.11}$$

The radial velocity component is derived using the momentum equations are follows:

$$V_r\frac{\partial V_\theta}{\partial r} + \frac{V_r V_\theta}{r} = \upsilon\left[\nabla^2 V_\theta - \frac{V_\theta}{r^2}\right],$$
$$V_r\left[\frac{\partial V_\theta}{\partial r} + \frac{V_\theta}{r}\right] = \upsilon\left[\nabla^2 V_\theta - \frac{V_\theta}{r^2}\right] \qquad \text{Where, } \nabla^2 = \frac{\partial^2 V_\theta}{\partial r^2} + \frac{1}{r}\frac{\partial V_\theta}{\partial r}$$

$$V_\theta(r) = \frac{\Gamma}{2\pi}\left[\frac{r}{r_c^2 + r^2}\right], \frac{\partial V_\theta}{\partial r} = \frac{\Gamma}{2\pi}\left[\frac{r_c^2 - r^2}{(r_c^2 + r^2)^2}\right] \& \frac{\partial^2 V_\theta}{\partial r^2} = \frac{\Gamma}{2\pi}\left[\frac{-2r}{(r_c^2 + r^2)^2} + \frac{-4r(r_c^2 - r^2)}{(r_c^2 + r^2)^3}\right]$$

$\bar{V}_r = -4\frac{\bar{r}}{1+\bar{r}^{-2}}$. Where $\bar{V}_r = \frac{V_r r_c}{\upsilon}$, if we normalize the radial velocity using V_c instead of using $\frac{r_c}{\upsilon}$, the radial velocity is

$$\bar{V}_r = \frac{-4}{R_e}\frac{\bar{r}}{1+\bar{r}^{-2}}, \tag{2.12}$$

where $\bar{V}_r = \frac{V_r}{V_c}$ & $R_e = \frac{V_c r_c}{\upsilon} = \frac{\Gamma}{2\pi\upsilon}$

Similarly, but now from the conservation of mass the axial velocity is given by

$$\frac{\bar{V}_z}{z} = \frac{8}{R_e}\frac{1}{(1+\bar{r}^{-2})^2} \qquad \text{Where} \qquad \bar{V}_z = \frac{V_z}{V_c} \tag{2.13}$$

Note that, $\upsilon_{air} \approx 10^{-5}$ & $\upsilon_{water} \approx 10^{-6}$ m^2/s

$R_e = \frac{V_c r_c}{\upsilon} = \frac{\Gamma}{2\pi\upsilon}$, which is a very large value, hence $\frac{1}{R_e} \approx 0$

Therefore, we realize that the axial and radial velocity components are very small compared with the tangential velocity. This implies that, the air vortices posse only substantial tangential velocity while the other two components are relatively small.

The static pressure distribution can easily found, if we assume that the radial and axial velocities are negligible everywhere. Therefore the static pressure will balance the centrifugal force. Based on the momentum equations and assumptions made, the momentum equation will be,

$$\bar{p} = 2\int_0^{\bar{r}} \frac{\bar{V}_\theta^2}{\bar{r}} d\bar{r} = \int_0^{\bar{r}} 2\frac{\bar{r}}{(1+\bar{r}^2)^2} d\bar{r} = [1 - \frac{1}{1+\bar{r}^2}] \tag{2.14}$$

The normalized axial vorticity for this model is given as well

$$\therefore \bar{\Omega} = \frac{\Omega}{\Gamma/r_c^2} = \frac{1}{\pi}[\frac{1}{(1+\bar{r}^2)^2}], \tag{2.15}$$

The above analysis showed that, the flow properties have neither singularity point nor discontinuity. The results of this model are shown in figures [2.10 to 2.14]. Although this formulation has been used previously in a variety of aerospace related applications. However this model severely underestimates the tangential velocity see figure [2.20]. This model is applicable for a limited number of physical applications, moreover it dose not fit most of the experimental results [14].

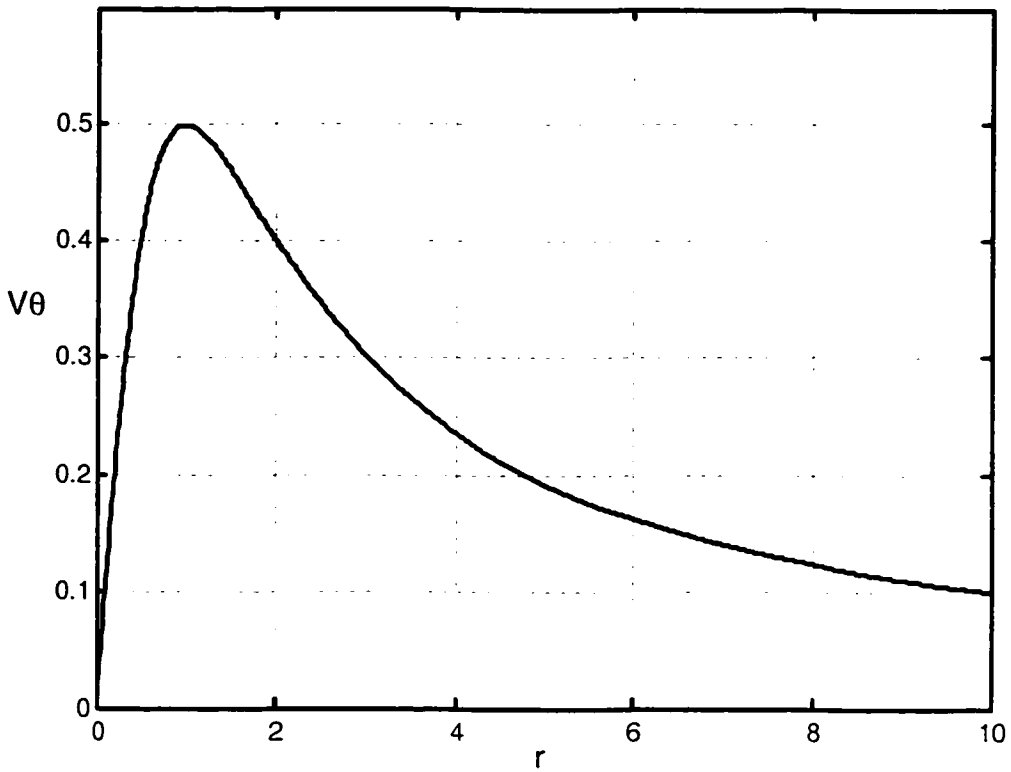

Fig. 2-10. Tangential velocity distribution of Scully vortex model

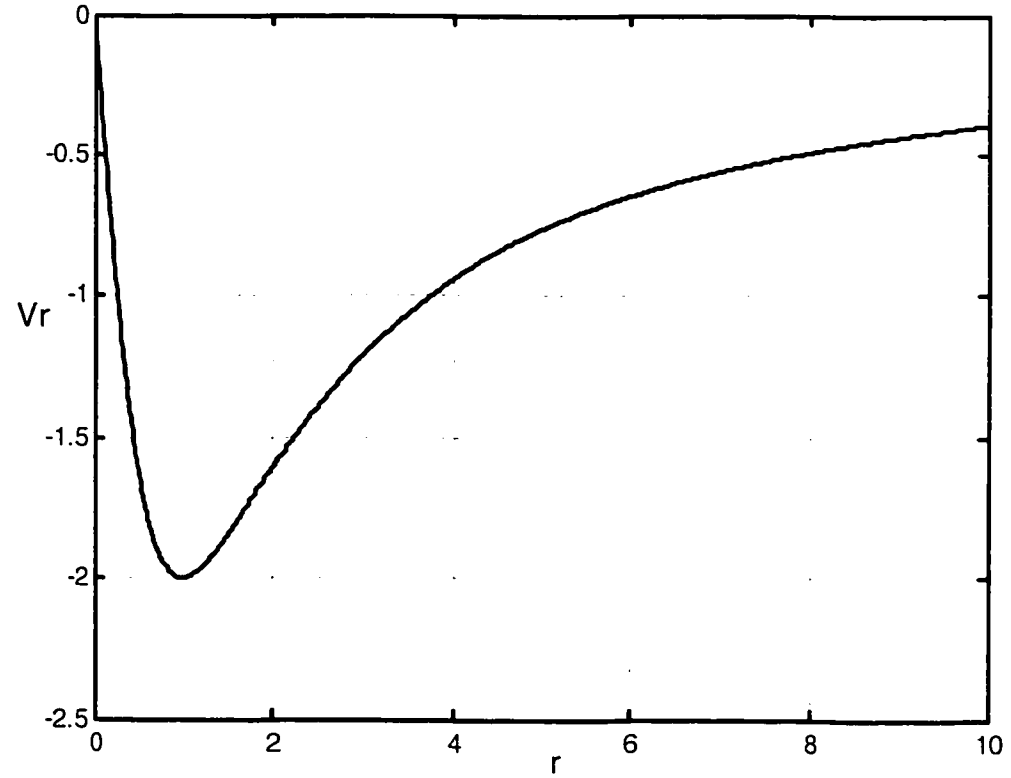

Fig. 2-11. Radial velocity distributions of Scully vortex model

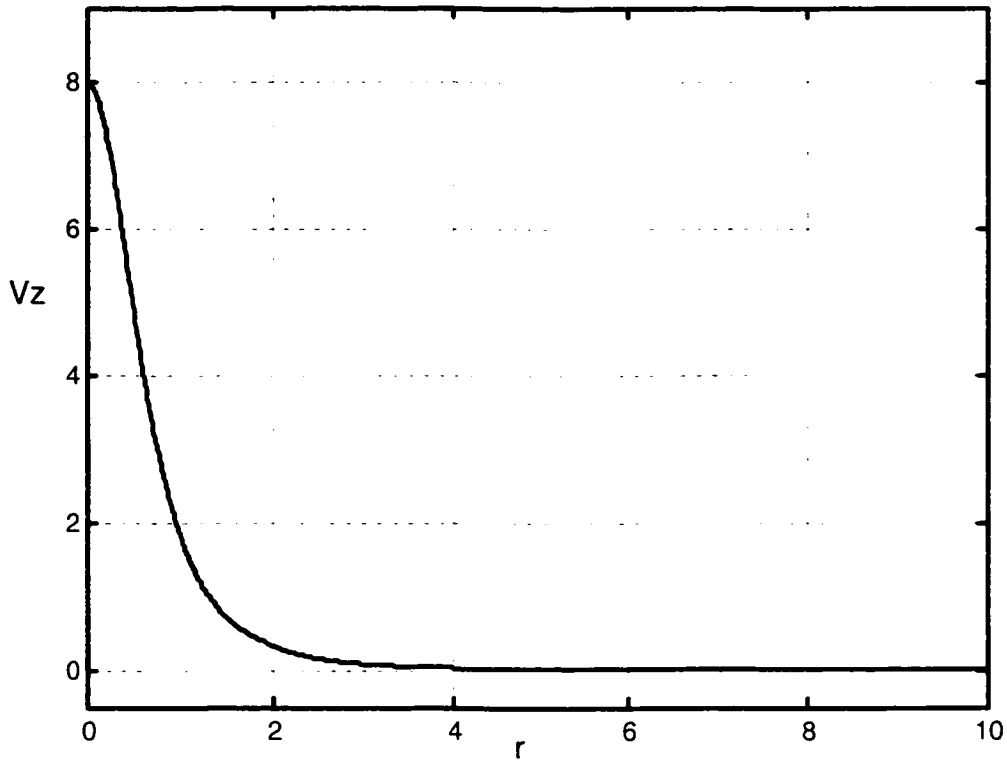

Fig. 2-12. Axial velocity distributions of Scully vortex model

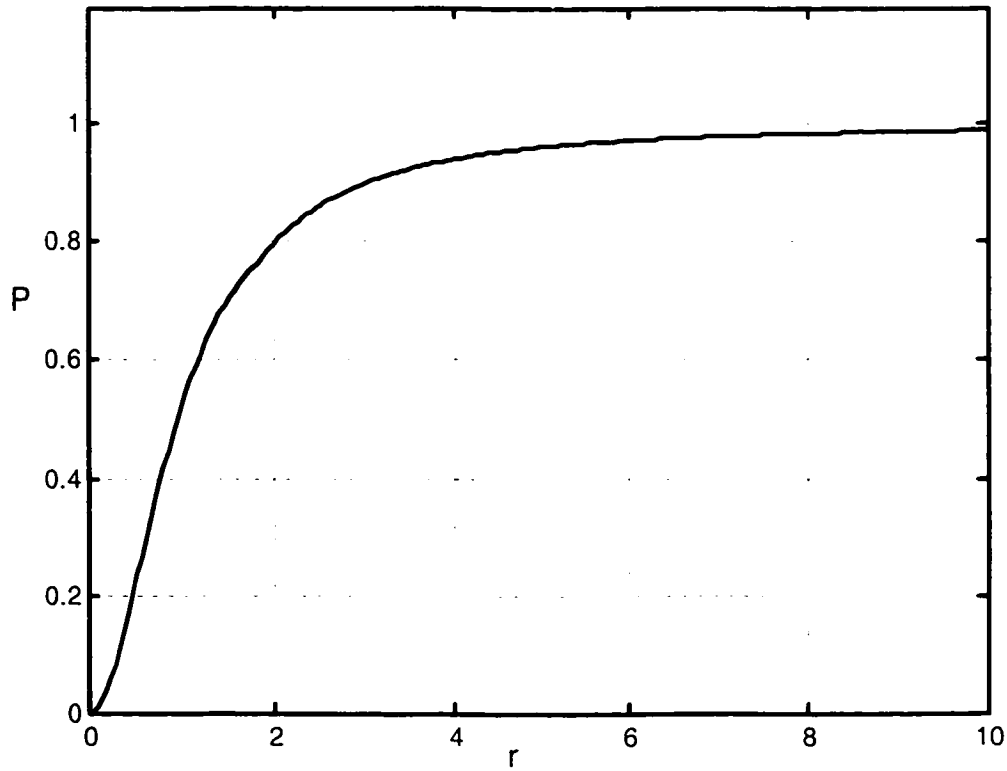

Fig. 2-13. Pressure distributions of Scully vortex model

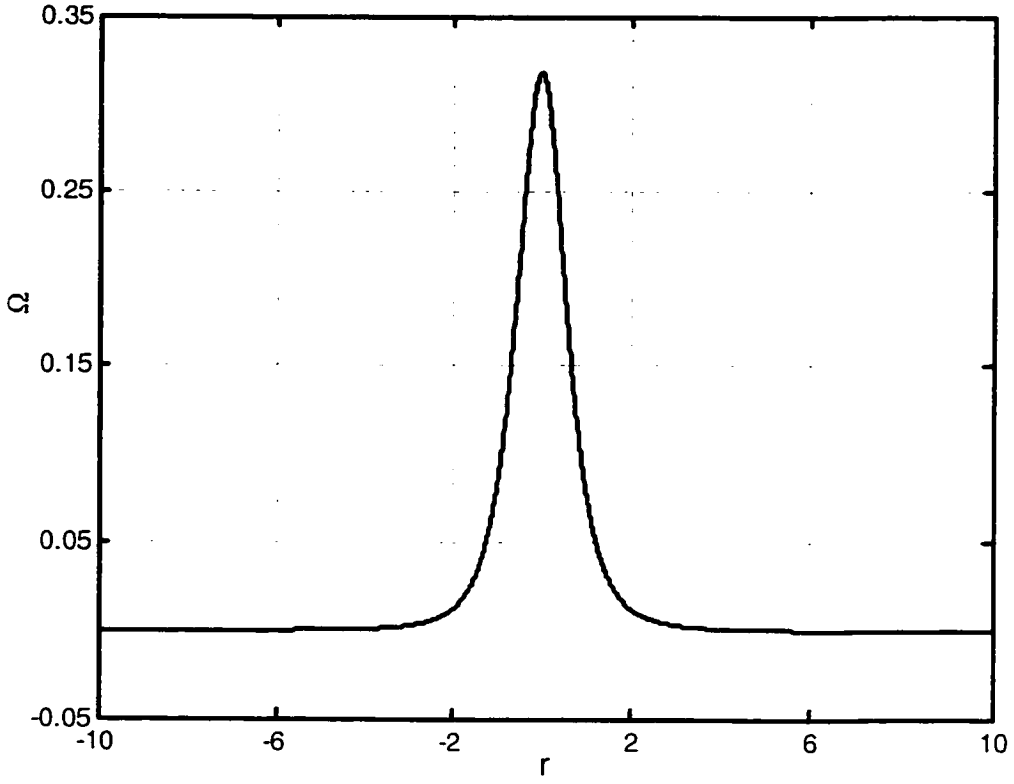

Fig. 2-14. Vorticity distributions of Scully vortex model

2.3.4 Vatistas et al n=2 Vortex Model [38]

Due to problems in previous formulations of the vortex flow, many scientists searched for a better realistic vortex model. Here we present Vatistas's model, which is an algebraic formula for the tangential velocity that fits the observations as shown in figure [2.1]. This model consists of a family of continuous algebraic swirl velocity profiles within and away from the core radius. The radial and axial velocity components can be derived easily using the momentum and mass conservation equations. This model is a generalized model, which produces a family of curves ranging between Rankine's model and Scully's model. This formulation is based on the hypothesis that, the tangential velocity and the static pressure are only radial dependent as indicated by most of the experimental observations.

The tangential velocity is given by

$$V_\theta(r) = \frac{\Gamma}{2\pi} \frac{r}{(r_c^{2n} + r^{2n})^{\frac{1}{n}}} \qquad 0 \le r \le \infty$$

where, n positive integer. If the equation is normalized based on the core size yields,

$$\bar{V}_\theta(\bar{r}) = \frac{V_\theta}{\Gamma/2\pi r_c} = \frac{\bar{r}}{(1 + \bar{r}^{-2n})^{\frac{1}{n}}} \quad , \quad \bar{r} = \frac{r}{r_c} \tag{2.16}$$

Similar analysis as previously shown, can be used to derive the radial and axial velocity components as

$$\bar{V}_r(\bar{r}) = \frac{V_r}{\Gamma/2\pi r_c} = \frac{-2(n+1)}{R_e} \frac{\bar{r}^{-(2n-1)}}{(1+\bar{r}^{-2n})} \tag{2.17}$$

Where $R_e = \frac{V_c r_c}{\upsilon}$ The vortex Reynolds number

$$\frac{\bar{V}_r(\bar{r})}{\bar{z}} = \frac{V_z}{\Gamma z/2\pi r_c^2} = \frac{4n(n+1)}{R_e} \frac{\bar{r}^{-2(n-1)}}{(1+\bar{r}^{-2n})^2} \text{ , Where } \bar{z} = \frac{z}{r_c} \tag{2.18}$$

The static pressure distribution can also be derived by resorting to the radial momentum equation and the fact that $\frac{1}{R_e} \approx 0$.

$$\bar{p} = 2\int_0^{\bar{r}} \frac{\bar{V}_\theta^2}{\bar{r}} d\bar{r} = \int_0^{\bar{r}} 2 \frac{\bar{r}}{(1+\bar{r}^{-2n})^{\frac{2}{n}}} d\bar{r} \tag{2.19}$$

Case of $n = 1$ $\bar{p} = [1 - \frac{1}{1+\bar{r}^{-2}}]$ (2.20)

Case of $n = 2$ $\bar{p} \equiv \frac{2}{\pi} \arctan(\bar{r}^{-2})$ (2.21)

Case of $n = \infty$ $\bar{P} = \begin{cases} \frac{1}{2}\bar{r}^{-2} & 0 \le \bar{r} \le 1 \\ 1 - \frac{1}{2\bar{r}^{-2}} & 1 < \bar{r} < \infty \end{cases}$ (2.28)

Similarly the normalized axial vorticity is given by

$$\overline{\Omega_z} = \frac{\Omega_z}{\Gamma/r_c^2} = \frac{1}{2\pi} \frac{1}{\bar{r}} \frac{\partial}{\partial \bar{r}} \left(\frac{\bar{r}^{-2n}}{(1+\bar{r}^{-2n})} \right)^{\frac{1}{n}} = \frac{1}{2\pi} \frac{1}{\bar{r}} \left(\frac{2\bar{r}}{(1+\bar{r}^{-2n})^{\frac{1}{n}}} - \frac{2\bar{r}^{-2n}}{(1+\bar{r}^{-2n})^{\frac{1}{n}+1}} \right)$$

$$\overline{\Omega_z} = \frac{1}{\pi} \left(\frac{1}{(1+\bar{r}^{-2n})^{\frac{1+n}{n}}} \right) \tag{2.29}$$

It quite interesting to study the limiting cases have the tangential, vorticity and the pressure for this model. The Therefore, the limiting velocity is given by:

a- $$\lim_{n\to 1}\bar{V}_\theta(\bar{r}) = \lim_{n\to 1}\frac{\bar{r}}{(1+\bar{r}^{-2n})^{\frac{1}{n}}} = \frac{\bar{r}}{(1+\bar{r}^{-2})} \quad \rightarrow \quad \text{Scully's Model}$$

b- $$\lim_{n\to\infty}\bar{V}_\theta(\bar{r}) = \lim_{n\to\infty}\frac{\bar{r}}{(1+\bar{r}^{-2n})^{\frac{1}{n}}} = \begin{cases}\bar{r} & 0\le\bar{r}\le 1\\ \dfrac{1}{\bar{r}} & 1<\bar{r}\le\infty\end{cases} \quad \rightarrow \quad \text{Rankine's Model}$$

c- $$\lim_{n\to 1}\overline{\Omega_z} = \lim_{n\to 1}\frac{1}{\pi}\left(\frac{1}{(1+\bar{r}^{-2n})^{\frac{1+n}{n}}}\right) = \frac{1}{\pi}\left(\frac{1}{(1+\bar{r}^{-2})^2}\right) \quad \rightarrow \quad \text{Scully's Model}$$

d- $$\lim_{n\to\infty}\overline{\Omega_z} = \lim_{n\to\infty}\frac{1}{\pi}\left(\frac{1}{(1+\bar{r}^{-2n})^{\frac{1+n}{n}}}\right) = \begin{cases}\dfrac{1}{\pi} & 0\le\bar{r}\le 1\\ 0 & 1<\bar{r}\le\infty\end{cases} \quad \rightarrow \quad \text{Rankine's Model}$$

a- $$\lim_{n\to 1}\bar{p} = \lim_{n\to 1}\int 2\frac{\bar{V}_\theta^2}{\bar{r}}d\bar{r} = \int\lim_{n\to 1}2\frac{\bar{r}}{(1+\bar{r}^{-2n})^{\frac{2}{n}}}d\bar{r} = \int 2\frac{\bar{r}}{(1+\bar{r}^{-2})2}d\bar{r}$$

$$\bar{P}_{n=1} = [1-\frac{1}{1+\bar{r}^{-2}}] \quad \rightarrow \quad \text{Scully's Model}$$

b- $$\lim_{n\to\infty}\bar{p} = \lim_{n\to\infty}\int\frac{\bar{V}_\theta^2}{\bar{r}}d\bar{r} = \int\lim_{n\to\infty}\frac{\bar{r}}{(1+\bar{r}^{-2n})^{\frac{2}{n}}}d\bar{r} = \begin{cases}\int\bar{r}d\bar{r} & 0\le\bar{r}\le 1\\ \int\dfrac{1}{\bar{r}^3}d\bar{r} & 1<\bar{r}<\infty\end{cases}$$

$$\bar{P}_{n\to\infty} = \begin{cases}\dfrac{1}{2}\bar{r}^{-2} & 0\le\bar{r}\le 1\\ 1-\dfrac{1}{2\bar{r}^2} & 1<\bar{r}<\infty\end{cases} \quad \rightarrow \quad \text{Rankine's Model}$$

The analysis showed that Vatistas's model tends to scully's model as n=1 and reaches Rankine's model as n tends to infinity. These results are plotted through figures [2.15 to 2.19]. It is clear that these family members are plagued from the previously mentioned mathematical and physical inconsistencies. In addition it simulates the actual tangential velocity reasonably well, see figure [2.1]. This family model can be used to predict the aircraft wakes. It has shown that, it gives good predications of the wing tip vortices. Therefore this general model is expected to be suitable for use in several aero acoustics applications that require a good physical interpretation [14]. A summary figure illustrates the distribution of induced swirl velocity inside a viscous vortex core on the basis of several models are shown in figure [2.20].

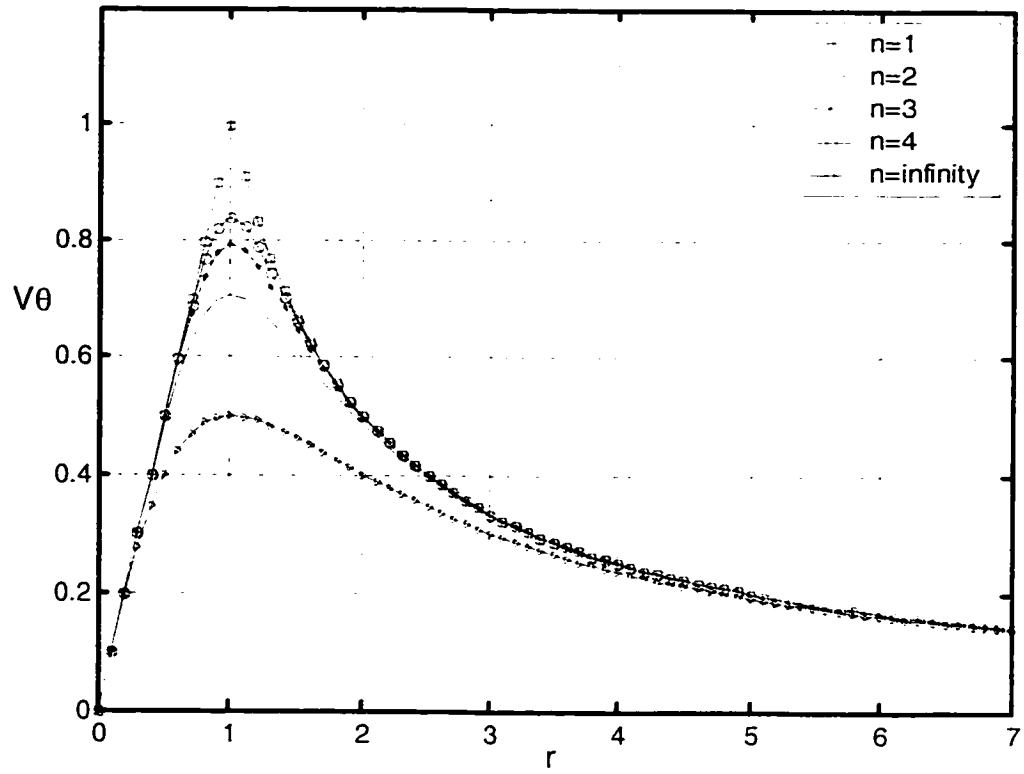

Fig. 2-15. Tangential velocity distribution of Vatistas vortex model

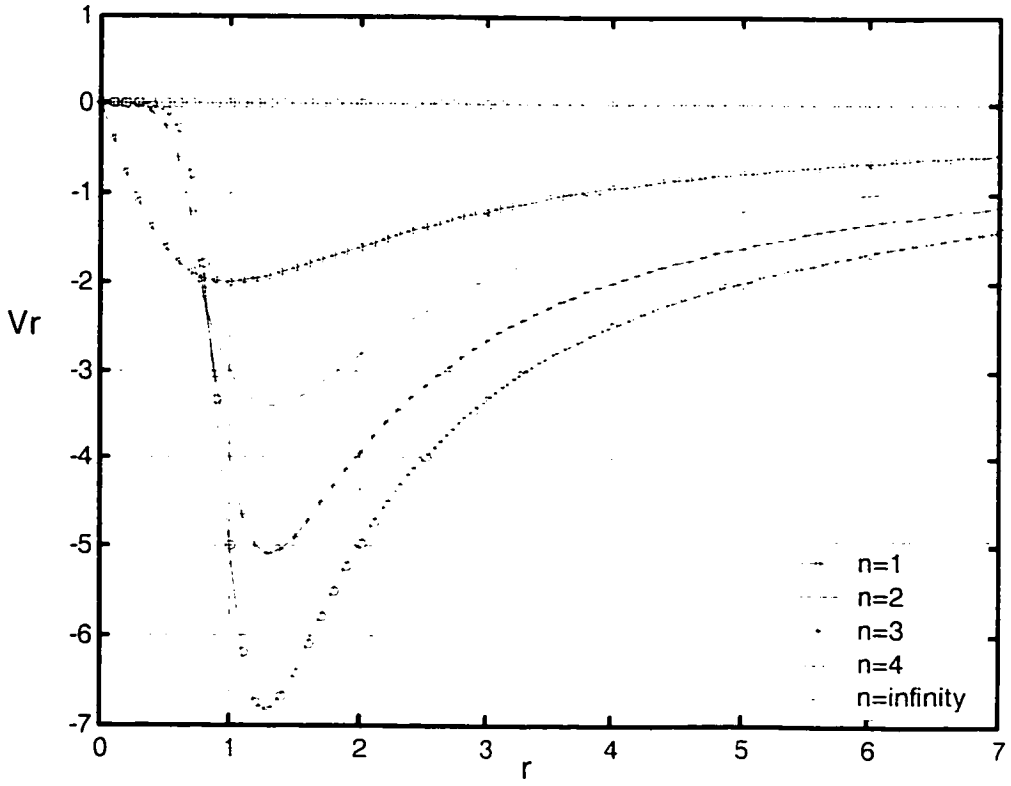

Fig. 2-16. Radial velocity distribution of Vatistas vortex model

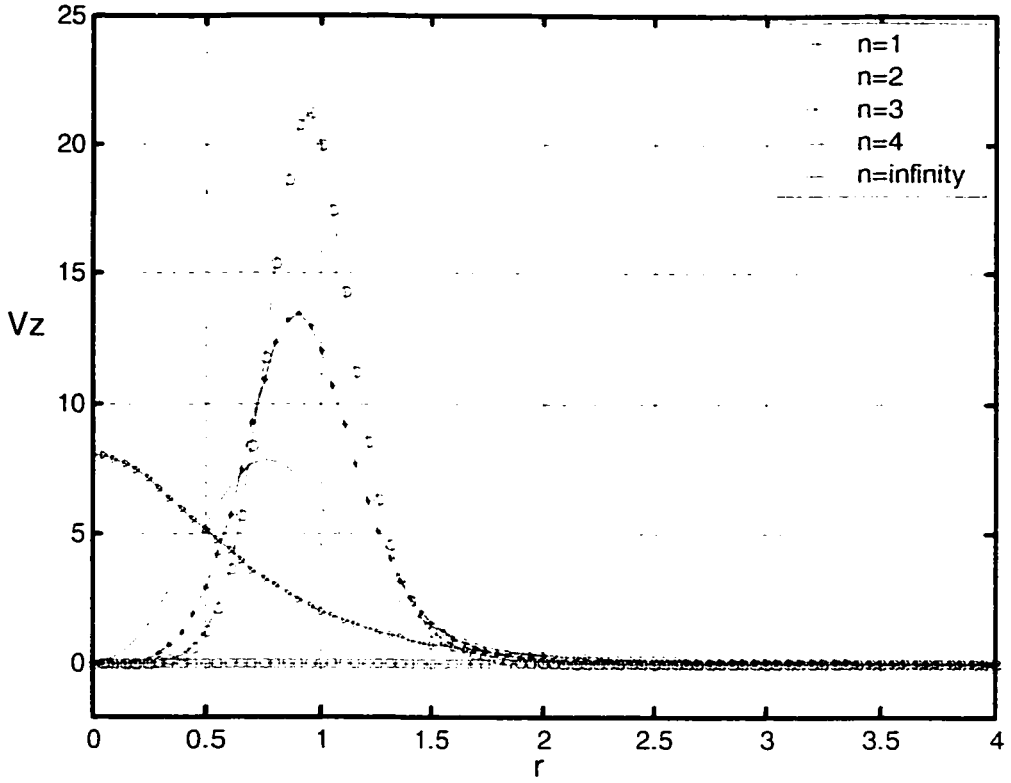

Fig. 2-17. Axial velocity distribution of Vatistas vortex model

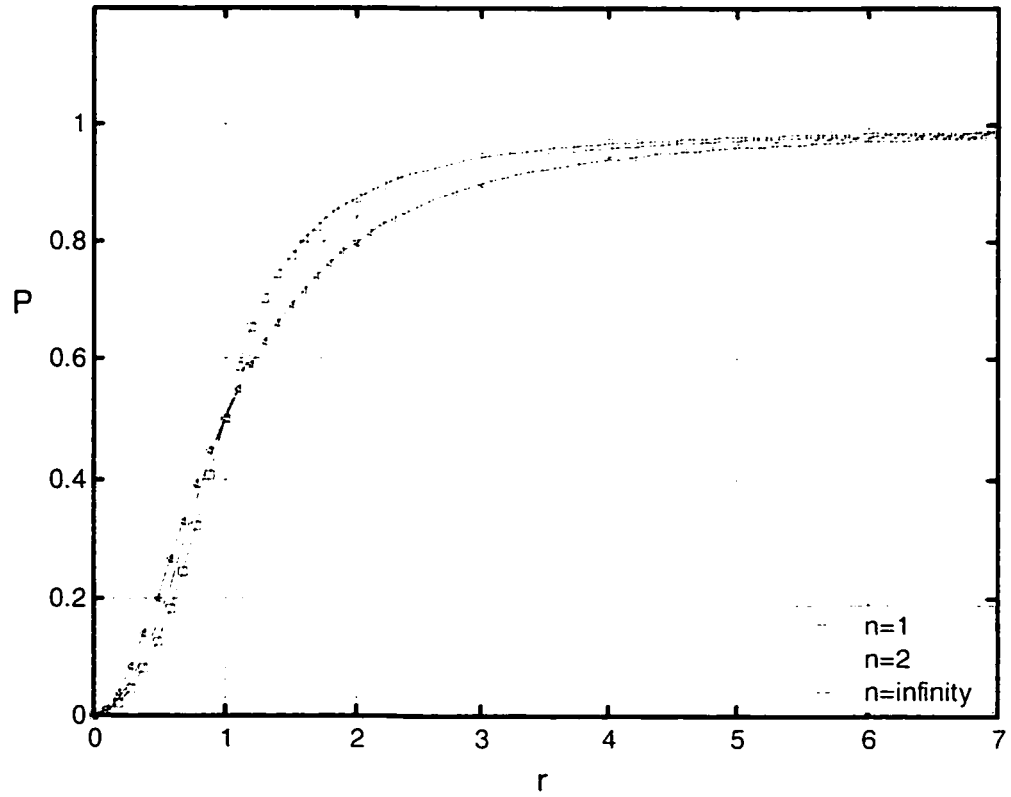

Fig. 2-18. Pressure distribution of Vatistas Vortex model

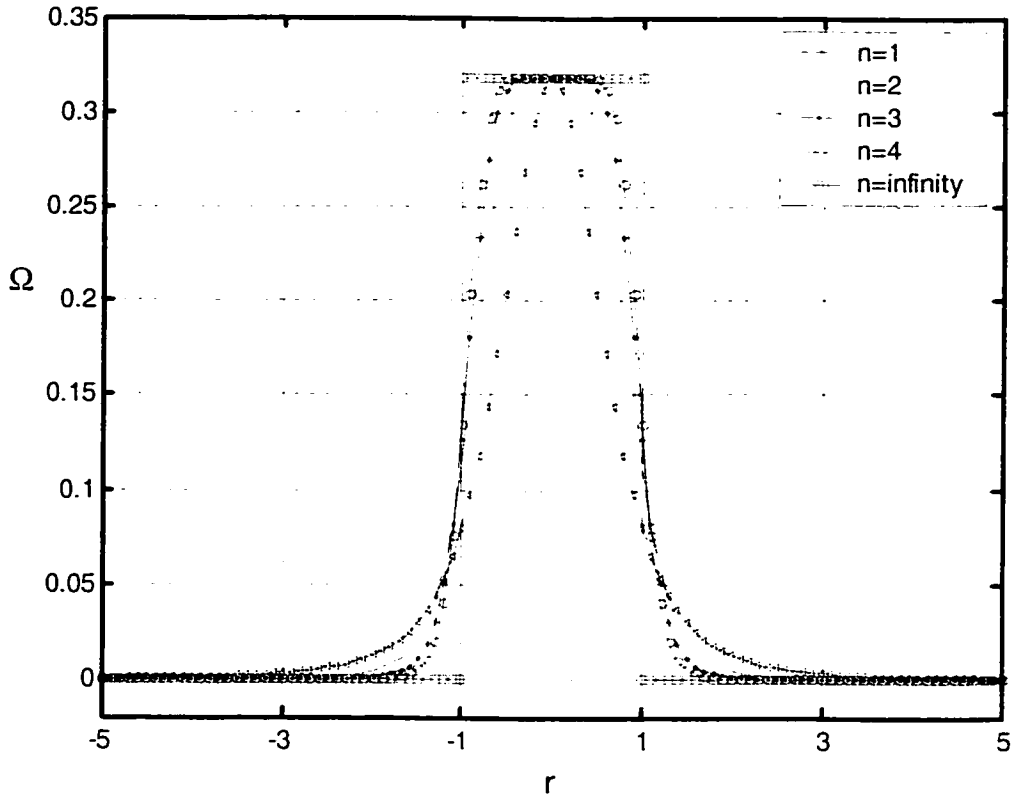

Fig. 2-19. Vorticity distribution of Vatistas's Vortex

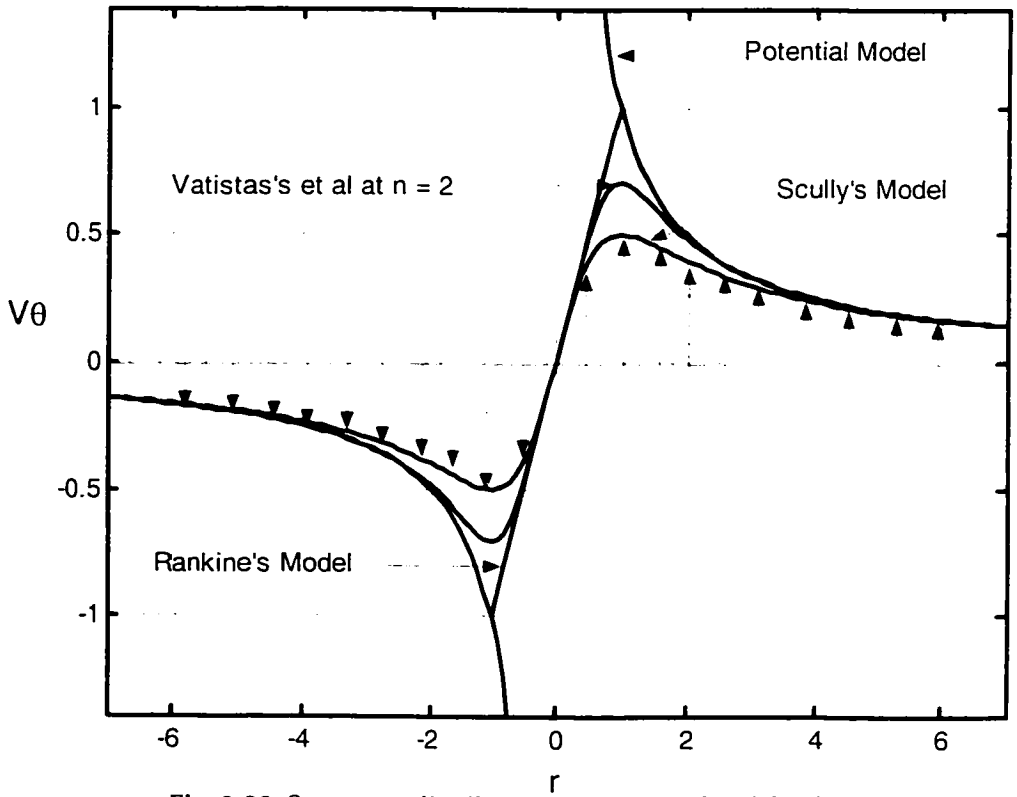

Fig. 2-20. Summary distributions of induced swirl velocity on the basis of several models.

Chapter 3

Decay of Confined Line Vortices

3.1 Overview

Confined steady and unsteady vortex flows are clearly appear in many of the fluid mechanics engineering applications of fluid mechanics. Some of these applications can be treated as confined flows without separation, such as the swirl flows in a duct/pipe, channel flows and confined jets. If we add the swirl intensity, pressure gradient or if we suddenly change the geometry of such applications, then we have to analyze them as confined flows with separation. Rotor stator interaction in turbine stage, mixing of the fuel-oxidizer during the combustion process inside the confined liner [combustor] within the gas turbine engine can be classified as unsteady confined flows.

Most of these confined flows are characterized by strong vortices. One of the most widely used techniques to generate confined strong vortex is to force the fluid in a cylindrical chamber [vortex chamber] through a series of tangential inlets or by wall rotation. The swirl velocity near and far from the vortex core and time dependent vortex flow field parameters can describe the natural characteristics of these confined vortices. Here we present a new simple scheme

to track how the vortex flow field parameters, such as the tangential velocity, radial static pressure and axial vorticity distributions decay with time.

3.2 Problem Formulation

Consider purely swirling motion of an unsteady, viscous, laminar, axisymmetric and incompressible vortex filament shown in figure [3.1]. The later is considered to be a self-similar line and concentrated vortex. Assumes further that, the tangential velocity is orders of magnitude greater than the other velocity components. Under these conditions the equations of motion in a simplified form yields,

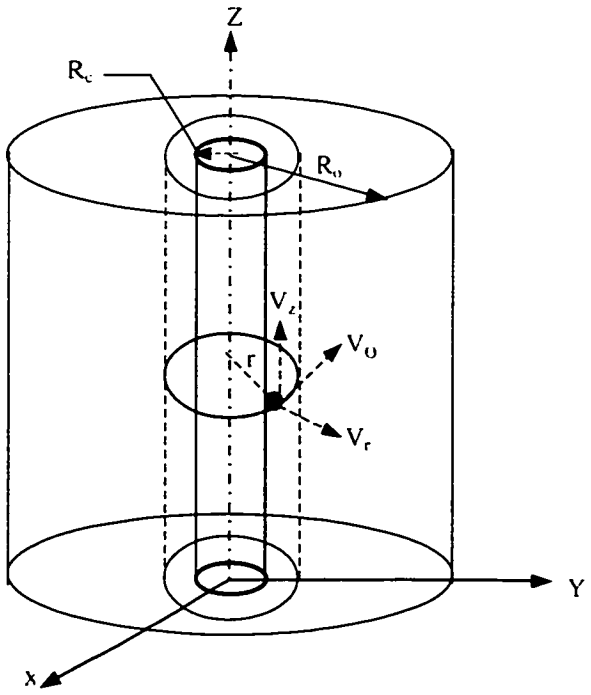

Fig. 3-1 Schematic illustrates the Confined Line Vortex

Radial Momentum: $$\frac{V_\theta^2}{r} = \frac{1}{\rho}\frac{\partial P}{\partial r} \tag{3.1}$$

Swirl Momentum: $$\frac{\partial V_\theta}{\partial t} = \upsilon[\nabla^2 V_\theta - \frac{V_\theta}{r^2}]$$

$$\nabla^2 V_\theta = \frac{\partial^2 [V_\theta]}{\partial r^2} + \frac{1}{r}\frac{\partial [V_\theta]}{\partial r}$$

$$\frac{\partial [V_\theta]}{\partial t} = \upsilon[\frac{\partial^2 V_\theta}{\partial r^2} + \frac{1}{r}\frac{\partial V_\theta}{\partial r} - \frac{V_\theta}{r^2}] \tag{3.2}$$

Axial Momentum: $$\frac{\partial P}{\partial z} = 0 \tag{3.3}$$

The continuity is automatically satisfied, which indicates that this flow is kinematical possible flow. The momentum balance equations suggest that static pressure distribution does not vary along the axial direction. Which further implies that the pressure is only a function of the time and the radius. Referring to equation (3.1), it is clear that the tangential velocity will depend only on time and radial location as well. Therefore the tangential velocity and static pressure are:

$$\vec{V}(r,t) = V_\theta(r,t)\vec{e_\theta}$$
$$P = P(r,t)$$

It is recommended to dimensionalize this set of equations. Therefore, we can use the free stream parameters V_{θ_i}, p_∞ and ρ_∞ to normalize the equations. The equations in normalized form are:

$$\frac{\partial \Pi}{\partial \bar{r}} = \frac{\bar{V}_\theta^2}{\bar{r}} \tag{3.4}$$

$$\frac{\partial [\bar{V}_\theta]}{\partial \bar{t}} = [\frac{\partial^2 \bar{V}_\theta}{\partial \bar{r}^2} + \frac{1}{\bar{r}} \frac{\partial \bar{V}_\theta}{\partial \bar{r}} - \frac{\bar{V}_\theta}{\bar{r}^2}] \tag{3.5}$$

While, the vorticity is given by:

$$\bar{\Omega}(r,t) = \frac{1}{r} \frac{\partial [rV_\theta]}{\partial r} \bar{e}_z \tag{3.6}$$

Where

$\bar{V}_\theta = \frac{V_\theta}{V_{a_0}}$ Non-dimensional Tangential velocity components

$\Pi = \frac{p - p_a}{\rho V_{a_0}^2}$ Non-dimensional Static Pressure

$\bar{t} = \frac{tv}{R_a^2}$ Non-dimensional Time Parameter

$\bar{r} = \frac{r}{R_a}$ Non-dimensional Radial distance

Solving the vortex flow field of purely swirling fluid motion will require two well-known boundary conditions for the velocity at the vortex center and at the outer core radius. Hence it is quite interesting to study how the vortex flow field parameters vary with time along the radial direction, provided that the velocity may be free to slip at the outer vortex diameter or the velocity is not allowed to slip [non-slip]. In the light of this, we present the solution, which can capture most of the decay characteristics of such a vortex.

3.3 Analysis and Solution

Referring back to equations (3.4), (3.5) and (3.6) we can observe that, these equations constitute an initial boundary value problem, which can be solved using the separation of variables technique. The latter is a generalized solution, which, is derived based on various steady vortex models as an initial conditions. This procedure is applicable for both confined and unconfined vortices, however mathematical transformations have been assumed separately to make sure that the boundary conditions are homogenous.

Since, we are using the separation of variables approach, the tangential velocity must assumed to consist of the following:

$$\bar{V}_\theta(\bar{t},\bar{r}) = T(\bar{t})R(\bar{r}) \tag{3.7}$$

$T(\bar{t})$ Considered to be only function of time

$R(\bar{r})$ Is considered to be only function of the vortex radius

Differentiating equation (3.7) with respect to t and r yields,

$$\left.\begin{aligned} \frac{\partial[\bar{V}_\theta]}{\partial\bar{t}} &= R(\bar{r})\frac{\partial T(\bar{t})}{\partial\bar{t}} \\ \frac{\partial[\bar{V}_\theta]}{\partial\bar{r}} &= T(\bar{t})\frac{\partial R(\bar{r})}{\partial\bar{r}} \\ \frac{\partial^2[\bar{V}_\theta]}{\partial\bar{r}^2} &= T(\bar{t})\frac{\partial^2 R(\bar{r})}{\partial\bar{r}^2} \end{aligned}\right\} \tag{3.8}$$

Substituting back from equation (3.8) into equation (3.5) yields,

$$\frac{1}{T(\bar{t})}\frac{\partial T(\bar{t})}{\partial\bar{t}} = \frac{1}{R(\bar{r})}\left[\frac{\partial^2 R(\bar{r})}{\partial\bar{r}^2} + \frac{1}{\bar{r}}\frac{\partial R(\bar{r})}{\partial\bar{r}} - \frac{R(\bar{r})}{\bar{r}^2}\right] \tag{3.9}$$

Since $T(\bar{t})$ & $R(\bar{r})$ are two dependent variables, while $\bar{t}$ & $\bar{r}$ are two independent parameters which indicates that equation (3.9) can only be satisfied if both sides equal to a constant.

$$\frac{1}{T(\bar{t})}\frac{\partial T(\bar{t})}{\partial \bar{t}} = -m^2 \tag{3.10}$$

$$\frac{1}{R(\bar{r})}\left[\frac{\partial^2 R(\bar{r})}{\partial \bar{r}^2} + \frac{1}{\bar{r}}\frac{\partial R(\bar{r})}{\partial \bar{r}} - \frac{R(\bar{r})}{\bar{r}^2}\right] = -m^2 \tag{3.11}$$

Where $-m^2$ is the separation constant

Solving Equation (3.10), hence

$$\frac{1}{T(\bar{t})}\frac{\partial T(\bar{t})}{\partial \bar{t}} = -m^2$$

$$\frac{\partial T(\bar{t})}{\partial \bar{t}} = -m^2 T(\bar{t}), \qquad \int\frac{\partial T(\bar{t})}{T(\bar{t})} = \int -m^2 d\bar{t}$$

$$\ln[T(t)] = -[m^2\bar{t} + A_o], \qquad e^{\ln[T(t)]} = e^{-[m^2\bar{t}+A_o]}$$

$$T(t) = e^{-[m^2\bar{t}]}e^{-A_o},$$

Letting $A = e^{-A_o}$

Where, A & A_o are constants, therefore

$$T(t) = Ae^{-[m^2\bar{t}]} \tag{3.12}$$

Solving equation (3.11), we obtain

$$\frac{1}{R(\bar{r})}\left[\frac{\partial^2 R(\bar{r})}{\partial \bar{r}^2} + \frac{1}{\bar{r}}\frac{\partial R(\bar{r})}{\partial \bar{r}} - \frac{R(\bar{r})}{\bar{r}^2}\right] = -m^2$$

$$\left[\frac{\partial^2 R(\bar{r})}{\partial \bar{r}^2} + \frac{1}{\bar{r}}\frac{\partial R(\bar{r})}{\partial \bar{r}} - \frac{R(\bar{r})}{\bar{r}^2}\right] = -m^2 R(\bar{r})$$

$$[\frac{\partial^2 R(\bar{r})}{\partial \bar{r}^2} + \frac{1}{\bar{r}}\frac{\partial R(\bar{r})}{\partial \bar{r}} + m^2 R(\bar{r}) - \frac{R(\bar{r})}{\bar{r}^2}] = 0$$

$$[\frac{\partial^2 R(\bar{r})}{\partial \bar{r}^2} + \frac{1}{\bar{r}}\frac{\partial R(\bar{r})}{\partial \bar{r}} + (m^2 - \frac{1}{\bar{r}^2})R(\bar{r})] = 0$$

$$[\bar{r}^2\frac{\partial^2 R(\bar{r})}{\partial \bar{r}^2} + \bar{r}\frac{\partial R(\bar{r})}{\partial \bar{r}} + (\bar{r}^2 m^2 - 1)R(\bar{r})] = 0 \qquad (3.13)$$

Recall that equation (3.13) is the general Bessel's differential equation, which is a standard form of the linear differential equation is given in form:

$$x^2\frac{\partial^2 y(x)}{\partial x^2} + x\frac{\partial y(x)}{\partial x} + (x^2 m^2 - z)y(x) = 0, \quad z \geq 0 \qquad (3.14)$$

By comparing equation (3.13) and equation (3.14) we realized that they are identical if z=1 hence the solution of equation (3.13) can be introduced in terms of the Bessel series function [15]:

$$R(\bar{r}) = BJ_1(m\bar{r}) + CY_1(m\bar{r}) \qquad (3.15)$$

Where

J_1	1st kind 1st order Bessel function
Y_1	2nd kind 1st order Bessel function
B&C	Constants

A physical restriction requires all the flow parameters to be finite over the entire domain, therefore the tangential velocity must satisfy this mathematical fact.

The latter is explained in detail, in Appendix A.

Since the tangential velocity is finite at the vortex center, therefore the constant C in equation (3.15) must vanish. Consequently the solution must be restricted to

$$R(\bar{r}) = BJ_1(m\bar{r}) \tag{3.16}$$

Using equations (3.12), (3.16) and substituting back into equation (3.7), then we can obtain,

$$\bar{V}_\theta(\bar{t},\bar{r}) = Ae^{-[m^2\bar{t}]}BJ_1(m\bar{r})$$

Letting $A_n = AB$,

Where A_n is constant, yields

$$\bar{V}_\theta(\bar{t},\bar{r}) = A_n e^{-[m^2\bar{t}]}J_1(m\bar{r}) \tag{3.17}$$

Determining these constants will depend on whether the velocity is allowed to slip at the vortex filament's outer radius or it is halted.

3.4 Case study 1

Free Slip of The Tangential Velocity at The Outer Radius

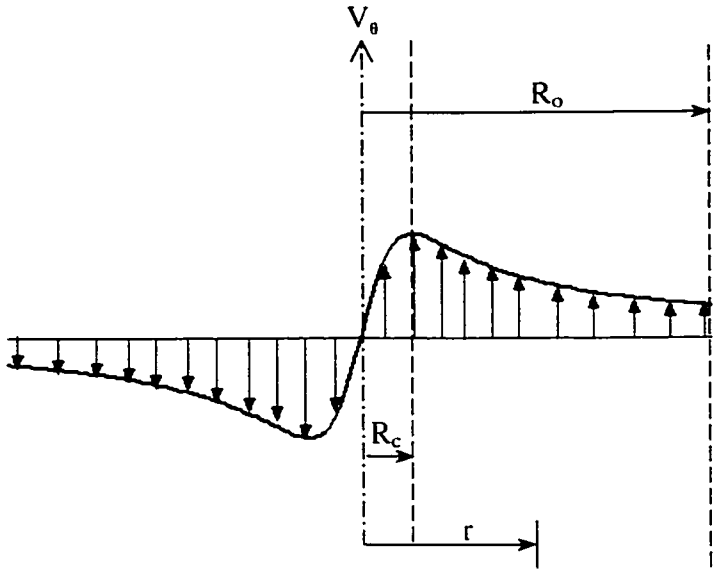

Fig. 3-2 Schematic illustrates the velocity slip at the outer radius

In this case we assumes that the swirl velocity is free to slip at the outer vortex filament's diameter as shown in figure [3.2]. Therefore the boundary conditions are given by:

For $\bar{t} \geq 0$,

1. The tangential velocity is zero at the vortex center i.e. $\bar{V}_\theta = 0$ at $\bar{r} = 0$

2. The tangential velocity is unity at the vortex outer radius i.e. $\bar{V}_\theta = 1$ at $\bar{r} = 1$

Appling the boundary conditions indicates that, the first boundary condition is automatically satisfied. While the second boundary condition gives:

$1 = A_n e^{-(m^2 \bar{t})} J_1(m)$ While, at $\bar{t} = 0$. $e^{-m\bar{t}^2} = 1$ therefore,

$$1 = A_n J_1(m) \tag{3.18}$$

From the definition of the Bessel function of the 1st kind 1st order, we have

$$J_1(m) = \sum_{S=0}^{\infty} \frac{(-1)^S (m/2)^{2S+1}}{S!\Gamma(2+S)}$$

Where Γ here is the Gamma function. Substituting equation (3.18) gives

$$1 = A_n \sum_{S=0}^{\infty} \frac{(-1)^S (m/2)^{2S+1}}{S!\Gamma(2+S)} \tag{3.19}$$

It is clear that equation (3.19) is a very complicated function; hence we can do some mathematically transformation without losing the generality of problem.

Letting $$\tilde{V}_\theta(\bar{t}, \bar{r}) = \bar{r} - \bar{V}_\theta(\bar{t}, \bar{r}) \tag{3.20}$$

Differentiate (3.20) with respect to $\bar{t}$, $\bar{r}$

$$\left.\begin{aligned}
&\frac{\partial \bar{V}_\theta(\bar{t}, \bar{r})}{\partial \bar{t}} = -\frac{\partial \tilde{V}_\theta(\bar{t}, \bar{r})}{\partial \bar{t}} \\
&\frac{1}{\bar{r}} \frac{\partial \bar{V}_\theta(\bar{t}, \bar{r})}{\partial \bar{r}} = \frac{1}{\bar{r}} - \frac{1}{\bar{r}} \frac{\partial \tilde{V}_\theta(\bar{t}, \bar{r})}{\partial \bar{r}} \\
&\frac{\partial^2 \bar{V}_\theta(\bar{t}, \bar{r})}{\partial \bar{r}^2} = -\frac{\partial^2 \tilde{V}_\theta(\bar{t}, \bar{r})}{\partial \bar{r}^2} \\
&\frac{-\bar{V}_\theta(\bar{t}, \bar{r})}{\bar{r}^2} = -\frac{1}{\bar{r}} + \frac{\tilde{V}_\theta(\bar{t}, \bar{r})}{\bar{r}^2}
\end{aligned}\right\} \tag{3.21}$$

Back substantiation of eq. (3.21) into eq. (3.5) will recover the governing equation.

$$\frac{\partial \tilde{V}_\theta}{\partial \bar{t}} = [\frac{\partial^2 \tilde{V}_\theta}{\partial \bar{r}^2} + \frac{1}{\bar{r}} \frac{\partial \tilde{V}_\theta}{\partial \bar{r}} - \frac{\tilde{V}_\theta}{\bar{r}^2}] \tag{3.22}$$

Solution of equation (3.22) is identical to solution of equation (3.5). Hence

$$\bar{V}_\theta(\bar{t},\bar{r}) = A_n e^{-(m^2\bar{t})} J_1(m\bar{r}) \tag{3.23}$$

The original boundary conditions must be rewritten again relative to the transformed one, which is given by equation (3.23). The homogeneous boundary conditions for the transformed equation are given by:

For $\bar{t} \geq 0$

1. $\bar{V}_\theta = 0$ for $\bar{r} = 0$ therefore, $V_\theta = 0$

2. $\bar{V}_\theta = 1$ for $\bar{r} = 1$ therefore, $V_\theta = 0$

Application of the 2nd boundary condition to the model equation (3.23)

$$0 = J_1(m) \tag{3.24}$$

Where, $\lambda_n = m$, λ_n are the zeros of the Bessel function J_1, which can be given as

$$\lambda_n = \pi[n + 0.25 - \frac{0.151985}{(4n+1)} + \frac{0.015399}{(4n+1)^3} - \frac{0.245275}{(4n+1)^5} \cdots\cdots\cdots\cdots], n = 1,2,3\cdots\cdots\cdots\infty$$

Since we are dealing with a linear differential equation, the principle of superposition applies. Thus the velocity can be expressed by terms summation.

$$\bar{V}_\theta(\bar{t},\bar{r}) = \sum_n^\infty A_n e^{-(\lambda_n^2\bar{t})} J_1(\lambda_n \bar{r}) \tag{3.25}$$

Where, A_n Can be found analytically as.

$$A_n = \frac{\int_0^1 r\bar{V}_\theta(\bar{t}=0,\bar{r}) J_1(\lambda_n \bar{r}) d\bar{r}}{\int_0^1 r J_1^2(\lambda_n \bar{r}) d\bar{r}} = \frac{2}{J_o^2(\lambda_n)} \int_0^1 r\bar{V}_\theta(\bar{t}=0,\bar{r}) J_1(\lambda_n \bar{r}) d\bar{r} \tag{3.26}$$

Substituting from equation (3.25) into equation (3.20), gives

$$\bar{V}_\theta(\bar{t},\bar{r}) = \bar{r} - \sum_n^{\infty} A_n e^{-(\lambda_n^2 \bar{t})} J_1(\lambda_n \bar{r}) \tag{3.27}$$

Once the tangential velocity is known, the axial vorticity and radial pressure distributions can be determined via Bessel series by back substitutions as well.

$$\bar{\Omega}(r,t) = \left(2 - \frac{1}{\bar{r}} \sum_n^{\infty} A_n e^{-(\lambda_n^2 \bar{t})} J_1(\lambda_n \bar{r}) - \frac{1}{2} \sum_n^{\infty} A_n e^{-(\lambda_n^2 \bar{t})} [J_0(\lambda_n \bar{r}) - J_2(\lambda_n \bar{r})]\right) \tag{3.28}$$

$$\Pi = \int_0^{\bar{r}} \frac{\left(\bar{r} - \sum_n^{\infty} A_n e^{-(\lambda_n^2 \bar{t})} J_1(\lambda_n \bar{r})\right)^2}{\bar{r}} \Bigg/ \int_0^1 \frac{\left(\bar{r} - \sum_n^{\infty} A_n e^{-(\lambda_n^2 \bar{t})} J_1(\lambda_n \bar{r})\right)^2}{\bar{r}} \tag{3.29}$$

The tangential velocity expression depends on the constant coefficient A_n, which can be found based on the initial velocity distribution. Here we present three different initial vortex swirl velocity models, which are the Potential, Rankine and Vatistas's n = 2 model. Each model is presented in a separate section, however a relative time comparison is shown in figure [3.12]. The steady vortex solution presented in chapter two can be used as an initial condition to predict the decay phase of the vortex field. This solution is an approximate solution to The Navier-Stokes's equation, assuming a pure swirling motion. These results are based on the assumptions that the vortex outer core radius is 20 times larger than the inner radius, which means that, β =0.05.

3.4.1 The Potential Vortex Decay [Slip]

In this section, we will use the potential vortex model as an initial velocity distribution. Let the initial potential vortex model is given by

$$\bar{V}_\theta(\bar{t}=0,\bar{r})=\frac{1}{\bar{r}} \qquad 0<\bar{r}\le 1$$

Using the general transformation made previously [see Eq. (3.20)], we have:

$$\bar{V}_\theta(\bar{t}=0,\bar{r})=\bar{r}-\bar{V}_\theta(\bar{t}=0,\bar{r})=\bar{r}-\frac{1}{\bar{r}} \tag{3.30}$$

In order to determine the tangential velocity distribution, one has to evaluate the coefficient A_n using this standard formulation:

$$A_n=\frac{\int_0^1 r\bar{V}_\theta(\bar{t}=0,\bar{r})J_1(\lambda_n\bar{r})d\bar{r}}{\int_0^1 rJ_1^2(\lambda_n\bar{r})d\bar{r}}=\frac{2}{J_o^2(\lambda_n)}\int_0^1 r\bar{V}_\theta(\bar{t}=0,\bar{r})J_1(\lambda_n\bar{r})d\bar{r}$$

$$A_n=\frac{2}{J_o^2(\lambda_n)}\int_0^1 \bar{r}\left(\bar{r}-\frac{1}{\bar{r}}\right)J_1(\lambda_n\bar{r})d\bar{r}$$

$$=\frac{2}{J_o^2(\lambda_n)}\int_0^1 (\bar{r}^2-1)J_1(\lambda_n\bar{r})d\bar{r}$$

By Referring to Appendix A

$$\int_0^1 J_1(\lambda_n\bar{r})d\bar{r}=\frac{-1}{\lambda_n}[J_o(\lambda_n)-1] \qquad \text{and} \qquad \int_0^1 \bar{r}^2 J_1(\lambda_n\bar{r})d\bar{r}=\frac{4}{\lambda_n^3}[-\frac{\lambda_n^2}{4}J_o(\lambda_n)+\frac{\lambda_n}{2}J_1(\lambda_n)]$$

$$A_n=\frac{2}{J_o^2(\lambda_n)}\left(\frac{4}{\lambda_n^3}[-\frac{\lambda_n^2}{4}J_o(\lambda_n)+\frac{\lambda_n}{2}J_1(\lambda_n)]+\frac{1}{\lambda_n}[J_o(\lambda_n)-1]\right), J_1(\lambda_n)=0$$

$$A_n=\frac{-2}{\lambda_n J_o^2(\lambda_n)} \tag{3.31}$$

The tangential velocity distribution can be determined by inserting equation (3.31) into equation (3.27), yields:

$$\bar{V}_\theta(\bar{t},\bar{r}) = \bar{r} - \sum_n^{\infty} \frac{-2}{\lambda_n J_o^2(\lambda_n)} e^{-[\lambda_n^2 \bar{t}]} J_1(\lambda_n \bar{r}) \tag{3.32}$$

Similarly, the vorticity and static pressure are given respectively

$$\bar{\Omega}(r,t) = \left(2 - \frac{1}{\bar{r}} \sum_n^{\infty} \frac{-2}{\lambda_n J_o^2(\lambda_n)} e^{-[\lambda_n^2 \bar{t}]} J_1(\lambda_n \bar{r}) - \frac{1}{2} \sum_n^{\infty} \frac{-2}{\lambda_n J_o^2(\lambda_n)} e^{-[\lambda_n^2 \bar{t}]} [J_o(\lambda_n \bar{r}) - J_2(\lambda_n \bar{r})] \right) \tag{3.33}$$

$$\Pi = \int_0^{\bar{r}} \frac{\left(\bar{r} - \sum_n^{\infty} \frac{-2}{\lambda_n J_o^2(\lambda_n)} e^{-[\lambda_n^2 \bar{t}]} J_1(\lambda_n \bar{r}) \right)^2}{\bar{r}} \Bigg/ \int_0^1 \frac{\left(\bar{r} - \sum_n^{\infty} \frac{-2}{\lambda_n J_o^2(\lambda_n)} e^{-[\lambda_n^2 \bar{t}]} J_1(\lambda_n \bar{r}) \right)^2}{\bar{r}} \tag{3.34}$$

The tangential velocity, vorticity and pressure distributions are shown in figures [3.3], [3.4] and [3.5] respectively. The entire analysis of the potential vortex must be restricted to times greater than the mean free length. Since for smaller times the continuum assumption is violated and hence the phenomena cannot be descried by the standard continuous equations assumed. The early decay of the potential model exhibit higher values of the tangential velocity inside the core. Since the steady the Potential model assume infinity tangential velocity at the vortex center. Therefore at the beginning it is expected to evolve higher values of the velocity, vorticity and pressure distributions.

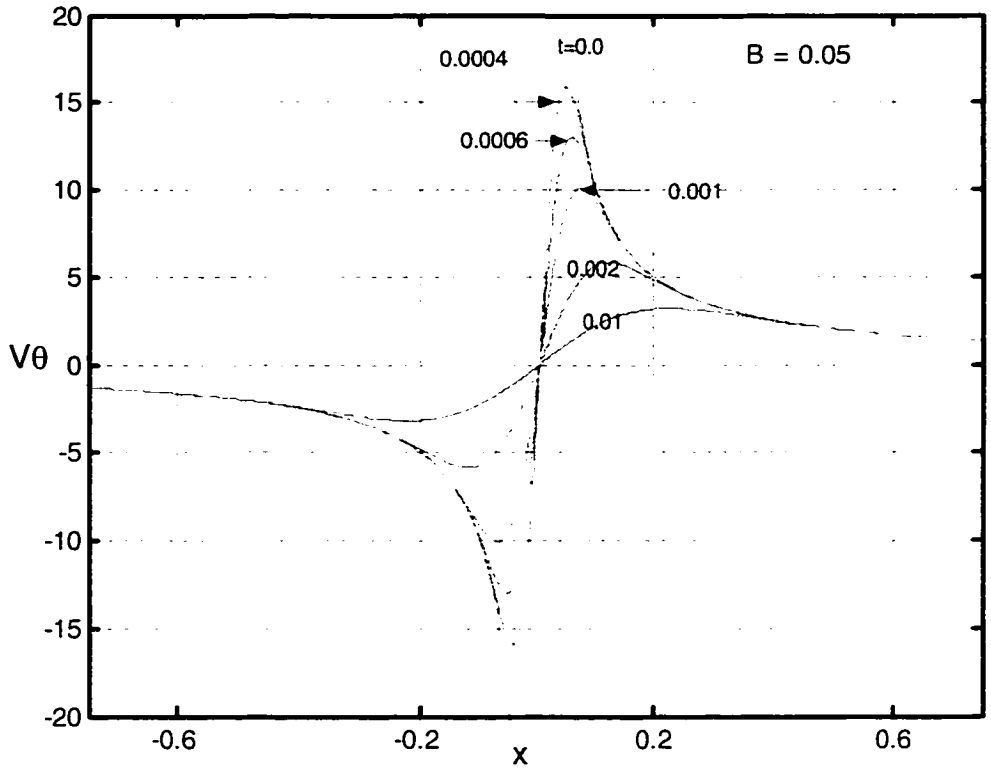

Fig. 3-3 Tangential velocity decays, using potential model [Case of Slip].

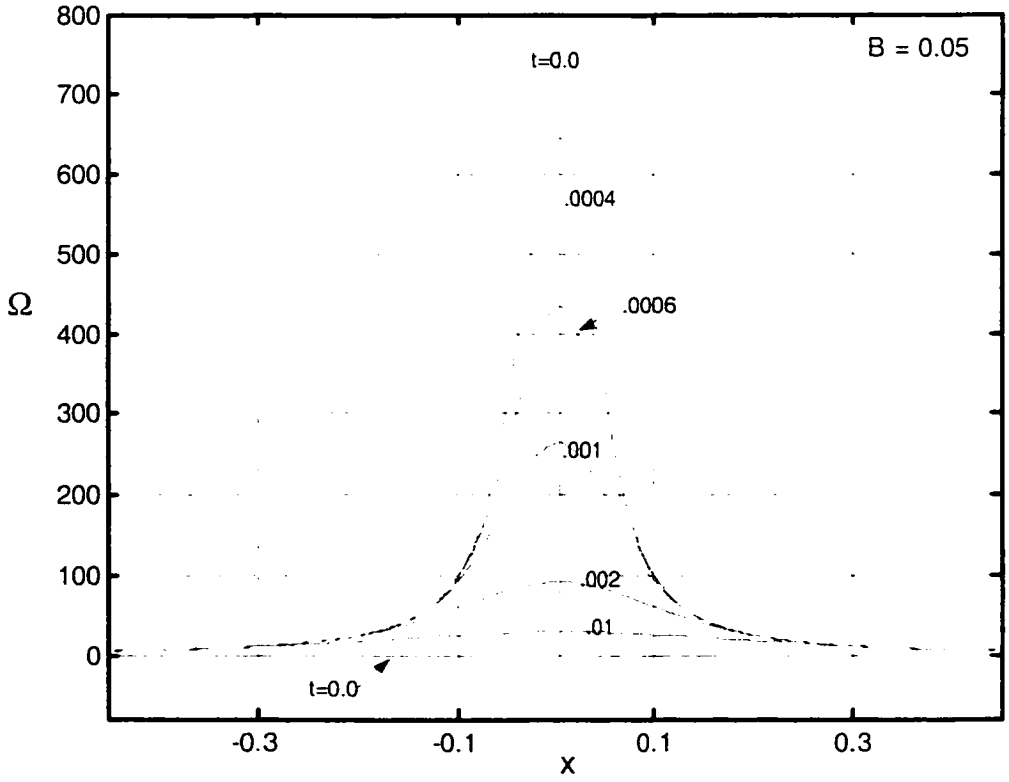

Fig. 3-4 Axial Vorticity decays, using potential model [Case of Slip]

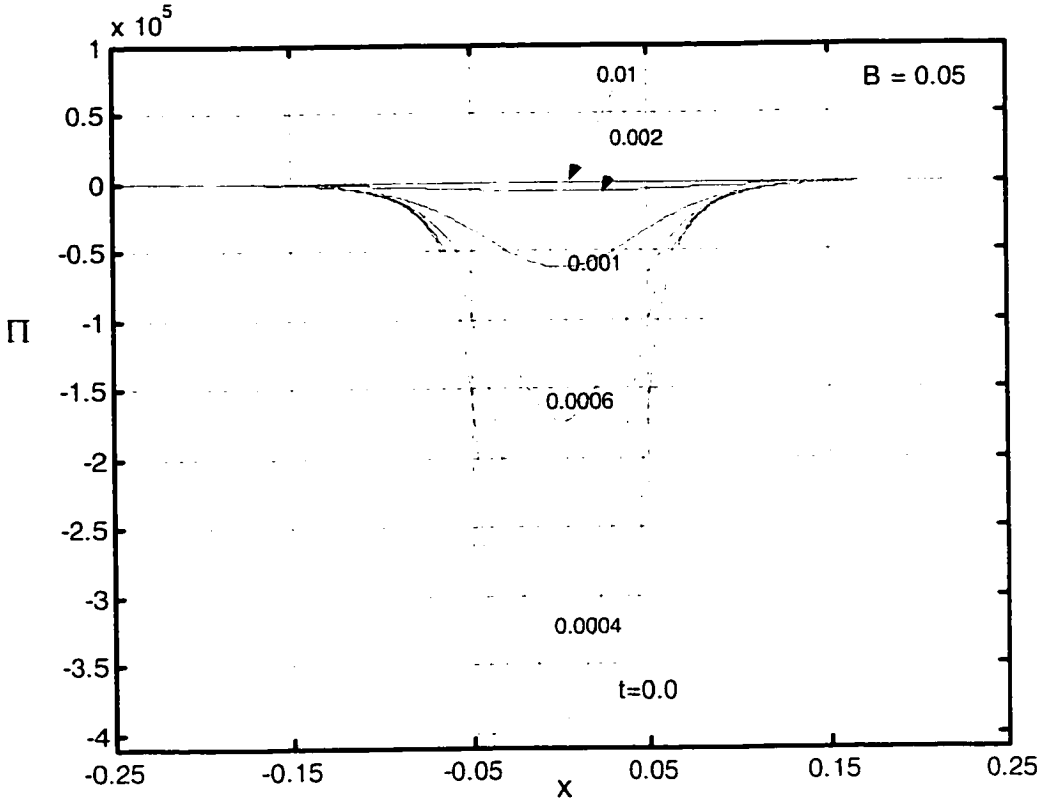

Fig. 3-5 Radial pressure decays, using potential model [Case of Slip]

3.4.2 Rankine's Vortex Decay [Slip]

Rankine's vortex model will now used as an initial velocity distribution. Similar analysis also applies, however the initial swirl velocity is now:

$$\bar{V}_\theta(\bar{t}=0,\bar{r}) = \begin{cases} \bar{r}\left[\dfrac{\beta^2-1}{\beta^2}\right] & 0 \le \bar{r} \le \beta \\ \bar{r} - \dfrac{1}{\bar{r}} & \beta < \bar{r} \le 1 \end{cases} \tag{3.35}$$

Where, $\beta = \dfrac{r_c}{R_o}, \bar{r} = \dfrac{r}{R_o}$

The coefficient A_n, can be derived in the same way as previously, [Appendix B detailed derivations].

$$A_n = \frac{-4J_1(\lambda_n\beta)}{\beta\lambda_n^2 J_o^2(\lambda_n)} \tag{3.36}$$

The tangential velocity distribution can be determined by inserting equation (3.36) into equation (3.27), yields:

$$\bar{V}_\theta(\bar{t},\bar{r}) = \bar{r} - \sum_n^\infty \frac{-4J_1(\lambda_n\beta)}{\beta\lambda_n^2 J_o^2(\lambda_n)} e^{-(\lambda_n)^2 \bar{t}} J_1(\lambda_n \bar{r}) \tag{3.37}$$

Similarly, the vorticity and static pressure are given respectively as,

$$\bar{\Omega}(r,t) = \begin{pmatrix} 2 - \dfrac{1}{\bar{r}}\displaystyle\sum_n^\infty \frac{-4J_1(\lambda_n\beta)}{\beta\lambda_n^2 J_o^2(\lambda_n)} e^{-(\lambda_n)^2 \bar{t}} J_1(\lambda_n \bar{r}) - \\ \dfrac{1}{2}\displaystyle\sum_n^\infty \frac{-4J_1(\lambda_n\beta)}{\beta\lambda_n^2 J_o^2(\lambda_n)} e^{-(\lambda_n)^2 \bar{t}} [J_o(\lambda_n \bar{r}) - J_2(\lambda_n \bar{r})] \end{pmatrix} \tag{3.38}$$

$$\Pi = \int_0^{\bar{r}} \frac{\left(\bar{r} - \sum_n^{\infty} \frac{-4J_1(\lambda_n\beta)}{\beta\lambda_n^2 J_o^2(\lambda_n)} e^{-(\lambda_n^2 \bar{t})} J_1(\lambda_n \bar{r})\right)^2}{\bar{r}} \Bigg/ \int_0^{1} \frac{\left(\bar{r} - \sum_n^{\infty} \frac{-4J_1(\lambda_n\beta)}{\beta\lambda_n^2 J_o^2(\lambda_n)} e^{-(\lambda_n^2 \bar{t})} J_1(\lambda_n \bar{r})\right)^2}{\bar{r}} \quad (3.39)$$

The tangential velocity, vorticity and pressure distributions are shown in figures [3.6], [3.7] and [3.8] respectively. Initially there is no singularity at the origin for this case. However the physical problem now has moved to the core where the derivative of the velocity is now singular. The latter will also violate the continuum assumption for times smaller than the mean free times. The results showed that, the early decay of the tangential velocity has value less than the one predicated by the potential model at the same time. However the late decay have almost the same values. One can notice that the static pressure has gradually decayed within radius equal to [0 –15%] of the vortex radius and it vanish fast after this radius. The Vorticity smoothly drops within radius equal to [0-30%] of the vortex outer radius and vanish beyond this value.

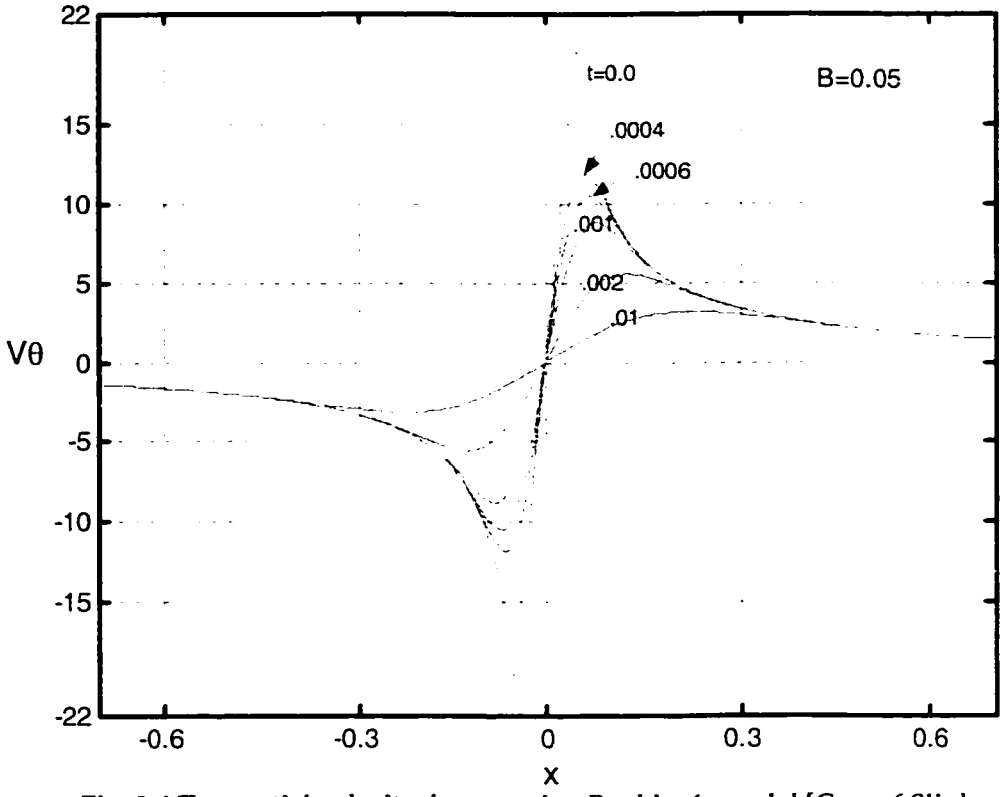

Fig. 3-6 Tangential velocity decays, using Rankine's model [Case of Slip]

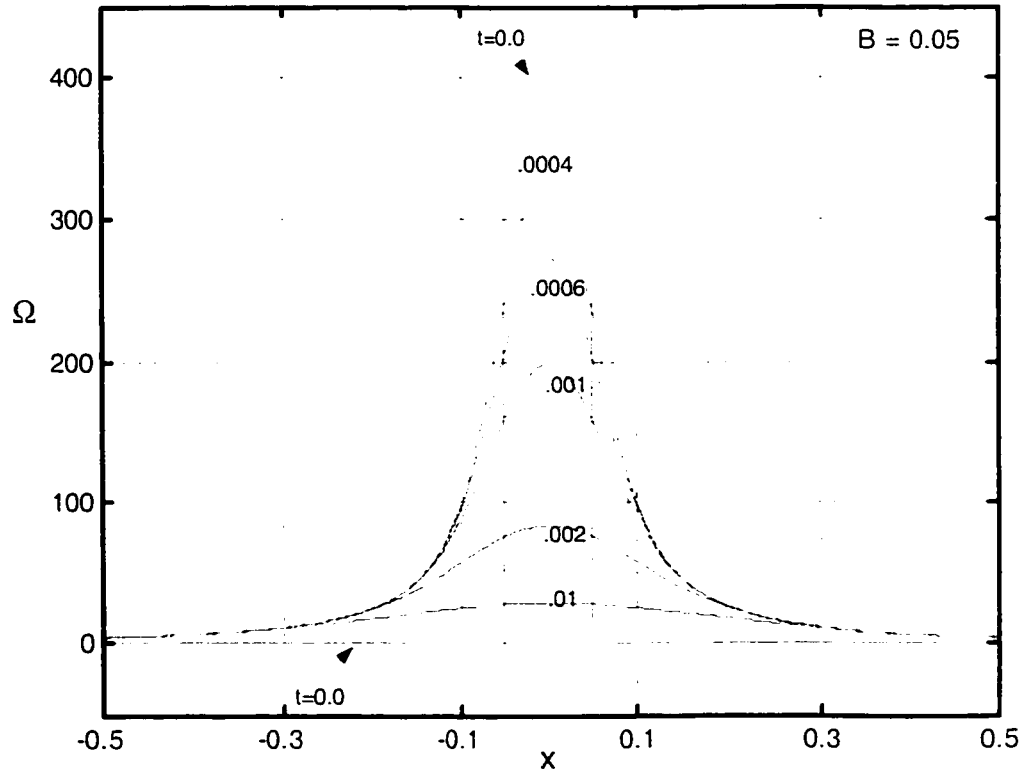

Fig. 3-7 Axial vorticity decays, using Rankine's model [Case of Slip]

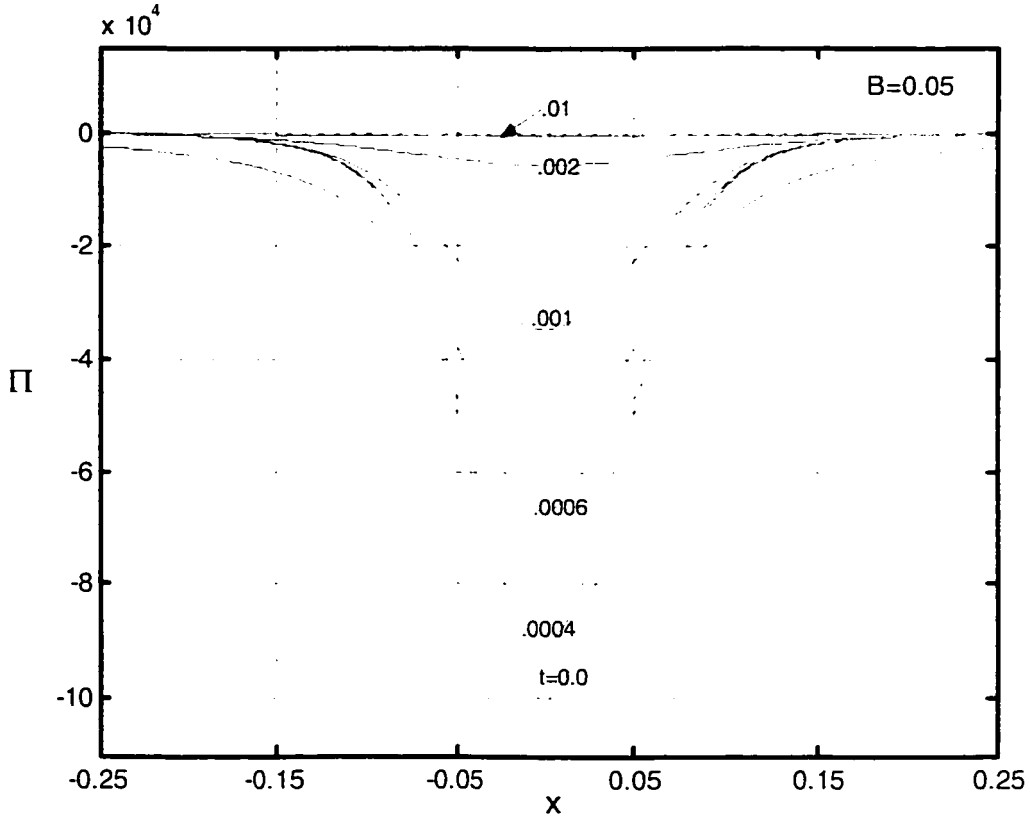

Fig. 3-8 Radial pressure decays, using Rankine's model [Case of Slip]

3.4.3 Vatistas's n=2 Vortex Decay [Slip]

In this section, we will employ Vatistas's vortex model as the initial velocity distribution,

$$\bar{V}_\theta(\bar{t}=0,\bar{r})=\frac{\bar{r}}{\left(\beta^{2n}+\bar{r}^{2n}\right)^{\frac{1}{n}}}.$$

Here, we will use another mathematical transformation. This transformation enables us to satisfy the boundary conditions. Therefore the tangential velocity is given by

$$\bar{V}_\theta(\bar{t}=0,\bar{r})=\frac{\bar{r}}{\left(\beta^{2n}+1\right)^{\frac{1}{n}}}-\bar{V}_\theta \tag{3.40}$$

Since the initial velocity satisfies the governing equations, so we can use the same procedure to find velocity decay in terms of Bessel function.

$$\bar{V}_\theta(\bar{t}=0,\bar{r})=\frac{1}{\left(\beta^{2n}+1\right)^{\frac{1}{n}}}\left(\bar{r}-\bar{r}\left(\frac{\beta^{2n}+1}{\beta^{2n}+\bar{r}^{2n}}\right)^{\frac{1}{n}}\right) \tag{3.41}$$

Where $\beta=\frac{r_c}{R_o}$ and let Vatistas's model exponent takes the value of $n=2$

Therefore, the coefficient A_n, is determined in the same manner as that outlined in Appendix B.

$$A_n=\frac{-2}{J^2{}_o(\lambda_n)}\left(\frac{1}{\lambda_n}\frac{J_0(\lambda_n)}{\left(\beta^4+1\right)^{\frac{1}{2}}}-H\right) \tag{3.42}$$

Where, $H = \left(\int_0^1 \left(\frac{\bar{r}^{-2}}{\beta^4 + \bar{r}^{-4}} \right)^{\frac{1}{2}} J_1(\lambda_n \bar{r}) d\bar{r} \right)$

The latter can be found by using the standard numerical integrations. Consequently, the tangential velocity is given by using equation (3.27) and substitute back into equation (3.42), yields:

$$\bar{V}_\theta(\bar{t}, \bar{r}) = \frac{\bar{r}}{(\beta^4 + 1)^{\frac{1}{2}}} - \sum_n \frac{-2}{J^2{}_o(\lambda_n)} \left(\frac{1}{\lambda_n} \frac{J_0(\lambda_n)}{(\beta^4 + 1)^{\frac{1}{2}}} - H \right) e^{-(\lambda_n^2 \bar{t})} J_1(\lambda_n \bar{r}) \tag{3.43}$$

The axial vorticity and the static pressure distributions are given by back substitution. $\bar{\Omega}(r, t) =$

$$\begin{pmatrix} \frac{2}{(\beta^4 + 1)^{\frac{1}{2}}} - \frac{1}{\bar{r}} \sum_n \frac{-2}{J^2{}_o(\lambda_n)} \left(\frac{1}{\lambda_n} \frac{J_0(\lambda_n)}{(\beta^4 + 1)^{\frac{1}{2}}} - H \right) e^{-(\lambda_n^2 \bar{t})} J_1(\lambda_n \bar{r}) \\ -\frac{1}{2} \sum_n \frac{-2}{J^2{}_o(\lambda_n)} \left(\frac{1}{\lambda_n} \frac{J_0(\lambda_n)}{(\beta^4 + 1)^{\frac{1}{2}}} - H \right) e^{-(\lambda_n^2 \bar{t})} [J_0(\lambda_n \bar{r}) - J_2(\lambda_n \bar{r})] \end{pmatrix} \tag{3.44}$$

$$\Pi = \frac{\int_0^{\bar{r}} \frac{\left(\frac{\bar{r}}{(\beta^4 + 1)^{\frac{1}{2}}} - \sum_n \frac{-2}{J^2{}_o(\lambda_n)} \left(\frac{1}{\lambda_n} \frac{J_0(\lambda_n)}{(\beta^4 + 1)^{\frac{1}{2}}} - H \right) e^{-(\lambda_n^2 \bar{t})} J_1(\lambda_n \bar{r}) \right)^2}{\bar{r}}}{\int_0^1 \frac{\left(\frac{\bar{r}}{(\beta^4 + 1)^{\frac{1}{2}}} - \sum_n \frac{-2}{J^2{}_o(\lambda_n)} \left(\frac{1}{\lambda_n} \frac{J_0(\lambda_n)}{(\beta^4 + 1)^{\frac{1}{2}}} - H \right) e^{-(\lambda_n^2 \bar{t})} J_1(\lambda_n \bar{r}) \right)^2}{\bar{r}}} \tag{3.45}$$

The tangential velocity, vorticity and pressure distributions are shown in figures [3.9], [3.10] and [3.11] respectively. This formulation has no mathematical shortcoming. Therefore, it must represent the physics of the problem better. The early decay of this model exhibit gradually velocity drop. The vorticity smoothly decrease within the 30% vortex radius and vanish beyond it. The pressure drops gradually within 15% core radius and maintain zero value along the rest of vortex radius.

The tangential velocity, axial vorticity and static pressure distributions on the basis of these vortex models are compared at the same time. The results are plotted in figure [3.12]. The first time represents the early decay phase, while the second choice indicates the late decay. The early decay shows that, the potential model and Rankine solution overestimates the swirl velocity. Unlike Vatistas's n=2 which predict smaller values. The late decay shows that the tangential velocity for each model almost has the same values. It also shows that the vorticity distributions for both potential and Rankine are asymptotically the same, while Vatistas's n=2 is not.

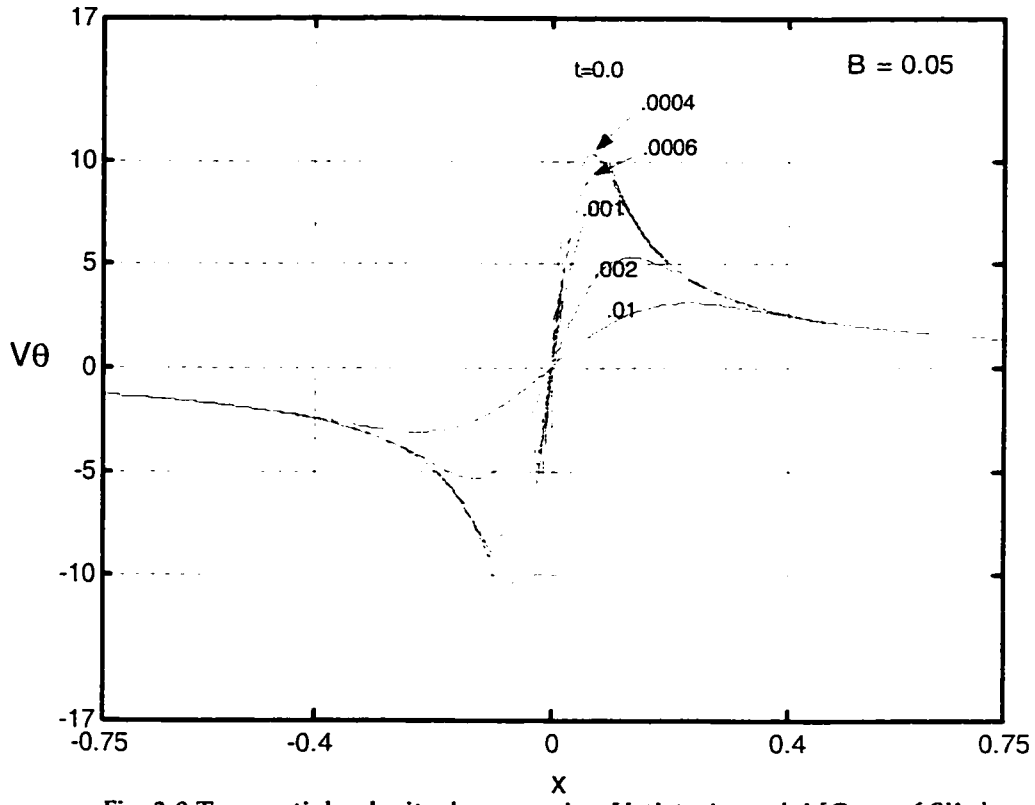

Fig. 3-9 Tangential velocity decays, using Vatistas's model [Case of Slip]

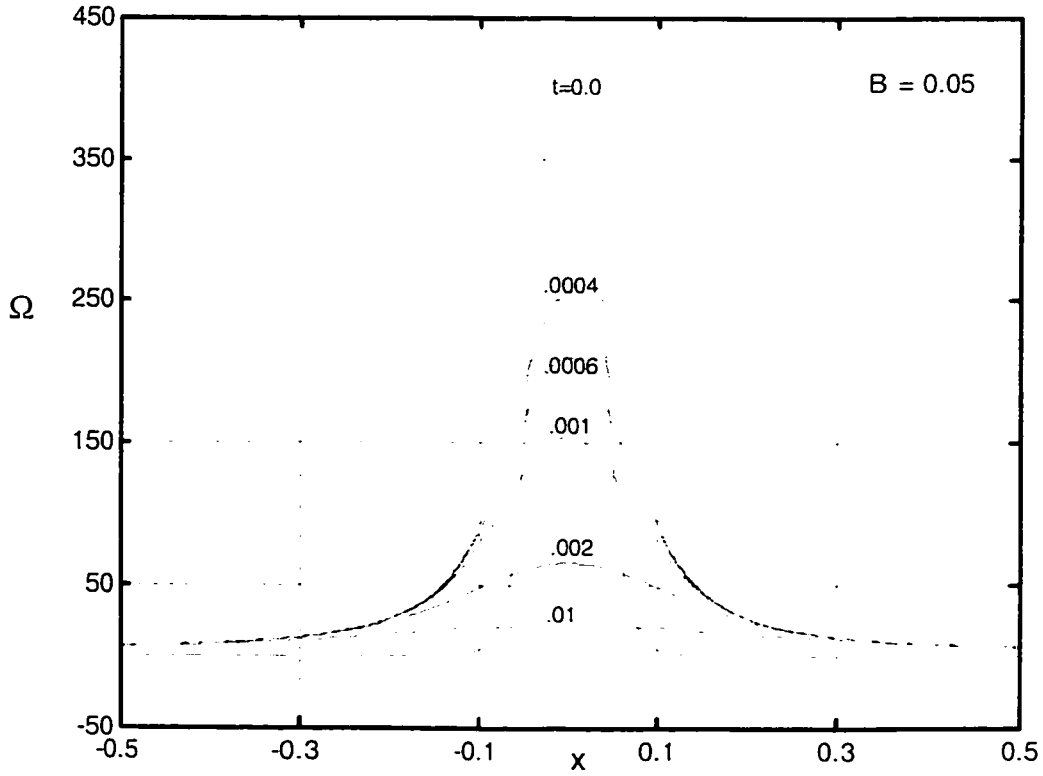

Fig. 3-10 Axial vorticity decays, using Vatistas's model [Case of Slip].

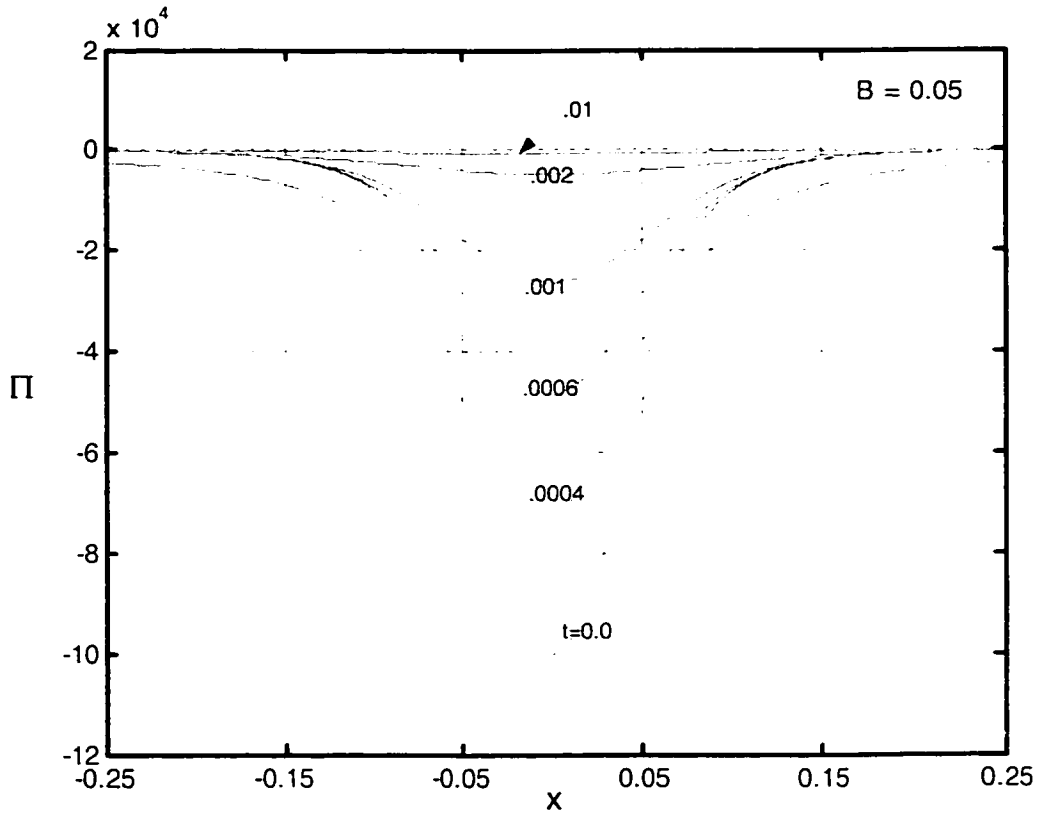

Fig. 3-11 Radial pressure decays, using Vatistas's model [Case of Slip].

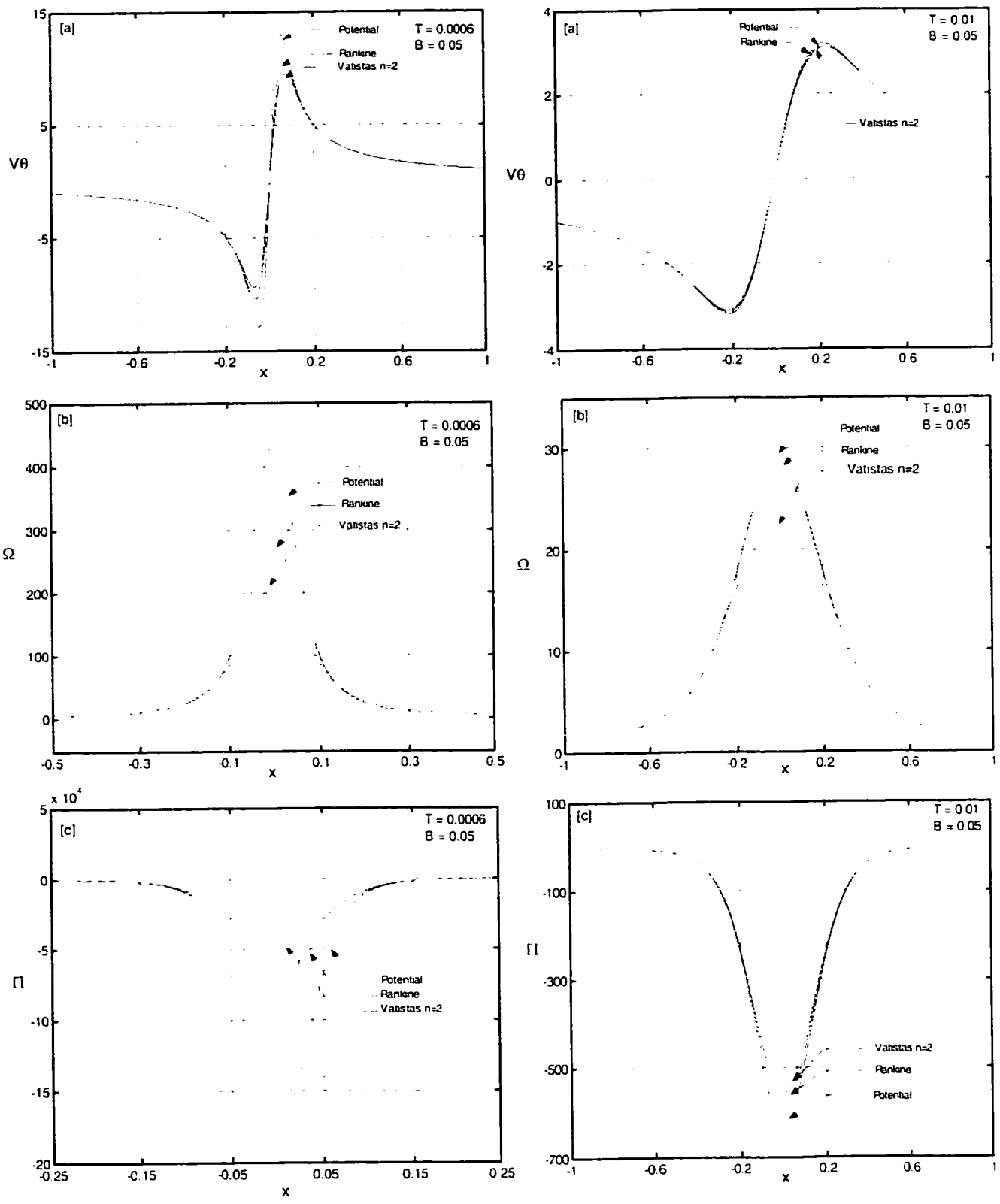

Fig. 3-12[a-c] Comparison between the velocity, vorticity and pressure distributions on the basis of different vortex model at t = 0.0006 and t = 0.01[Case of Slip].

3.5 Case study 2

No Slip of Tangential Velocity at The Outer Radius

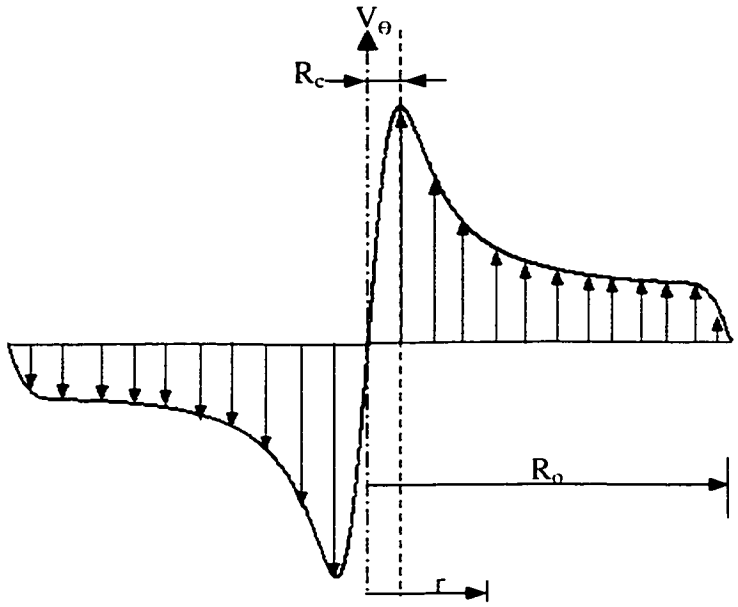

Fig. 3-13 Schematic illustrates the Non- slip velocity slip at the outer radius

In this case it is assumed that the vortex induced swirl velocity is not allowed to slip at the filament's outer cylinder, as shown in figure [3.13]. The solution can also be derived via the standard Bessel function. However, the new boundary conditions of the tangential velocity are:

1. For $\bar{t} \geq 0$, the tangential velocity is null at the vortex center i.e.

   $\bar{V}_\theta = 0$ at $\bar{r} = 0$

2. For $\bar{t} > 0$, the tangential velocity is null at the vortex outer radius i.e.

   $\bar{V}_\theta = 0$ at $\bar{r} = 1$

The same analysis similar to the previous one can be used here. One can realize that, in this case we don't have to do mathematical transformation. Therefore the Bessel constants can be easily determined, consequently the tangential velocity is

$$\bar{V}_\theta(\bar{t},\bar{r}) = \sum_n^{\infty} A_n e^{-[\lambda_n^2 \bar{t}]} J_1(\lambda_n \bar{r}) \tag{3.50}$$

Where in this case the coefficient A_n is defined as

$$A_n = \frac{\int_0^1 r\bar{V}_\theta(\bar{t}=0,\bar{r})J_1(\lambda_n\bar{r})d\bar{r}}{\int_0^1 rJ_1^2(\lambda_n\bar{r})d\bar{r}} = \frac{2}{J_o^2(\lambda_n)}\int_0^1 r\bar{V}_\theta(\bar{t}=0,\bar{r})J_1(\lambda_n\bar{r})d\bar{r} \tag{3.51}$$

$\bar{V}_\theta(\bar{t}=0.\bar{r})$ is the initial swirl velocity distribution

Once again, the axial vorticity and the static pressure distributions are given by:

$$\bar{\Omega}(r,t) = \frac{1}{r}\frac{\partial[\bar{r}\bar{V}_\theta]}{\partial\bar{r}}$$

$$= \frac{1}{r}\left(\bar{V}_\theta + \bar{r}\frac{\partial[\bar{V}_\theta]}{\partial\bar{r}}\right) = \frac{\bar{V}_\theta}{\bar{r}} + \frac{\partial[\bar{V}_\theta]}{\partial\bar{r}}$$

$$\frac{\partial J_n(\lambda_n\bar{r})}{\partial\bar{r}} = \frac{1}{2}[J_{n-1}(\lambda_n r) - J_{n+1}(\lambda_n r)]$$

$$\frac{\partial J_1(\lambda_1\bar{r})}{\partial\bar{r}} = \frac{1}{2}[J_o(\lambda_n r) - J_2(\lambda_n r)]$$

$$\bar{\Omega}(r,t) = \left(\frac{1}{r}\sum_n^{\infty} A_n e^{-[\lambda_n^2\bar{t}]}J_1(\lambda_n\bar{r}) + \frac{1}{2}\sum_n^{\infty} A_n e^{-[\lambda_n^2\bar{t}]}[J_o(\lambda_n\bar{r}) - J_2(\lambda_n\bar{r})]\right) \tag{3.52}$$

$$\frac{\partial\Pi}{\partial\bar{r}} = \frac{\bar{V}_\theta^2}{\bar{r}} = \frac{\left(\sum_n^{\infty} A_n e^{-[\lambda_n^2\bar{t}]}J_1(\lambda_n\bar{r})\right)^2}{\bar{r}}$$

$$\Pi = \frac{\int_0^{\bar{r}} \frac{\left(\sum_n^{\infty} A_n e^{-[\lambda_n^2 \bar{t}]} J_1(\lambda_n \bar{r})\right)^2}{\bar{r}}}{\int_0^1 \frac{\left(\sum_n^{\infty} A_n e^{-[\lambda_n^2 \bar{t}]} J_1(\lambda_n \bar{r})\right)^2}{\bar{r}}} \tag{3.53}$$

As can be seen from the above analysis, the tangential velocity expression depends on the summation coefficient A_n, which further depends on the initial velocity distribution. Here we will introduce the same three initial vortex swirl velocity models that have been used in case study 1.

Each vortex model is presented in separate section with separate analysis, however a distinct time comparisons are addressed in figure [3.23]. All the results are based on the assumption that the vortex outer radius is 20 times the inner radius.

3.5.1 The Potential Vortex Decay [No Slip]

The decay of the potential vortex model is presented in this section. We assume the potential model as an initial velocity for our model solution. Therefore,

$$\bar{V}_\theta(\bar{t}=0,\bar{r}) = \frac{1}{\bar{r}} \qquad 0 \le \bar{r} \le \infty \tag{3.55}$$

The coefficient A_n, is derived in detail in Appendix B and given by:

$$A_n = \frac{-2}{J_o^2(\lambda_n)}\left(J_o(\lambda_n)-1\right) \tag{3.55}$$

Also, the swirl velocity distribution can be written in the form of

$$\bar{V}_\theta(\bar{t},\bar{r}) = \sum_n^\infty \frac{-2}{\lambda_n J_o^2(\lambda_n)}\left(J_o(\lambda_n)-1\right)e^{-(\lambda_n^2\bar{t})}J_1(\lambda_n\bar{r}) \tag{3.56}$$

And the axial vorticity and static pressure distributions are given respectively as:

$$\bar{\Omega}(r,t) = \begin{pmatrix} \frac{1}{\bar{r}}\sum_n^\infty \frac{-2}{\lambda_n J_o^2(\lambda_n)}\left(J_o(\lambda_n)-1\right)e^{-(\lambda_n^2\bar{t})}J_1(\lambda_n\bar{r}) + \\ \frac{1}{2}\sum_n^\infty \frac{-2}{\lambda_n J_o^2(\lambda_n)}\left(J_o(\lambda_n)-1\right)e^{-(\lambda_n^2\bar{t})}\left[J_o(\lambda_n\bar{r})-J_2(\lambda_n\bar{r})\right] \end{pmatrix} \tag{3.57}$$

$$\Pi = \frac{\int_0^{\bar{r}} \frac{\left(\sum_n^\infty \frac{-2}{\lambda_n J_o^2(\lambda_n)}\left(J_o(\lambda_n)-1\right)e^{-(\lambda_n^2\bar{t})}J_1(\lambda_n\bar{r})\right)^2}{\bar{r}}}{\int_0^1 \frac{\left(\sum_n^\infty \frac{-2}{\lambda_n J_o^2(\lambda_n)}\left(J_o(\lambda_n)-1\right)e^{-(\lambda_n^2\bar{t})}J_1(\lambda_n\bar{r})\right)^2}{\bar{r}}} \tag{3.58}$$

Figures [3.14], [3.15] and [3.16], shows respectively the decay distributions of the tangential velocity, axial vorticity and static pressure. Obviously the analysis of the potential vortex in case of non-slip must be restricted to times greater than the mean free length as well.

The early decay of the potential model predicts higher values of the tangential velocity inside the core. While, the late decay has gradually dropped.

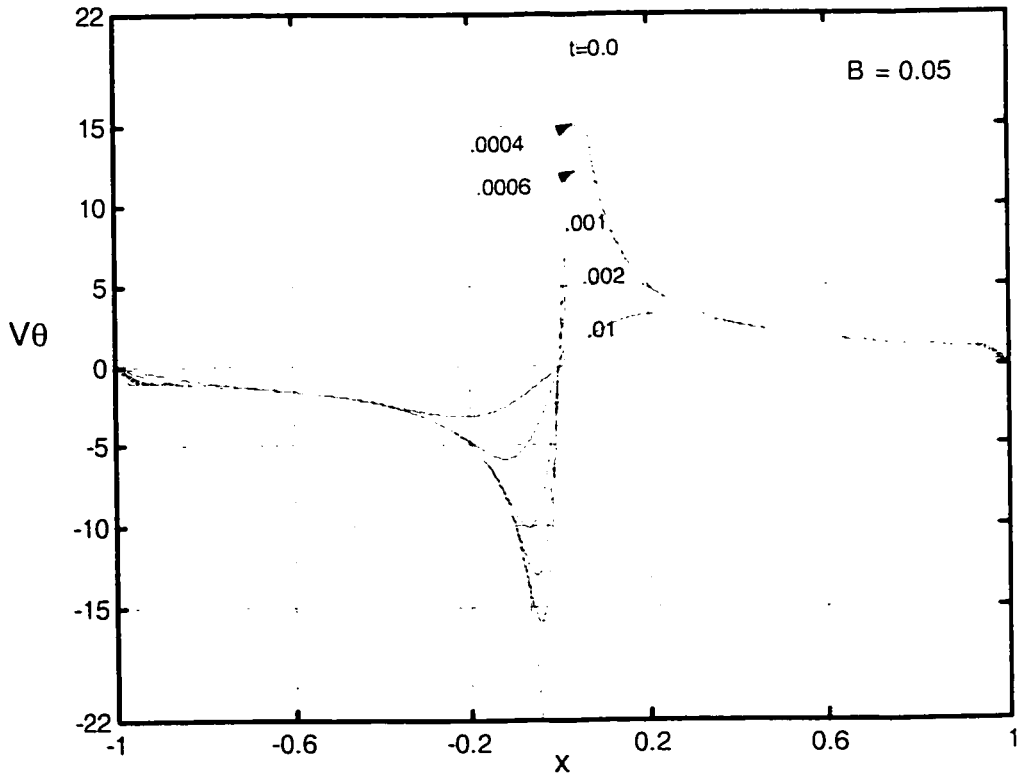

Fig. 3-14 Tangential velocity decays, using Potential model [Non-slip]

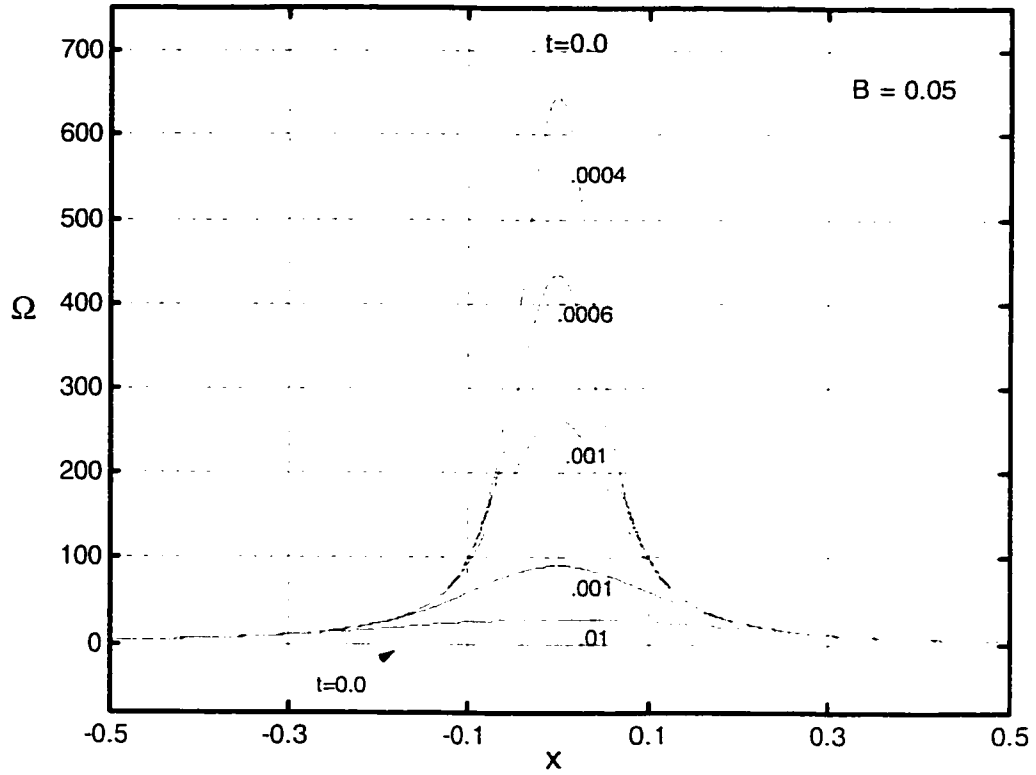

Fig. 3-15 Axial vorticity decays, using Potential model [Non-slip]

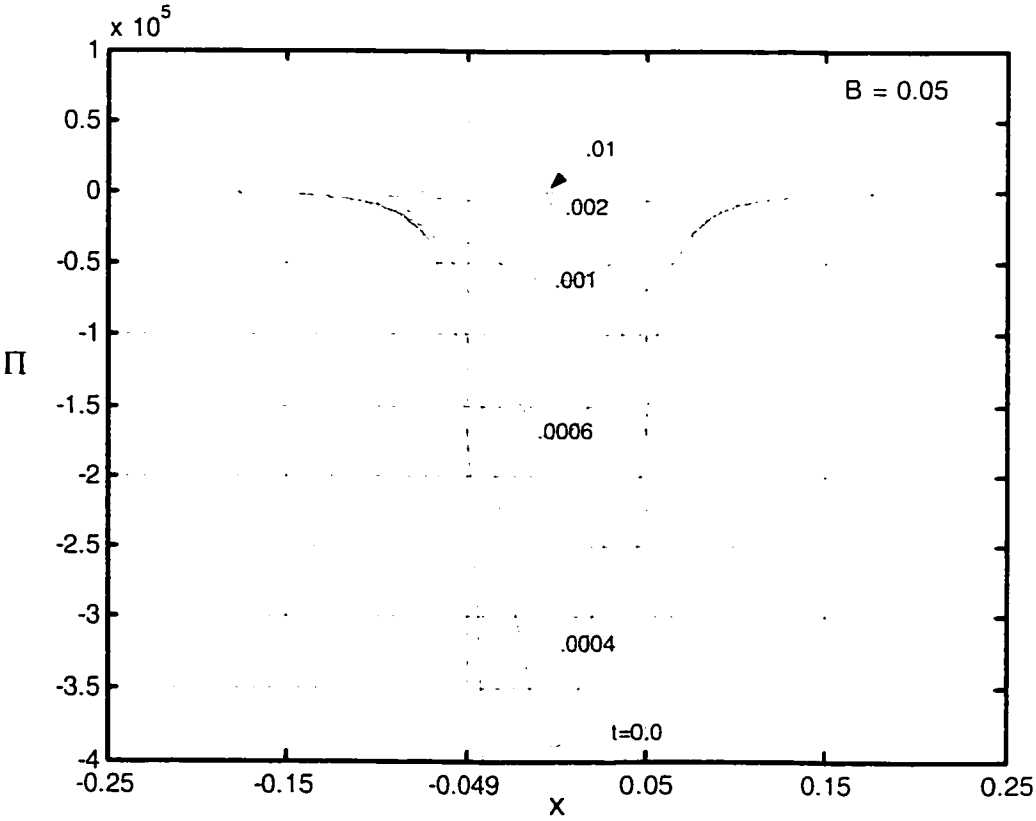

Fig. 3-16 Radial pressure decays, using Potential model [Non-slip]

3.5.2 Rankine's Vortex Decay [No Slip]

Rankine's vortex decay is presented in this section. Here we will use the Rankine's vortex model as an initial velocity distribution. Therefore,

$$\bar{V}_\theta(\bar{t}=0,\bar{r}) = \begin{cases} \dfrac{\bar{r}}{\beta^2} & 0 \le \bar{r} \le \beta \\ \dfrac{1}{\bar{r}} & \beta < \bar{r} \le 1 \end{cases} \tag{3.59}$$

The coefficient A_n is derived in detail. See Appendix B and is given by:

$$A_n = \frac{2}{\lambda_n J_o(\lambda_n)}\left(\frac{2J_1(\lambda_n\beta)}{\beta\lambda_n J_o(\lambda_n)} - 1\right) \tag{3.60}$$

The swirl velocity distribution is given by substituting equation (3.56) into equation (3.65). Therefore,

$$\bar{V}_\theta(\bar{t},\bar{r}) = \sum_n^\infty \frac{2}{\lambda_n J_o(\lambda_n)}\left(\frac{2J_1(\lambda_n\beta)}{\beta\lambda_n J_o(\lambda_n)} - 1\right) e^{-(\lambda_n^2)\bar{t}} J_1(\lambda_n\bar{r}) \tag{3.61}$$

The axial vorticity and static pressure distributions are given by:

$$\bar{\Omega}(r,t) = \begin{pmatrix} \dfrac{1}{\bar{r}}\displaystyle\sum_n^\infty \frac{2}{\lambda_n J_o(\lambda_n)}\left(\frac{2J_1(\lambda_n\beta)}{\beta\lambda_n J_o(\lambda_n)} - 1\right) e^{-(\lambda_n^2)\bar{t}} J_1(\lambda_n\bar{r}) \\ + \\ \dfrac{1}{2}\displaystyle\sum_n^\infty \frac{2}{\lambda_n J_o(\lambda_n)}\left(\frac{2J_1(\lambda_n\beta)}{\beta\lambda_n J_o(\lambda_n)} - 1\right) e^{-(\lambda_n^2)\bar{t}} [J_o(\lambda_n\bar{r}) - J_2(\lambda_n\bar{r})] \end{pmatrix} \tag{3.62}$$

$$\Pi = \int_0^{\bar{r}} \frac{\left(\displaystyle\sum_n^\infty \frac{2}{\lambda_n J_o(\lambda_n)}\left(\frac{2J_1(\lambda_n\beta)}{\beta\lambda_n J_o(\lambda_n)} - 1\right) e^{-(\lambda_n^2)\bar{t}} J_1(\lambda_n\bar{r})\right)^2 \partial\bar{r}}{\bar{r}} \Bigg/ \int_0^1 \frac{\left(\bar{V}_\theta(\bar{t},\bar{r})\right)^2}{\bar{r}} \partial\bar{r} \tag{3.63}$$

The tangential velocity, vorticity and pressure distributions are shown in figures [3.17], [3.18] and [3.19] respectively. Initially this formulation will also violate the continuum assumption for times smaller than the mean free times. The results showed that, the early decay of the tangential velocity has almost the same value as predicated by the potential model at the same time. However the late decay is different from the potential.

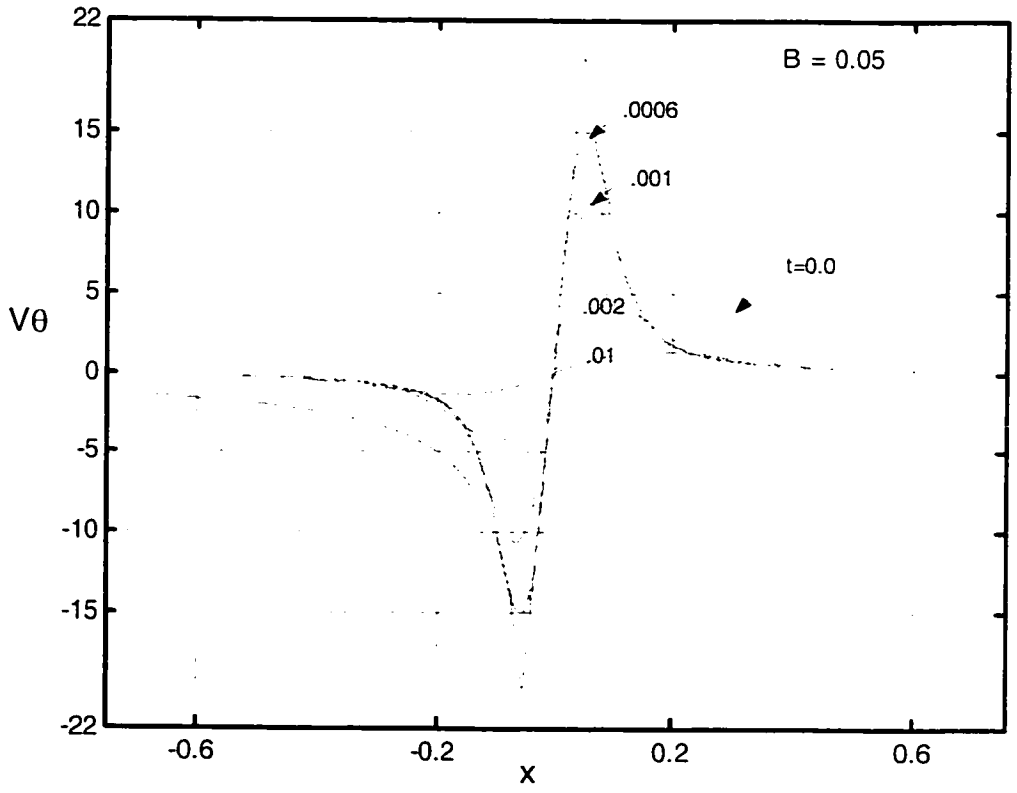

Fig. 3-17 Tangential velocity decays, using Rankine's model [Non-slip]

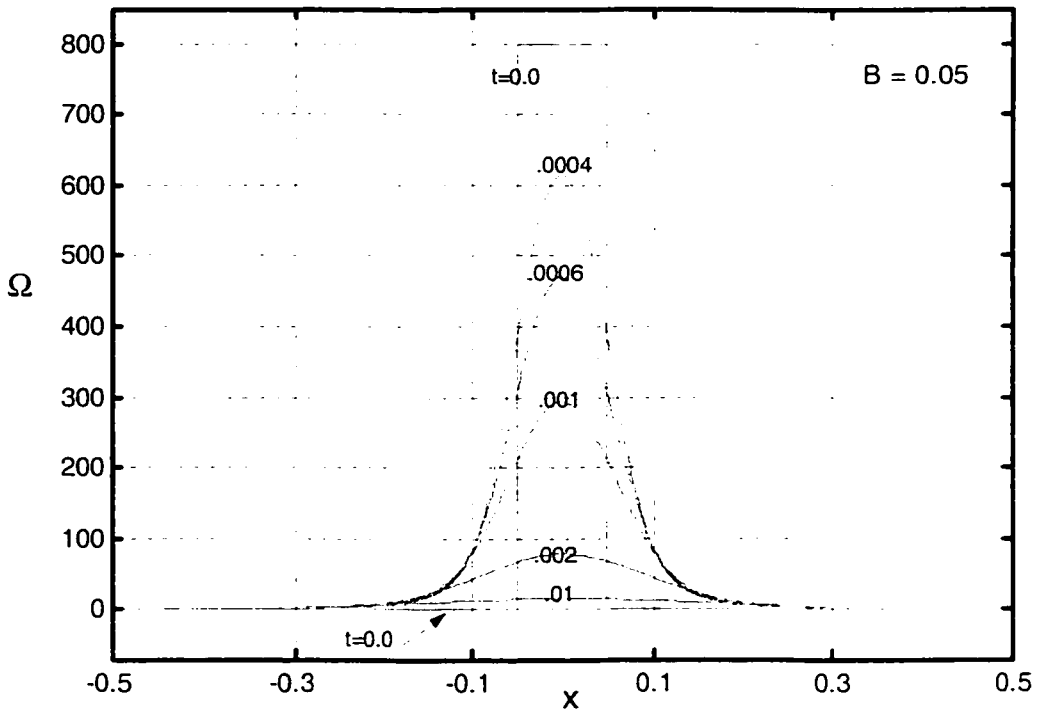

Fig. 3-18 Axial vorticity decays, using Rankine's model [Non-slip]

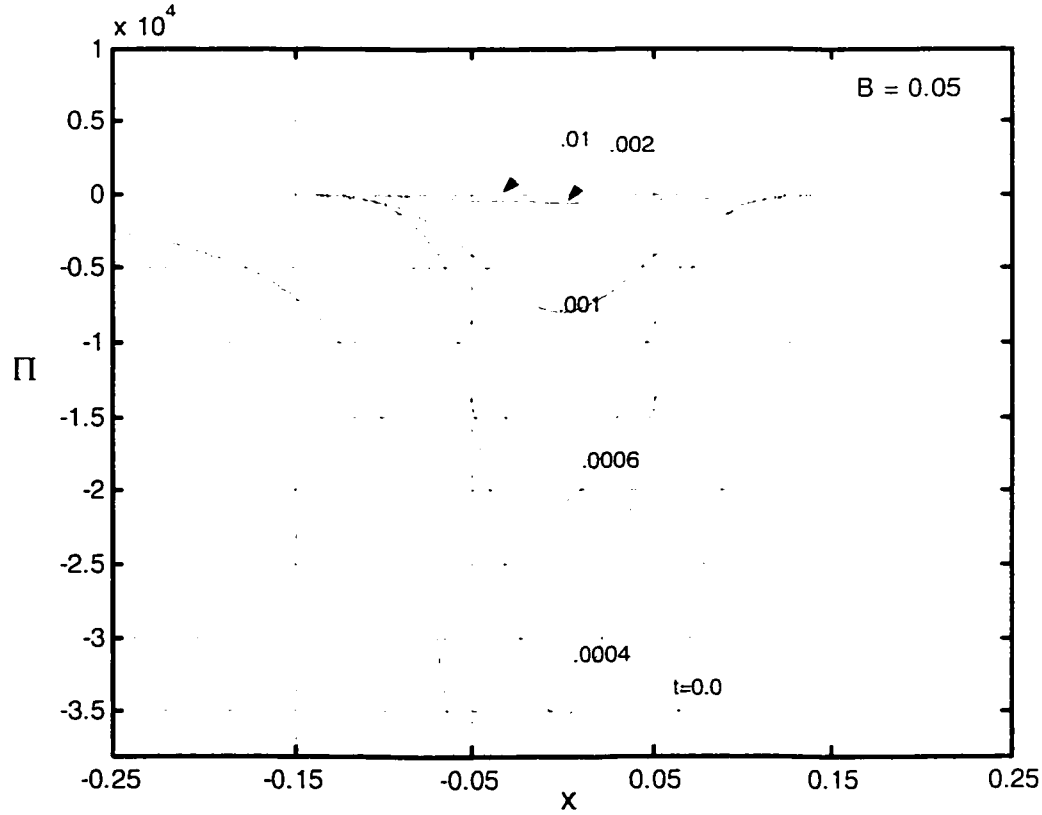

Fig. 3-19 Radial pressure decays, using Rankine's model [Non-slip]

3.5.3 Vatistas's n=2 Vortex Decay [No Slip]

The decay of Vatistas's vortex is examined as well. In this section we will use Vatistas's model at n=2 as an initial velocity distribution.

$$\text{Let, } \bar{V}_\theta(\bar{t}=0,\bar{r}) = \frac{\bar{r}}{\left(\beta^4 + \bar{r}^4\right)^{\frac{1}{2}}} \tag{3.64}$$

The coefficient A_n is derived in details based on Vatistas's initial velocity distribution, see Appendix B and it is given by:

$$A_n = \frac{2H}{J^2{}_o(\lambda_n)} \tag{3.65}$$

Where, $H = \int_0^1 \frac{\bar{r}^2}{\left(\beta^4 + \bar{r}^4\right)^{\frac{1}{2}}} J_1(\lambda_n \bar{r}) d\bar{r}$, Can be found using numerical integration

The tangential velocity is given by substituting back using equation (3.51) into equation (3.65). Therefore,

$$\therefore \bar{V}_\theta(\bar{t},\bar{r}) = \sum_n^\infty \left(\frac{2H}{J^2{}_o(\lambda_n)}\right) e^{-[\lambda_n^2 \bar{t}]} J_1(\lambda_n \bar{r}) \tag{3.66}$$

The axial vorticity and static pressure distributions are given respectively as:

$$\bar{\Omega}(r,t) = \begin{pmatrix} \frac{1}{\bar{r}} \sum_n^\infty \left(\frac{2H}{\lambda_n J_o(\lambda_n)}\right) e^{-[\lambda_n^2 \bar{t}]} J_1(\lambda_n \bar{r}) \\ -\frac{1}{2} \sum_n^\infty \left(\frac{2H}{J^2{}_o(\lambda_n)}\right) e^{-[\lambda_n^2 \bar{t}]} [J_o(\lambda_n \bar{r}) - J_2(\lambda_n \bar{r})] \end{pmatrix} \tag{3.67}$$

$$\Pi = \int_0^{\bar{r}} \frac{\left(\sum_n^\infty \left(\frac{2H}{J^2{}_o(\lambda_n)}\right) e^{-[\lambda_n^2 \bar{t}]} J_1(\lambda_n \bar{r})\right)^2 \partial \bar{r}}{\bar{r}} \Bigg/ \int_0^1 \frac{\left(\bar{V}_\theta(\bar{t},\bar{r})\right)^2}{\bar{r}} \partial \bar{r} \tag{3.68}$$

The tangential velocity, vorticity and pressure distributions are shown in figures [3.20], [3.20] and [3.22] respectively. The early decay of this model shows a moderate velocity distribution. At t=0.0004 there is a 50% velocity difference compared with Rankine or Potential results. While the vorticity value smoothly decrease and shows 75% difference than Rankine results. The late decay shows that the parameters are consistence with both Rankine and potential models.

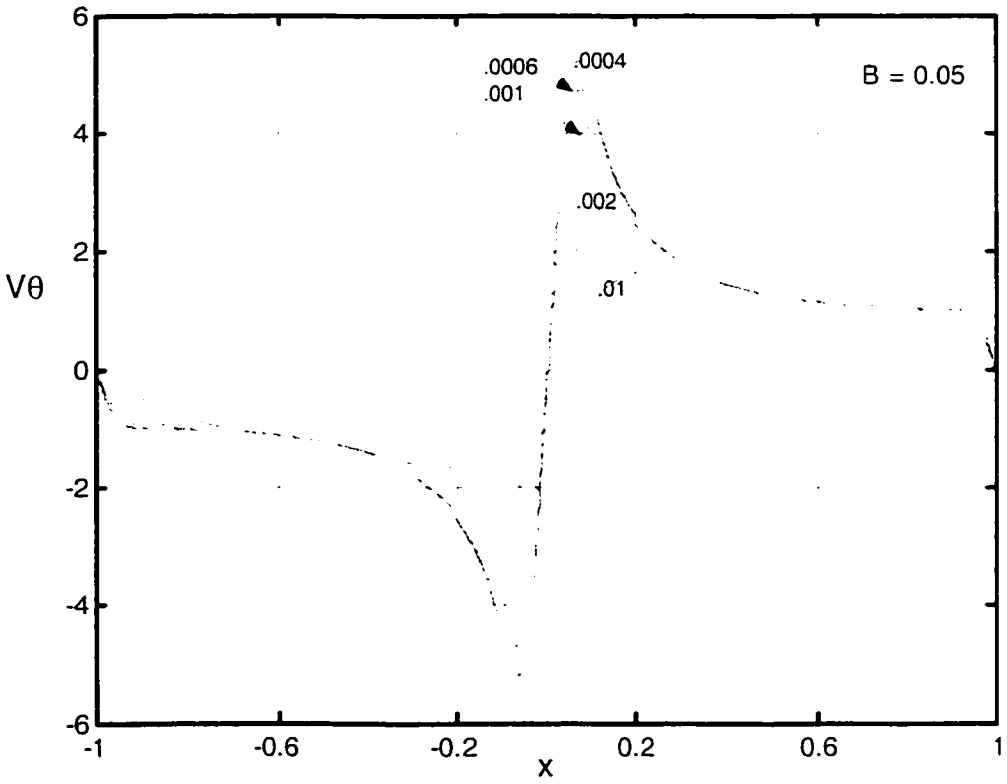

Fig. 3-20 Tangential velocity decays, using Vatistas's model [Non-slip]

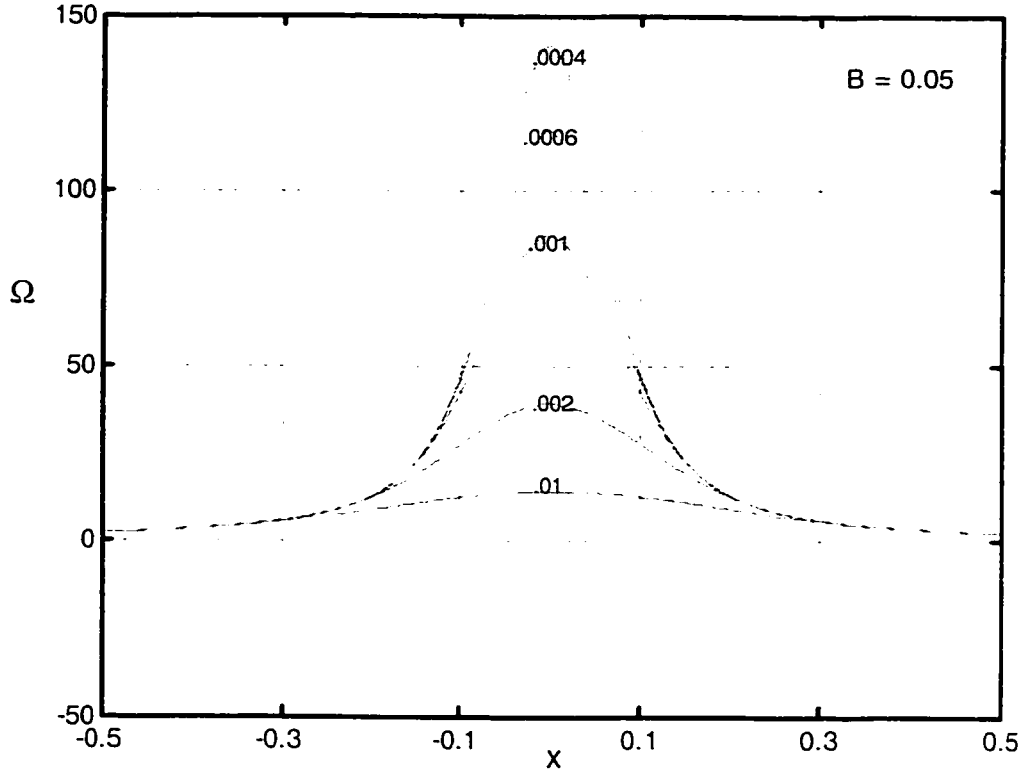

Fig. 3-21 Axial vorticity decays, using Vatistas's model [Non-slip]

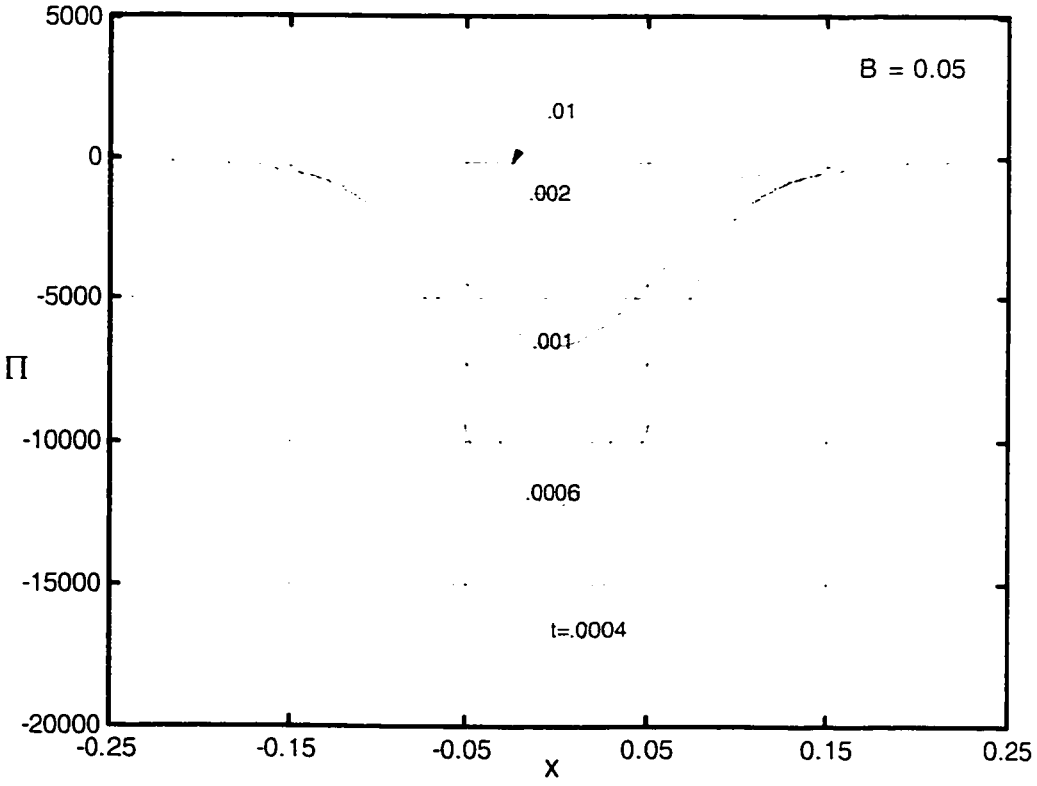

Fig. 3-22 Radial pressure decays, using Vatistas's model [Non-slip]

The tangential velocity, axial vorticity and static pressure distributions on the basis of these vortex models are compared at the same time. The results are plotted in figure [3.23]. It is quite interesting to notice that, during the early decay phases both potential and Rankine overestimates the velocity and the vorticity. While the pressure distributions for both Rankine and Vatistas are closer. Potential model exhibit larger pressure values of both early and late times. The late decay showed that, the velocity distribution for each model is not closes. The late phase also indicated that, the vorticity and the pressure of Rankine and Vatistas have almost the same values.

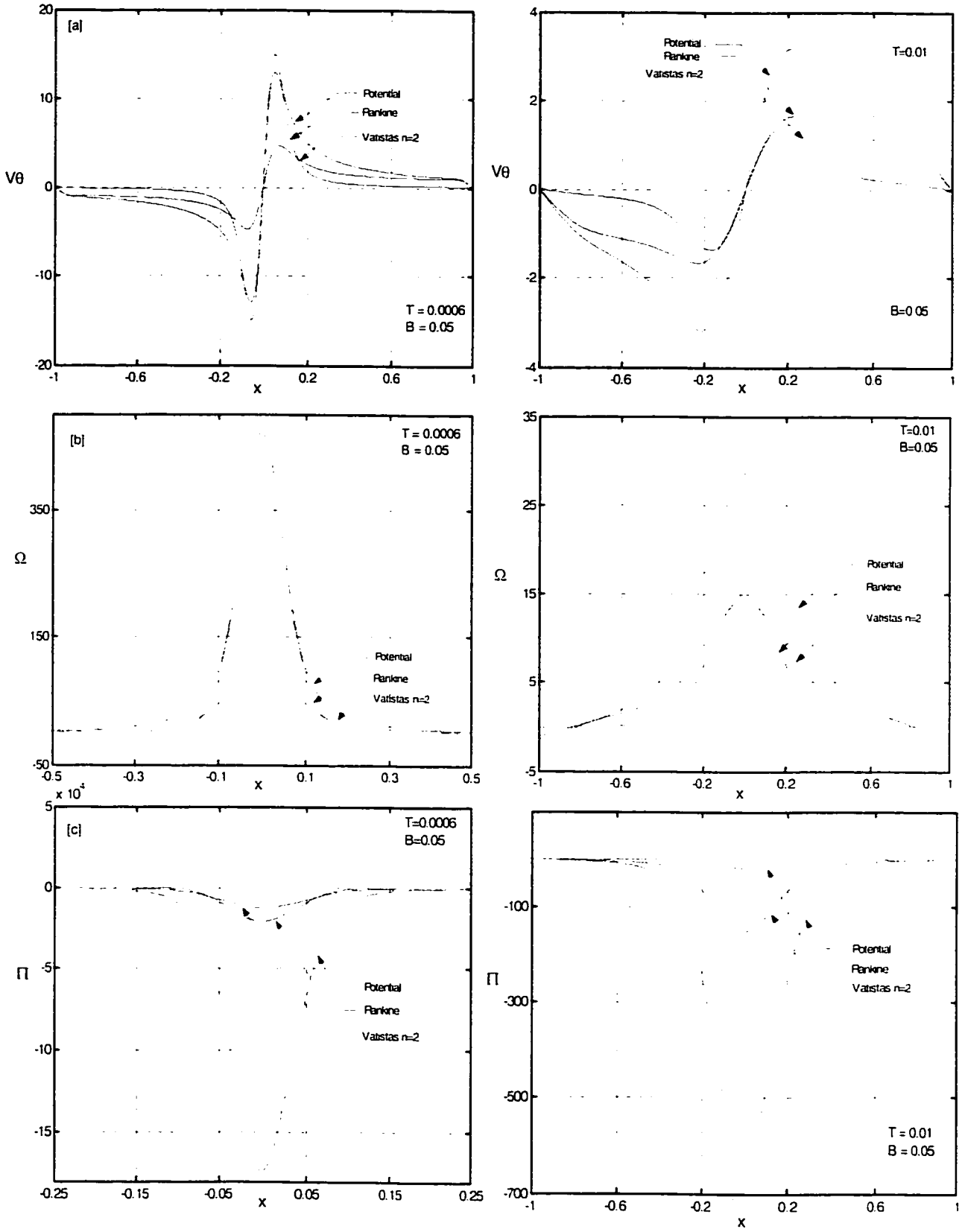

Fig. 3-23[a-c] Comparison between the velocity, vorticity and pressure distributions on the basis of different vortex model at t = 0.0006 and t = 0.01[Case of Non-slip].

Chapter 4

Decay of Unconfined Line Vortices

4.1 Overview

The decay of unconfined vortices, such as those generated in the wake of high lift aircrafts for both fixed and rotating wings is complicated. This difficulty is due to the complexity of the mathematical models, which govern the decay process in both turbulence and quiescent atmospheric conditions. The early development of the sheet vortices is not affected by atmospherics turbulence [7]. However, the sheet vortex decay process is affected by whether the neighboring atmospheric field is quiescent or turbulent.

One of the techniques used recently to investigate the decay process, is via the Large Eddy Simulation [LES] method [11], which must be initiated by appropriate measurements data collected from different aircrafts at different atmospheric conditions. This method provides appropriate results for both quiescent and weak turbulent conditions, but it gives poor results in case of strong turbulence atmospheric conditions. The vortex decay in a quiescent neighboring field is influenced by the interaction of short wave disturbances induced by aircraft and vorticity field. Conversely, if the neighboring field is turbulent enough the decay

process is controlled by large wave instability. Vortex decay is an essential aspect in the issue of the wake dissipation. However, a simplified mathematical analysis as the present can set a light into the basic mechanisms involved in this phenomenon.

4.2 Problem Formulation

The time dependent solution of unconfined line vortices will be solved based on the same assumptions that have been made in chapter 3. Consider the vortex filament to be an isolated and intense vortex as shown in figure [4.1]. The simulation of unconfined vortex is achieved by letting the vortex filament's outer radius extends to a very large value.

To be able to tackle the unconfined vortex, the value of β which describes how far the outer radius should extend in relative to the core radius is required. The decay solution of the potential model based on this theory and Oseen Hamel vortex are compared. The error between both solutions is examined for the value of β=0.01.

Hence, in this chapter we are going to present a simplified analytical solution, using the same approach. It will consider the decay of the same steady vortex models used to find the confined vortices solution. However in this case different boundary conditions are needed.

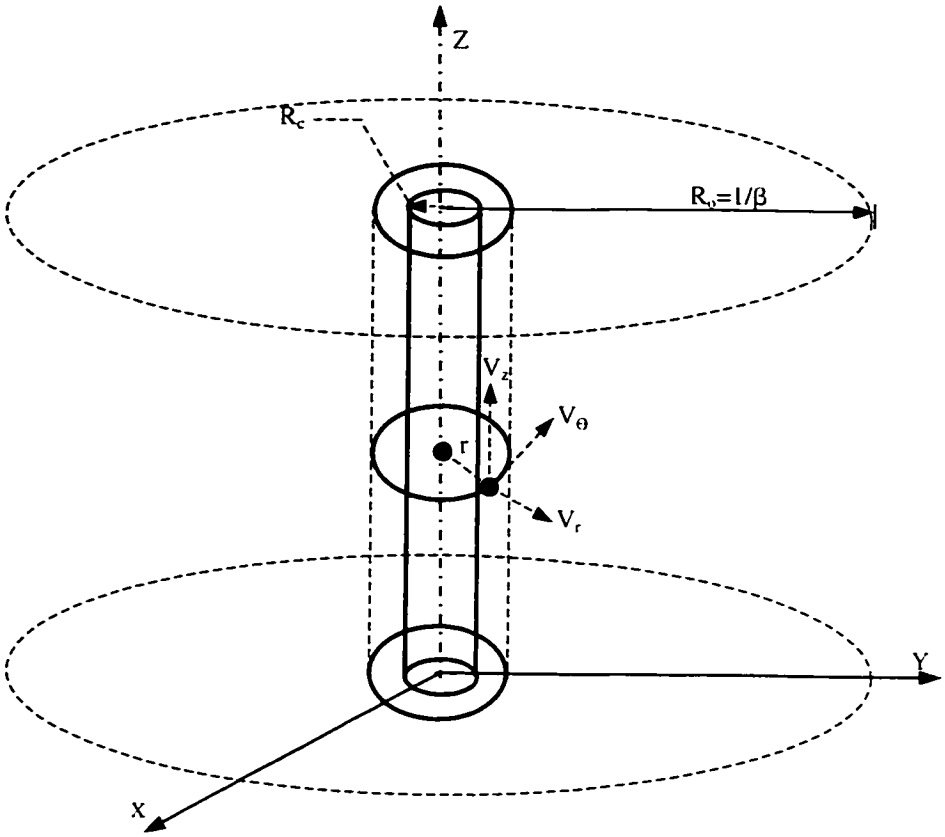

Fig. 4-1 Schematic illustrates the Unconfined Line Vortex

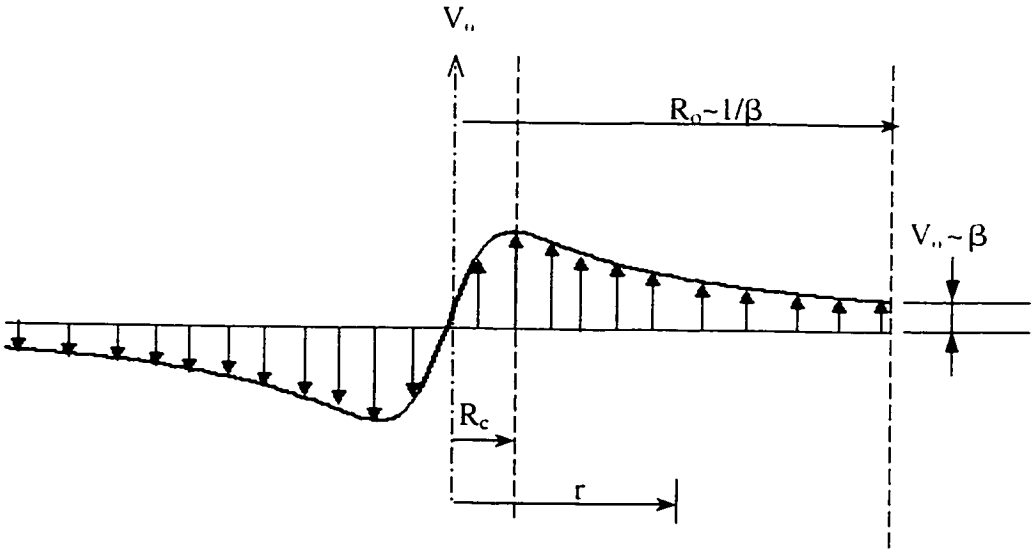

Fig. 4-2 Schematic shows the velocity distribution in case of unconfined vortex

We will also predict the vortex maximum core radius growth, maximum induced swirl velocity, maximum pressure and maximum vorticity distributions as a function of time.

A distinct mathematical normalization based on the parameters at the maximum core radius is also addressed. The later shows that it is possible to collapse the velocity time distributions into one single curve, which also exhibits a self-similarity distribution.

Since the outer filament's diameter will extend to a larger value, it is recommended to use the core radius as a reference scale. Based on the governing equations of swirling fluid motion i.e. those presented in chapter 2 and the set of assumptions given in chapter 3, we can normalize the governing equations using the parameters at the core radius, see figure [4.2]. Therefore the dimensionless set of equation are given by:

$$\frac{\partial[\bar{V}_\theta]}{\partial \bar{t}} = [\frac{\partial^2 \bar{V}_\theta}{\partial \bar{r}^2} + \frac{1}{\bar{r}}\frac{\partial \bar{V}_\theta}{\partial \bar{r}} - \frac{\bar{V}_\theta}{\bar{r}^2}] \tag{4.1}$$

$$\frac{\partial \Pi}{\partial \bar{r}} = \frac{\bar{V}_\theta^2}{\bar{r}} \tag{4.2}$$

$$\bar{\Omega}(\bar{r},\bar{t}) = \frac{1}{\bar{r}}\frac{\partial[\bar{r}\bar{V}_\theta]}{\partial \bar{r}}\bar{e}_z \tag{4.3}$$

Where, $\bar{r} = \frac{r}{R_c}, \bar{V}_\theta = \frac{V_\theta}{V_{\theta c}}, \beta = \frac{R_c}{R_o}$ & $\bar{t} = \frac{t\upsilon}{R_c^2}$

This set of equations describes how is tangential velocity; axial vorticity and radial static pressure can vary along the vortex radial direction at different time levels. Since the static pressure and the axial vorticity distributions depend on the tangential velocity, therefore, we have to start solving the radial momentum equation first. We can apply directly the solution derived via Bessel function based on the separation of variables used to solve the case of confined vortices. However, according to the unconfined natural boundary conditions the solution will be slightly different

Refer to the unconfined line vortex presented in figure [4.2], provided that the vortex induced swirl velocity must satisfies the unconfined boundary conditions. Which implies that, the swirl velocity is null at the vortex center i.e. at $\bar{r}=0$ therefore, $\bar{V}_\theta=0$ and it tends to zero as the vortex outer radius tends to infinity i.e. at $\bar{r}=\infty$, therefore $\bar{r}\bar{V}_\theta=1$. Theoretically we can't let $\bar{r}$ tends to infinity, however it is possible to assume that can reach maximum possible value which is, $\frac{1}{\beta}$. Consequently $\bar{V}_\theta$ will tends to a minimum value, which is β.

Since the general solution of swirl velocity is given by:

$$\bar{V}_\theta(\bar{t},\bar{r}) = A_n e^{-[m^2\bar{t}]} J_1(m\bar{r})$$

Where, A_n and m are constants. Determination of the constants requires applying the set of boundary conditions that were outlined. The first boundary condition is automatically satisfied, while the second boundary conditions leads to a complicated equation.

$$\beta = A_n e^{-(m^2 \bar{t})} J_1(\frac{m}{\beta}) \tag{4.4}$$

This equation cannot be solved explicitly to find the constants. Therefore, a mathematical transformation is required in order to make the boundary conditions homogeneous. This transformation is given by:

$$\bar{V}_\theta(\bar{t}, \bar{r}) = \beta^2 \bar{r} - \bar{V}_\theta(\bar{t}, \bar{r}) \tag{4.5}$$

One can prove that, the transformed velocity satisfies the momentum governing equations. Therefore the solution will be similar to the previous solution derived in chapter 3. However the detailed analysis is listed in Appendix B. The original boundary conditions are then given by:

For $\bar{t} \geq 0$

1. As $\bar{r} = 0$, yields $\bar{V}_\theta = 0$ consequently $\tilde{V}_\theta = 0$

2. As $\bar{r} = \frac{1}{\beta}$, yields $\bar{V}_\theta = \beta$ consequently $\tilde{V}_\theta = 0$

The solution of the transformed swirl velocity is then given as,

$$\tilde{V}_\theta(\bar{t}, \bar{r}) = \sum_{n=1}^{\infty} A_n e^{-(\beta^2 \lambda_n^2 \bar{t})} J_1(\beta \lambda_n \bar{r}) \tag{4.6}$$

Where,

$$A_n = \frac{2\beta^2}{J_n^2(\lambda_n)} \int_0^{1/\beta} r \tilde{V}_\theta(\bar{t} = 0, \bar{r}) J_1(\beta \lambda_n \bar{r}) d\bar{r} \tag{4.7}$$

Since we are looking for the unconfined solution based on the swirl velocity, therefore reverse substantiation should be made by using equation (4.6) and (4.5). That will give the analytical time-radial vortex induced velocity distribution.

$$\bar{V}_\theta(\bar{t},\bar{r}) = \beta^2\bar{r} - \sum_{n=1}^{\infty} A_n e^{-(\beta^2\lambda_n^2\bar{t})} J_1(\beta\lambda_n\bar{r}) \tag{4.8}$$

Consequently, the distributions for both vorticity and pressure are given respectively,

$$\bar{\Omega}(r,t) = \left(2\beta^2 - \frac{1}{\bar{r}}\sum_{n=1}^{\infty} A_n e^{-(\beta^2\lambda_n^2\bar{t})} J_1(\beta\lambda_n\bar{r}) - \frac{1}{2}\sum_{n=1}^{\infty} A_n e^{-(\beta^2\lambda_n^2\bar{t})} [J_n(\beta\lambda_n\bar{r}) - J_2(\beta\lambda_n\bar{r})] \right) \tag{4.9}$$

$$\Pi = \int_0^{\bar{r}} \frac{\left(\beta^2\bar{r} - \sum_{n=1}^{\infty} A_n e^{-(\lambda_n^2\bar{t})} J_1(\lambda_n\bar{r}) \right)^2}{\bar{r}} \Bigg/ \int_0^{1} \frac{\left(\beta^2\bar{r} - \sum_{n=1}^{\infty} A_n e^{-(\lambda_n^2\bar{t})} J_1(\lambda_n\bar{r}) \right)^2}{\bar{r}} \tag{4.10}$$

This solution is examined for the same three initial velocity distribution. However each vortex model is presented in a separate section. A distinct comparison between the three models at the early [t=0.1] and late [t=5.0] decay is addressed.

4.3 Decay of The Potential Vortex

In this section, we will examine the potential vortex model as an initial velocity distribution. Since the induced swirl velocity is expressed as:

$$\bar{V}_\theta(\bar{t}=0,\bar{r}) = \frac{1}{\bar{r}} \qquad 0 < \bar{r} \le \infty$$

Based on the transformation, the velocity will take the form:

$$\bar{V}_\theta(\bar{t},\bar{r}) = \beta^2 \bar{r} - \bar{V}_\theta(\bar{t}=0,\bar{r}) = \beta^2 \bar{r} - \frac{1}{\bar{r}} \tag{4.11}$$

The coefficient A_n, see Appendix B is given by:

$$A_n = \frac{-2\beta}{\lambda_n J_o^2(\lambda_n)} \tag{4.12}$$

The swirl velocity, axial vorticity and static pressure distributions are given as:

$$\bar{V}_\theta(\bar{t},\bar{r}) = \beta^2 \bar{r} - \sum_{n=1}^{\infty} \frac{-2\beta}{\lambda_n J_o^2(\lambda_n)} e^{-(\beta^2 \lambda_n^2 \bar{t})} J_1(\beta\lambda_n \bar{r}) \tag{4.13}$$

$$\bar{\Omega}(r,t) = \begin{pmatrix} 2\beta^2 - \frac{1}{\bar{r}} \sum_{n=1}^{\infty} \frac{-2\beta}{\lambda_n J_o^2(\lambda_n)} e^{-(\beta^2 \lambda_n^2 \bar{t})} J_1(\beta\lambda_n \bar{r}) - \\ \frac{1}{2} \sum_{n=1}^{\infty} \frac{-2\beta}{\lambda_n J_o^2(\lambda_n)} e^{-(\beta^2 \lambda_n^2 \bar{t})} [J_o(\beta\lambda_n \bar{r}) - J_2(\beta\lambda_n \bar{r})] \end{pmatrix} \tag{4.14}$$

$$\Pi = \frac{\int_0^{\bar{r}} \left(\beta^2 \bar{r} - \sum_{n=1}^{\infty} \frac{-2\beta}{\lambda_n J_o^2(\lambda_n)} e^{-(\beta^2 \lambda_n^2 \bar{t})} J_1(\beta\lambda_n \bar{r}) \right)^2 \partial \bar{r} \,/\, \bar{r}}{\int_0^{1} \left(\beta^2 \bar{r} - \sum_{n=1}^{\infty} \frac{-2\beta}{\lambda_n J_o^2(\lambda_n)} e^{-(\beta^2 \lambda_n^2 \bar{t})} J_1(\beta\lambda_n \bar{r}) \right)^2 \partial \bar{r} \,/\, \bar{r}} \tag{4.15}$$

The tangential velocity, axial vorticity and static pressure distributions are shown respectively in figures [4.3], [4.4] and [4.5].

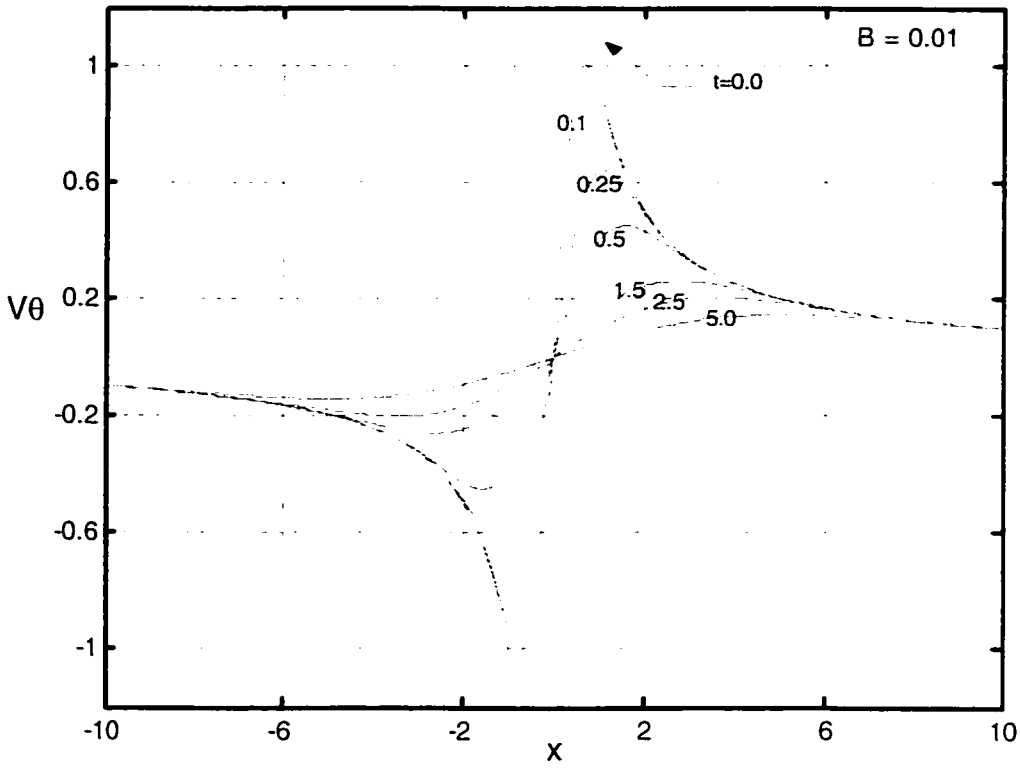

Fig. 4-3 Tangential velocity decays, using potential model. [Unconfined Vortex]

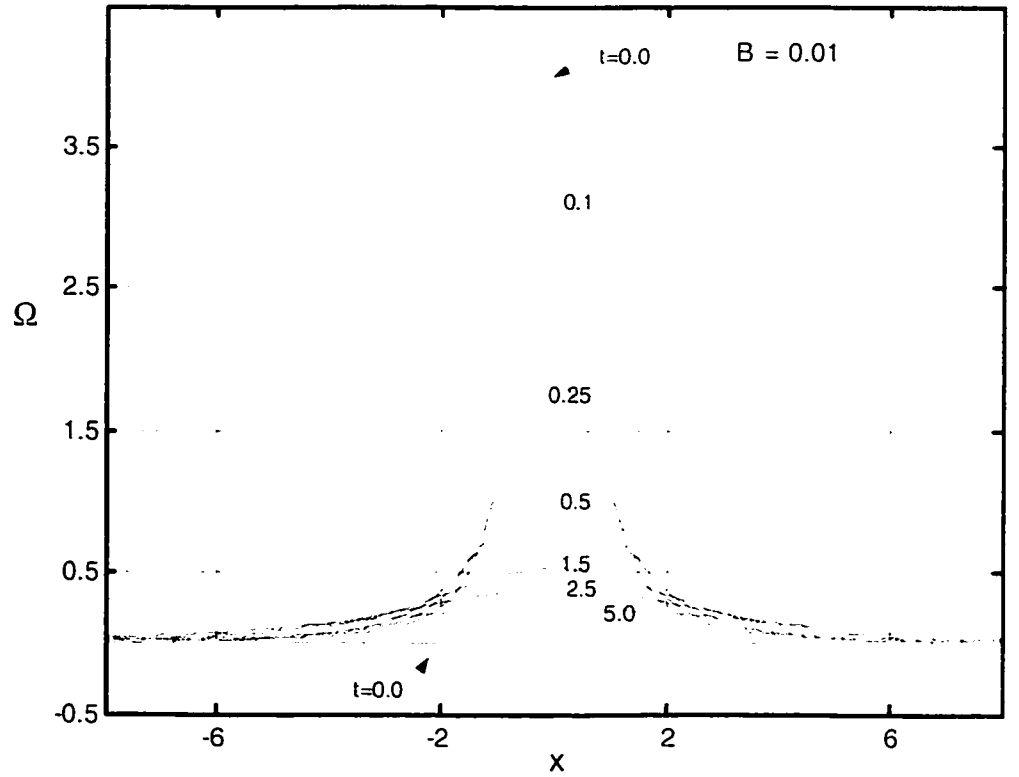

Fig. 4-4 Axial vorticity decays, using potential model. [Unconfined Vortex]

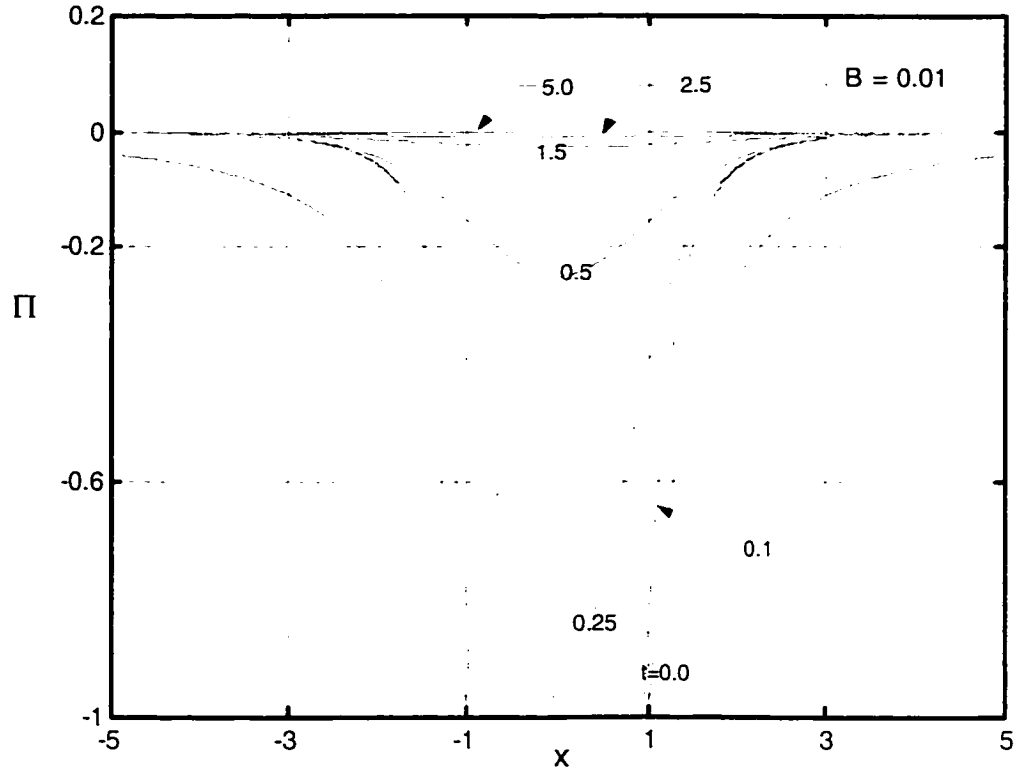

Fig. 4-5 Radial pressure decays, using potential model. [Unconfined Vortex]

It is quite interesting to compare the results between the present theory and solution given by Oseen Hamel model.

The time dependent vortex model of Ossen Hamel is given by:

$$\bar{V}_\theta = \frac{1}{\bar{r}}\left[1 - \exp\left(\frac{-\bar{r}^2}{4t_c}\right)\right]$$

Where, $\bar{V}_\theta = \frac{V_\theta}{V_{\theta_c}}$, $\bar{r} = \frac{r}{r_c}$ & $t_c = \frac{\upsilon t}{r_c^2}$

The tangential velocity distribution of the potential model is compared with results obtained by Ossen model at [t=0.1]. The results are tabulated and plotted in table [4.1] and figure [4.6], respectively. This comparison shows that, when [β=0.01] the similarity and that obtained by separation of variables solutions

produce no differences up to and including fourth decimal place. Therefore, we find that this value of β gives a radius, which is sufficiently far to represent the unconfined vortex flow.

Table [4-1] Comparison of the tangential velocity on the basis of present theory and Ossen solution at t=0.1 and β=0.01

r	Vθ-Bessel	Vθ-Oseen	Error
0	0	N/A	0
0.125	0.306441	0.306475	0.0034
0.25	0.578585	0.578619	0.0034
0.375	0.790429	0.790432	0.0003
0.5	0.929498	0.929477	0.0021
0.625	0.99745	0.997434	0.0016
0.75	1.006579	1.006586	0.0007
0.875	0.974292	0.974309	0.0017
1	0.917911	0.917915	0.0004
1.125	0.851342	0.85133	0.0012
1.25	0.783918	0.783907	0.0011
1.375	0.720828	0.720831	0.0003
1.5	0.664251	0.664262	0.0011
1.625	0.614544	0.614549	0.0005
1.75	0.571165	0.571158	0.0007
1.875	0.533261	0.533252	0.0009
2	0.499977	0.499977	0
2.125	0.470574	0.470582	0.0008
2.25	0.444438	0.444443	0.0005
2.375	0.421056	0.421052	0.0004
2.5	0.400007	0.4	0.0007
2.625	0.380954	0.380952	0.0002
2.75	0.363631	0.363636	0.0005
2.875	0.347821	0.347826	0.0005
3	0.333335	0.333333	0.0002
3.125	0.320005	0.32	0.0005
3.25	0.307695	0.307692	0.0003
3.375	0.296293	0.296296	0.0003
3.5	0.28571	0.285714	0.0004
3.625	0.275862	0.275862	0
3.75	0.266671	0.266667	0.0004
3.875	0.258067	0.258065	0.0002
4	0.249998	0.25	0.0002

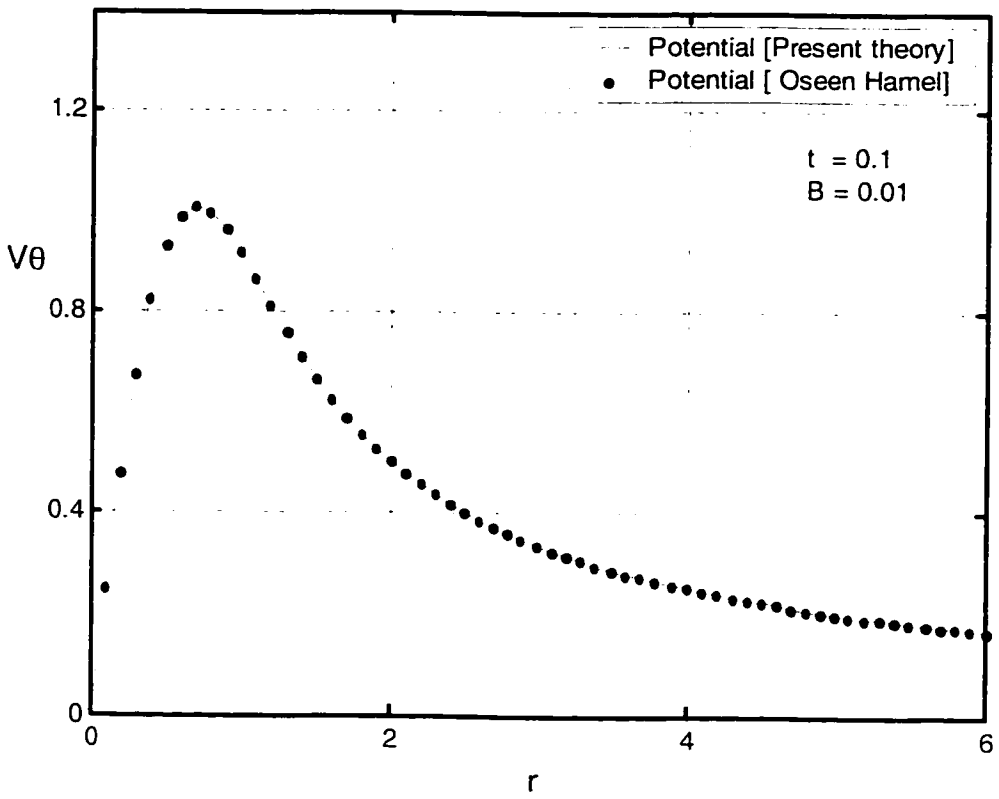

Fig. 4-6 The tangential velocity comparison between the present theory and Ossen solution at t=0.1 and β=0.01

4.4. Decay of Rankine's Vortex

Using Rankine's vortex model as an initial velocity distribution. That is,

$$\bar{V}_\theta(\bar{t}=0,\bar{r}) = \begin{cases} \bar{r} & 0 \le \bar{r} \le 1 \\ \dfrac{1}{\bar{r}} & 1 < \bar{r} \le \dfrac{1}{\beta} \end{cases}$$

Using the transformation mentioned before yields,

$$\bar{V}_\theta(\bar{t}=0,\bar{r}) = \begin{cases} \bar{r}[\beta^2 - 1] & 0 \le \bar{r} \le 1 \\ \beta^2 \bar{r} - \dfrac{1}{\bar{r}} & 1 < \bar{r} \le \dfrac{1}{\beta} \end{cases} \tag{4.16}$$

From Appendix B, the coefficient is given by:

$$A_n = \frac{-4J_1(\lambda_n\beta)}{\lambda_n^2 J_o^2(\lambda_n)} \tag{4.17}$$

Similarly, the swirl velocity, axial vorticity and static pressure formulas and their distributions can be found. Results are shown in figures [4.7], [4.8] and [4.9] respectively.

$$\bar{V}_\theta(\bar{t},\bar{r}) = \beta^2\bar{r} - \sum_{n=1}^{\infty} \frac{-4J_1(\lambda_n\beta)}{\lambda_n^2 J_o^2(\lambda_n)} e^{-(\beta^2\lambda_n^2)\bar{t}} J_1(\beta\lambda_n\bar{r}) \tag{4.18}$$

$$\bar{\Omega}(r,t) = \begin{pmatrix} 2\beta^2 - \dfrac{1}{\bar{r}}\displaystyle\sum_{n=1}^{\infty} \frac{-4J_1(\lambda_n\beta)}{\lambda_n^2 J_o^2(\lambda_n)} e^{-(\beta^2\lambda_n^2)\bar{t}} J_1(\beta\lambda_n\bar{r}) \\ -\dfrac{1}{2}\displaystyle\sum_{n=1}^{\infty} \frac{-4J_1(\beta\lambda_n\beta)}{\lambda_n^2 J_o^2(\lambda_n)} e^{-(\beta^2\lambda_n^2)\bar{t}} [J_o(\beta\lambda_n\bar{r}) - J_2(\beta\lambda_n\bar{r})] \end{pmatrix} \tag{4.19}$$

$$\Pi = \frac{\displaystyle\int_0^{\bar{r}} \frac{\left(\beta^2\bar{r} - \sum_{n=1}^{\infty} \frac{-4J_1(\lambda_n\beta)}{\lambda_n^2 J_o^2(\lambda_n)} e^{-(\beta^2\lambda_n^2)\bar{t}} J_1(\beta\lambda_n\bar{r})\right)^2}{\bar{r}}}{\displaystyle\int_0^{1} \frac{\left(\beta^2\bar{r} - \sum_{n=1}^{\infty} \frac{-4J_1(\lambda_n\beta)}{\lambda_n^2 J_o^2(\lambda_n)} e^{-(\beta^2\lambda_n^2)\bar{t}} J_1(\beta\lambda_n\bar{r})\right)^2}{\bar{r}}} \tag{4.20}$$

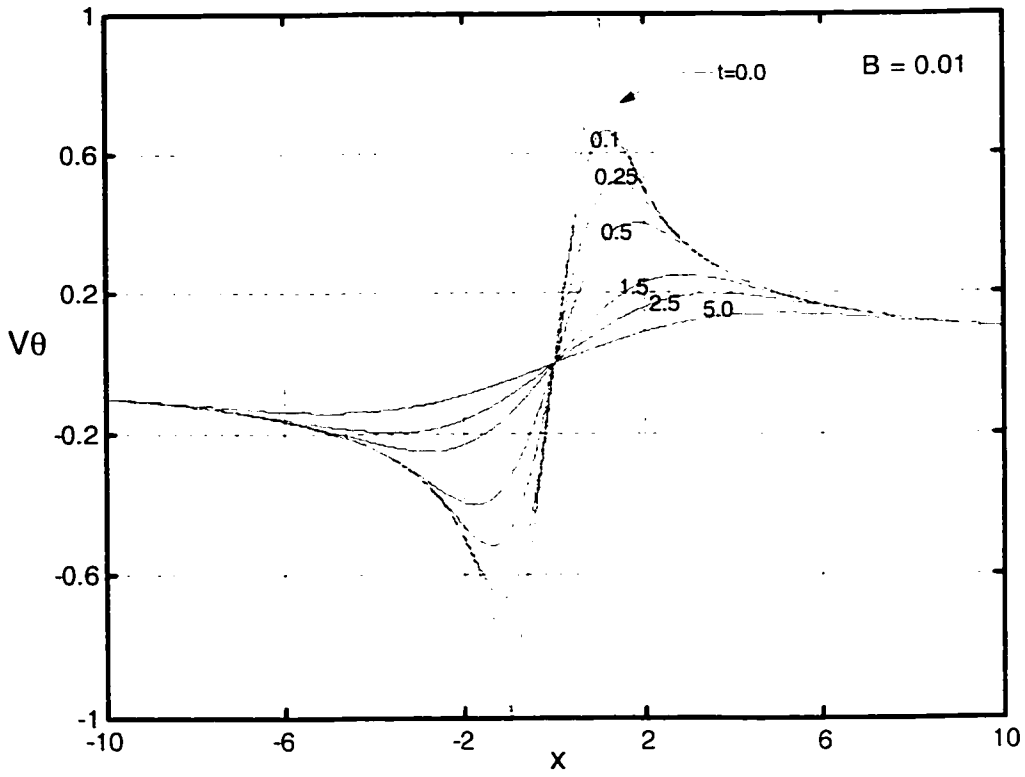

Fig. 4-7 Tangential velocity decays, using Rankine's model. [Unconfined Vortex]

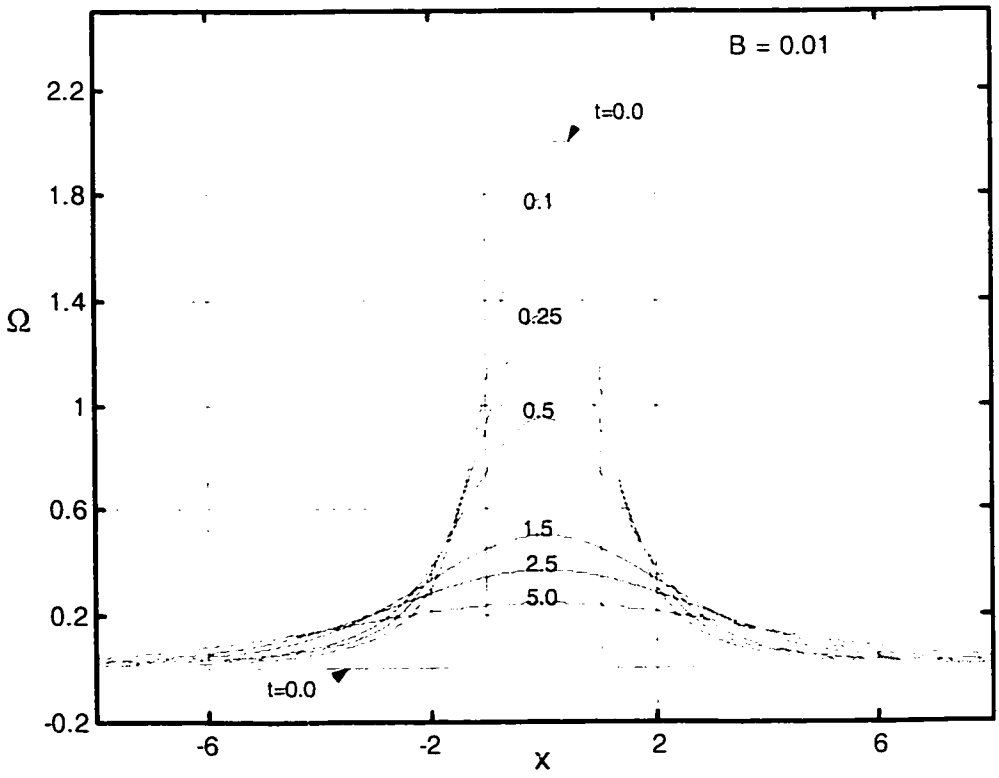

Fig. 4-8 Axial vorticity decays, using Rankine's model. [Unconfined Vortex]

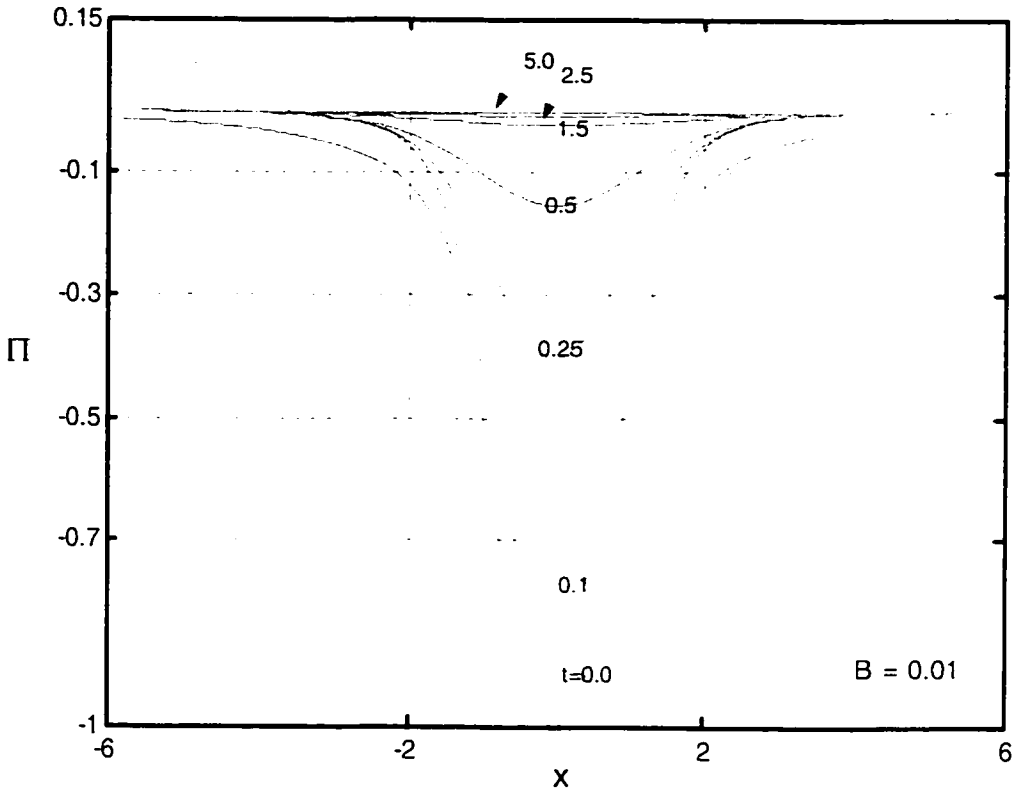

Fig. 4-9 Radial pressure decays, using Rankine's model. [Unconfined Vortex]

4.5 Decay of Vatistas's n=2 Vortex

Using Vatistas's vortex model at n=2 as an initial velocity distribution. Yields.

$$\bar{V}_\theta(\bar{t}=0,\bar{r})=\frac{\bar{r}}{\left(1+\bar{r}^4\right)^{\frac{1}{2}}}.$$

Here we had to use another transformation, which is given by:

$$\bar{V}_\theta(\bar{t}=0,\bar{r})=\frac{\beta^2\bar{r}}{\left(1+\beta^4\right)^{\frac{1}{2}}}-\frac{\bar{r}}{\left(1+\bar{r}^4\right)^{\frac{1}{2}}} \tag{4.21}$$

From Appendix B, the coefficient is given by:

$$A_n=\frac{2\beta^2}{J_o^2(\lambda_n)}\left(\frac{1}{\lambda_n\beta\sqrt{1+\beta^4}}(-J_o(\lambda_n))-H\right) \tag{4.22}$$

Where $H=\int_0^{1/\beta}\left(\frac{\bar{r}^4}{1+\bar{r}^4}\right)^{\frac{1}{2}}J_1(\beta\lambda_n\bar{r})d\bar{r}$. H can be found using numerical integration methods. Similarly, the swirl velocity, axial vorticity and static pressure formulas are:

$$\bar{V}_\theta(\bar{t},\bar{r})=\frac{\beta^2\bar{r}}{\sqrt{1+\beta^4}}-\sum_{n=1}^{\infty}\frac{2\beta^2}{J_o^2(\lambda_n)}\left(\frac{1}{\lambda_n\beta\sqrt{1+\beta^4}}(-J_o(\lambda_n))-H\right)e^{-(\beta^2\lambda_n^2)\bar{t}}J_1(\beta\lambda_n\bar{r}) \tag{4.23}$$

$$\bar{\Omega}(r,t)=\begin{pmatrix}\frac{2\beta^2}{\sqrt{1+\beta^4}}-\frac{1}{\bar{r}}\sum_{n=1}^{\infty}\frac{2\beta^2}{J_o^2(\lambda_n)}\left(\frac{1}{\lambda_n\beta\sqrt{1+\beta^4}}(-J_o(\lambda_n))-H\right)e^{-(\beta^2\lambda_n^2)\bar{t}}J_1(\beta\lambda_n\bar{r})\\ -\frac{1}{2}\sum_{n=1}^{\infty}\frac{2\beta^2}{J_o^2(\lambda_n)}\left(\frac{1}{\lambda_n\beta\sqrt{1+\beta^4}}(-J_o(\lambda_n))-H\right)e^{-(\beta^2\lambda_n^2)\bar{t}}[J_o(\beta\lambda_n\bar{r})-J_2(\beta\lambda_n\bar{r})]\end{pmatrix} \tag{4.24}$$

$$\Pi = \frac{\int_0^{\bar{r}} \frac{\left(\frac{\beta^2 \bar{r}}{\sqrt{1+\beta^4}} - \sum_{n=1}^{\infty} \frac{2\beta^2}{J_o^2(\lambda_n)} \left(\frac{1}{\lambda_n \beta \sqrt{1+\beta^4}} (-J_o(\lambda_n)) - H \right) e^{-(\beta^2 \lambda_n^2 \bar{t}} J_1(\beta \lambda_n \bar{r}) \right)^2}{\bar{r}}}{\int_0^{1} \frac{\left(\frac{\beta^2 \bar{r}}{\sqrt{1+\beta^4}} - \sum_{n=1}^{\infty} \frac{2\beta^2}{J_o^2(\lambda_n)} \left(\frac{1}{\lambda_n \beta \sqrt{1+\beta^4}} (-J_o(\lambda_n)) - H \right) e^{-(\beta^2 \lambda_n^2 \bar{t}} J_1(\beta \lambda_n \bar{r}) \right)^2}{\bar{r}}} \qquad (4.25)$$

The results for the tangential velocity, axial vorticity and the radial static pressure distributions are given in figures [4.10], [4.11] and [4.12] respectively. Also figure [4.13 a-c] shows a comparison between these parameters at the early [t=0.2] and late [t=5.0] decay. The results showed that, the early decay of the potential overestimate the tangential velocity, vorticity and pressure. While Rankine's decay have almost 20% difference from Vatistas et al n=2. Therefore, the early decay has considerable differences among parameters. These results were expected from the steady solution. The late decay showed that, the tangential velocities of the three models have almost the same value asymptotically. However the vorticity and the pressure of the potential and Rankine model are slightly different from Vatistas et al n=2 model.

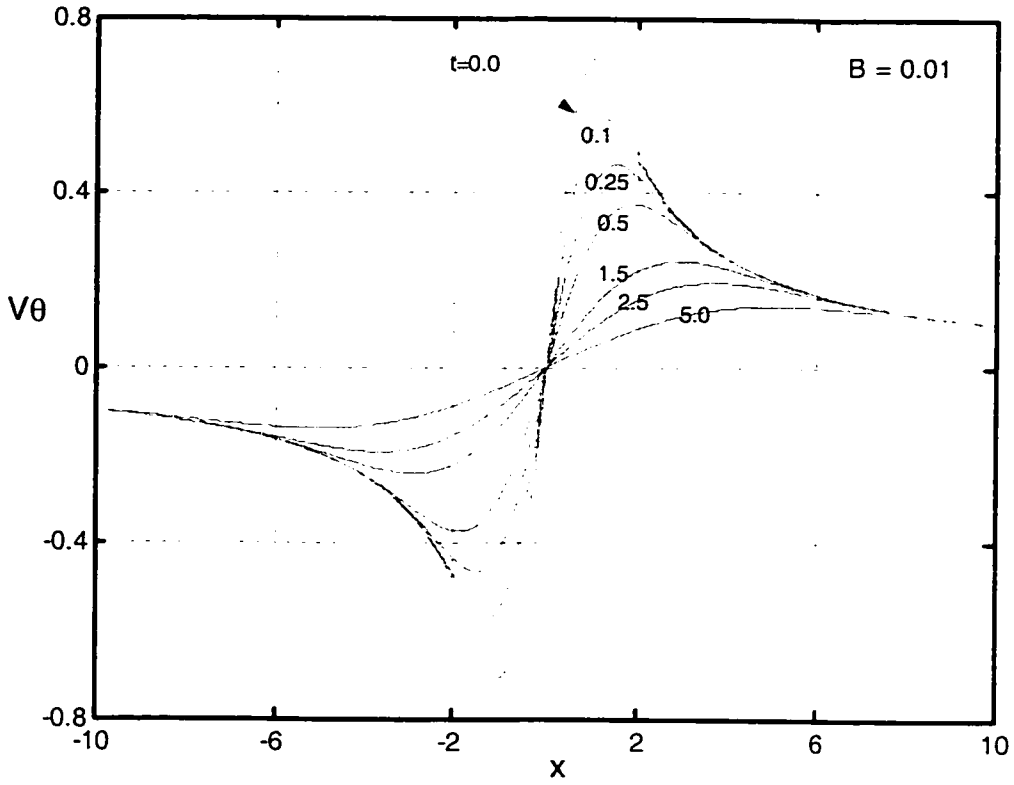

Fig. 4-10 Tangential velocity decays, using Vatistas's model [Unconfined Vortex]

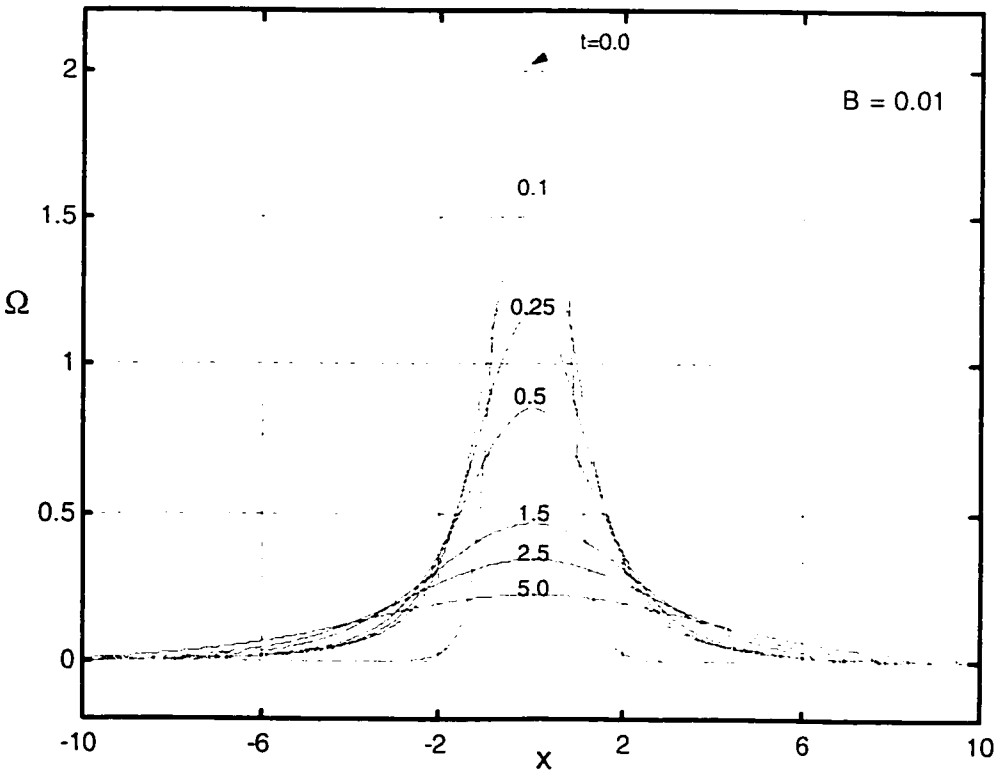

Fig. 4-11 Axial vorticity decays, using Vatistas's model. [Unconfined Vortex]

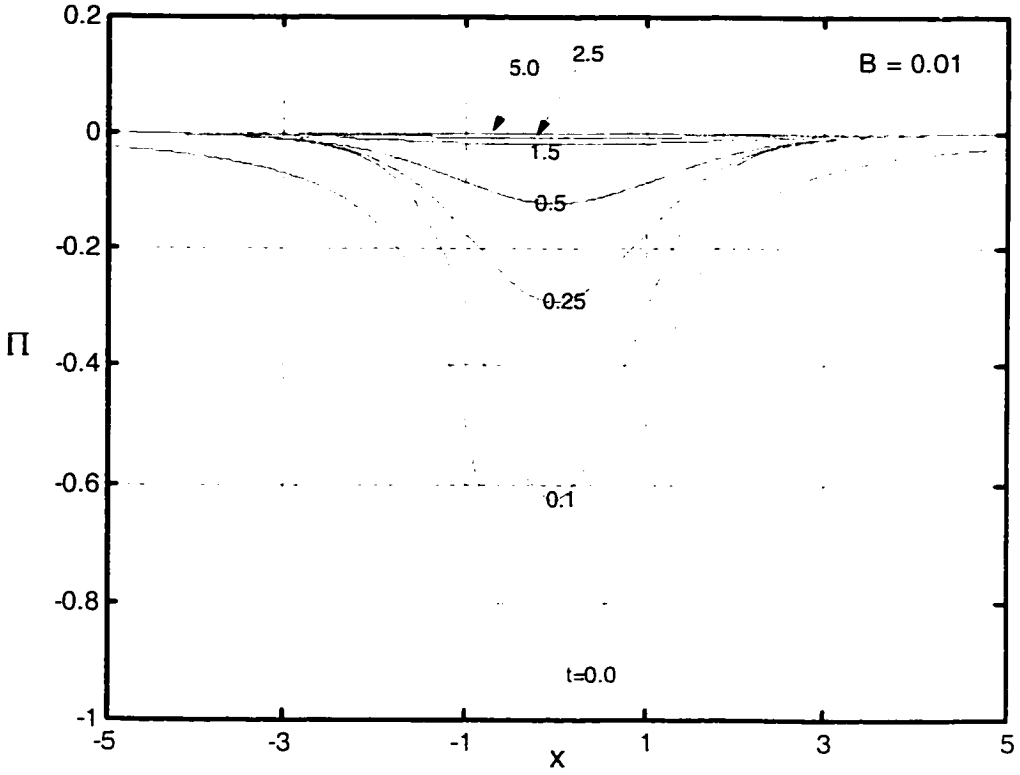

Fig. 4-12 Radial pressure decays, using Vatistas's model. [Unconfined Vortex]

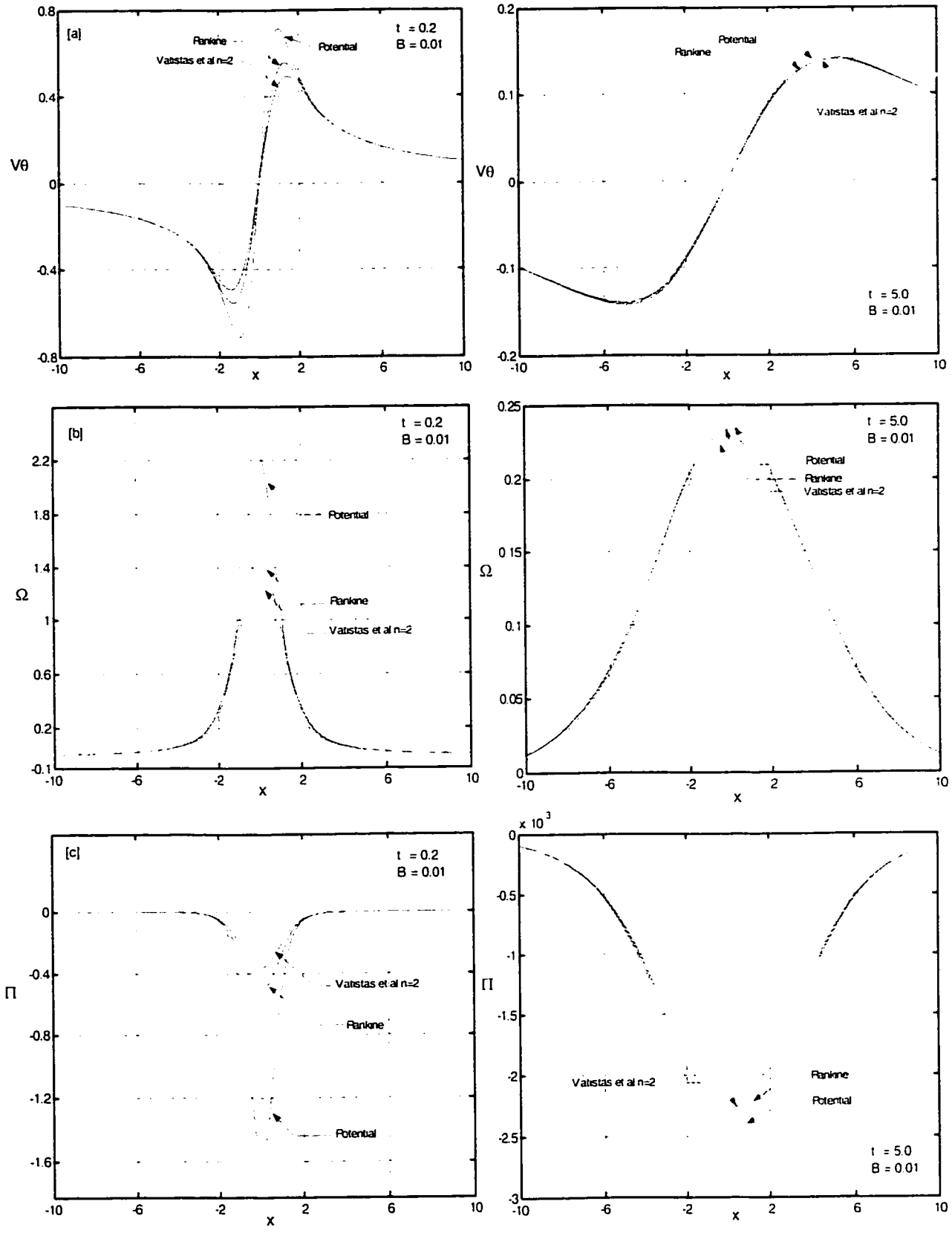

Fig. 4-13[a-c] Comparison between the velocity, vorticity and pressure distributions on the basis of different vortex model at t = 0.2 and t = 5.0 [Unconfined vortex].

4.6 Maximum Viscous Vortex Core Growth

The vortex-induced velocity is sensitive to the vortex core structure and the viscous vortex core growth. The induced velocity of the simple vortex models assumes constant viscous core size. The diffusive core growth with time was firstly explained by Oseen-Hamel. In this part, we will address the maximum viscous vortex core radius growth for various initial vortex models (see figure [4.14]). Using curve-fitting techniques, we can build simplified equations that can approximately describe the growth of maximum core radius and maximum velocity. The results are tabulated, see table [4.2] and [4.3]. Maximum induced swirl velocity, maximum vorticity and maximum radial pressure with time for each initial vortex model have been investigated as well, see figure [4.14 b-d]. Based on the previous analysis an analytical expression can be derived. Recall equation (4.8), which is:

$$\bar{V}_\theta(\bar{t},\bar{r}) = \beta^2\bar{r} - \sum_{n=1}^{\infty} A_n e^{-(\beta^2\lambda_n^2)\bar{t}} J_1(\beta\lambda_n\bar{r})$$

$$\frac{V_\theta}{V_\alpha} = \beta^2\left(\frac{r}{R_c}\right) - \sum_{n=1}^{\infty} A_n e^{-(\beta^2\lambda_n^2)\bar{t}} J_1(\beta\lambda_n\frac{r}{R_c}) \qquad (4.26)$$

Since the induced swirl velocity attains its maximum value at the core radius, hence the slope of the swirl velocity at the maximum core radius must vanish at this point yields,

$$\frac{\partial V_\theta}{\partial r_{t=\infty}} = 0.0 \qquad (4.27)$$

$$0.0 = \beta^2\left(\frac{1}{R_c}\right) - \sum_{n=1}^{\infty} A_n e^{-(\beta^2\lambda_n^2 t)} \frac{\partial}{\partial r} J_1(\beta\lambda_n \frac{r}{R_c}) \downarrow_{r=r_m}$$

$$\beta^2 = \sum_{n=1}^{\infty} A_n e^{-(\beta^2\lambda_n^2 t)} \frac{\lambda_n\beta}{2}\left(J_o(\lambda_n\beta\frac{r}{R_c}) - J_2(\beta\lambda_n \frac{r}{R_c})\right) \downarrow_{r=r_m}$$

$$\beta^2 = \sum_{n=1}^{\infty} A_n e^{-(\beta^2\lambda_n^2 t)} \frac{\lambda_n\beta}{2}\left(J_o(\lambda_n\beta\frac{r_m}{R_c}) - J_2(\beta\lambda_n \frac{r_m}{R_c})\right)$$

Let $\overline{r_m} = \frac{r_m}{R_c}$

$$\beta^2 = \sum_{n=1}^{\infty} A_n e^{-(\beta^2\lambda_n^2 t)} \frac{\lambda_n\beta}{2}\left(J_o(\lambda_n\beta\overline{r_m}) - J_2(\beta\lambda_n \overline{r_m})\right) \tag{4.28}$$

The Bessel function definition in terms of positive integer (n), can be expanded as.

$$J_o(\lambda_n\beta\overline{r_m}) = 1 - \frac{1}{4}(\lambda_n\beta)^2(\overline{r_m})^2 + \frac{1}{81}(\lambda_n\beta)^4(\overline{r_m})^4 - \frac{1}{2^2 4^2 6^2}(\lambda_n\beta)^6(\overline{r_m})^6 + \ldots\ldots\ldots$$

$$J_2(\lambda_n\beta\overline{r_m}) = \frac{1}{8}(\lambda_n\beta)^2(\overline{r_m})^2 - \frac{1}{96}(\lambda_n\beta)^4(\overline{r_m})^4 + \frac{1}{6*8^3}(\lambda_n\beta)^6(\overline{r_m})^6 - \ldots\ldots\ldots\ldots$$

Since the order of magnitude of $\beta\overline{r_m}$ is relatively small, consequently we can neglect higher order terms such as $(\beta\overline{r_m})^4$ & $(\beta\overline{r_m})^6$ with respect to $(\beta\overline{r_m})^2$

$$J_o(\lambda_n\beta\overline{r_m}) = 1 - \frac{1}{4}(\lambda_n\beta)^2(\overline{r_m})^2 + O(\beta\overline{r_m})^4$$

$$J_2(\lambda_n\beta\overline{r_m}) = \frac{1}{8}(\lambda_n\beta)^2(\overline{r_m})^2 + O(\beta\overline{r_m})^4$$

$$J_o(\lambda_n\beta\overline{r_m}) - J_2(\lambda_n\beta\overline{r_m}) = 1 - \frac{3}{8}(\lambda_n\beta)^2(\overline{r_m})^2 + O(\beta\overline{r_m})^4 \tag{4.29}$$

Since we have $\beta^2 = \sum_{n=1}^{\infty} A_n e^{-(\beta^2\lambda_n^2 t)} \frac{\lambda_n\beta}{2}\left(1 - \frac{3}{8}(\lambda_n\beta)^2(\overline{r_m})^2 + O(\beta\overline{r_m})^4\right)$, therefore we can solve for $\overline{r_m}$:

$$\overline{r_m} = \sqrt{\frac{\sum_{n=1}^{\infty} A_n \left(\frac{\lambda_n \beta}{2}\right) e^{-(\beta^2 \lambda_n^2 \bar{t}]} - \beta^2}{\frac{3}{2}\sum_{n=1}^{\infty} A_n \left(\frac{\lambda_n \beta}{2}\right)^3 e^{-(\beta^2 \lambda_n^2 \bar{t}]}} + O(\beta \overline{r_m})^4} \tag{4.30}$$

Equation (4.30) is an explicit expression that determines, how the maximum vortex viscous core growth varies with time, for given values of β & A_n corresponding to each initial vortex model. Simplified equation that can predict the maximum vortex viscous core radius as function of time is presented based on the curve fitting approach. Therefore, the core grows expressed as

$$\overline{r_m} = a\left(\bar{t}_c\right)^b \tag{4.31}$$

Where a & b are arbitrary constants varies from initial vortex model to another see table [4.2].

Since, that the maximum viscous vortex core radius growth can be formulated in the form of $\overline{r_m} = a\left(\bar{t}_{\cdot}\right)^b$, hence the normalized time parameter can also be introduced in terms of the maximum core radius. Therefore,

$$\bar{t}_{\cdot} = \left(\frac{\overline{r_m}}{a}\right)^{\frac{1}{b}} \tag{4.32}$$

Consequently, the maximum induced swirl velocity can be expressed as a function of the maximum core radius as well.

$$\overline{V}_{\theta})_{\max} = \beta^2 \overline{r_m} - \sum_{n=1}^{\infty} A_n e^{-(\beta^2 \lambda_n^2 \left(\frac{\overline{r_m}}{a}\right)^{\frac{1}{b}})} J_1(\beta\lambda_n \overline{r_m}) \tag{4.33}$$

If we now dimensionless the induced velocity expression of equation (4.8) using the maximum swirl velocity given in equation (4.33), that led to another swirl velocity expression, which is:

$$\overline{V}_{\theta} = \frac{\overline{V}_{\theta}(\bar{t}, \bar{r})}{\overline{V}_{\theta})_{\max}} = \frac{\beta^2 \bar{r} - \sum_{n=1}^{\infty} A_n e^{-(\beta^2 \lambda_n^2 \bar{t})} J_1(\beta\lambda_n \bar{r})}{\beta^2 \overline{r_m} - \sum_{n=1}^{\infty} A_n e^{-(\beta^2 \lambda_n^2 \left(\frac{\overline{r_m}}{a}\right)^{\frac{1}{b}})} J_1(\beta\lambda_n \overline{r_m})} \tag{4.34}$$

A simplified equation that can also predict the maximum swirl velocity as function of time is introduced based on the curve fitting approach. Therefore, the maximum induced swirl velocity takes the form of:

$$\overline{V}_{\theta \max} = \frac{c}{\left(\bar{t}\right)^d} \tag{4.35}$$

Where c & d are arbitrary constants varies from initial vortex model to another see table [4.3].

Here the swirl velocity is based on the maximum core radius as a reference scale. While the non-dimensional time enter the expression in a parametric way. Therefore, the distinct time distributions of the induced swirl velocity based on various initial vortex model shown in figures [4.3,4.7,4.10], will fall into a single curve as shown in figure [4.15]. This results shows that Rankine model

overestimate the tangential velocity in percentage of 4% at the early decay relative to the other formulations.

Also it is evident from figure [4.14] that the divergence of maximum core radius and the maximum velocity versus time among the three profiles of different initial conditions is largest during the beginning of the decaying process. The early phase decay of the potential model shows that, it over estimate the maximum parameters. Therefore this model has a considerable decay lag at the beginning. Although, initially the maximum vorticity and maximum pressure for both Rankine's and Vatistas's n=2 are equal. The later show leading vanishes. The late decay such as at t>~ 5.0, the curve representing The potential, Rankine's vortex and Vatistas'n=2 tends asymptotically which implying that beyond this time level, there are no appreciable differences between the three models.

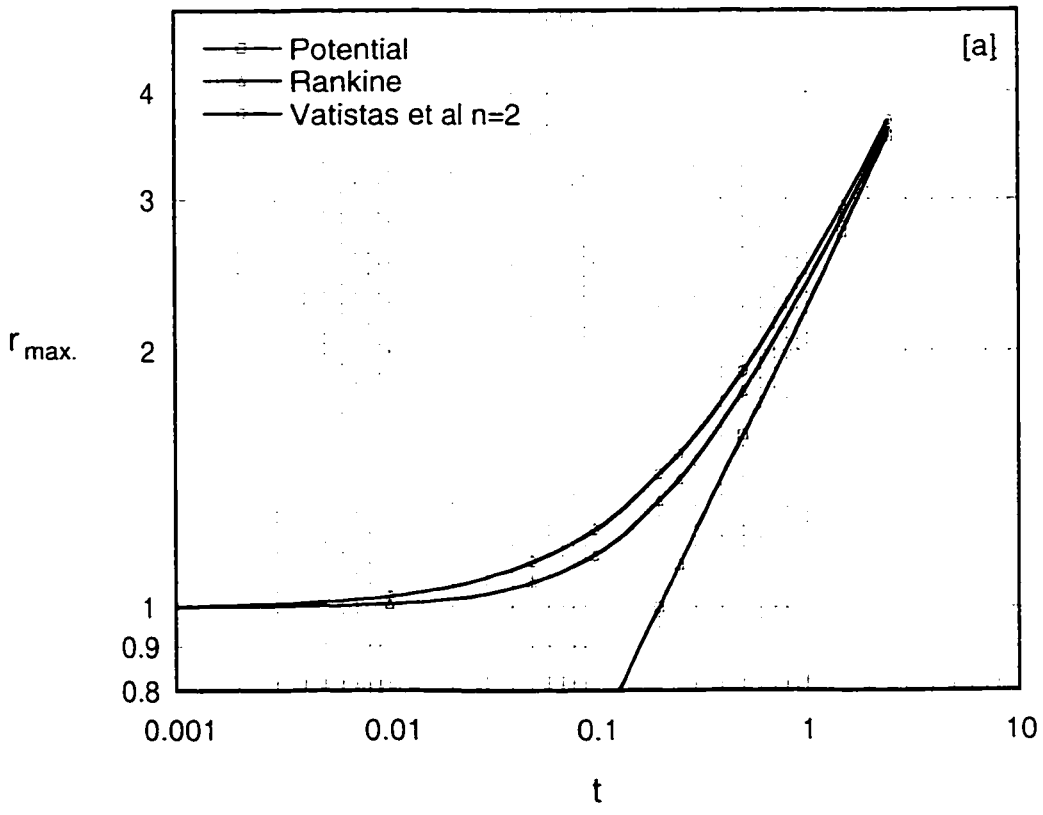

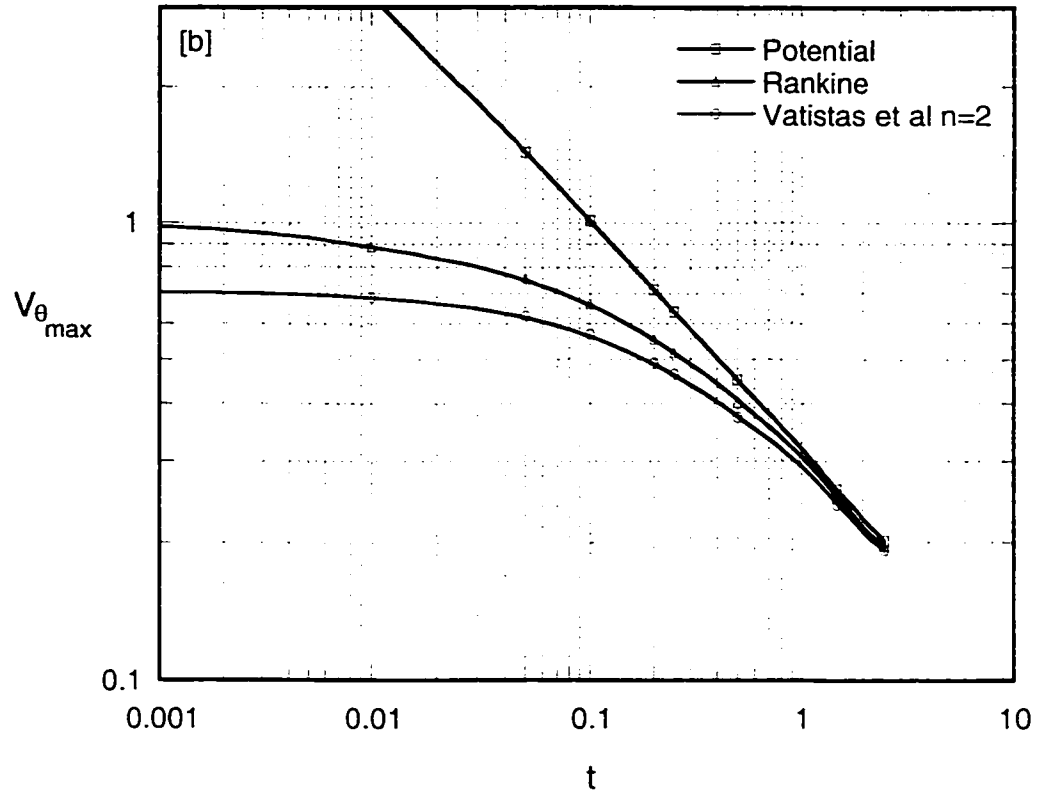
[b]
Potential
Rankine
Vatistas et al n=2
1
0.1
$V_{\theta_{max}}$
0.001
0.01
0.1
1
10
t

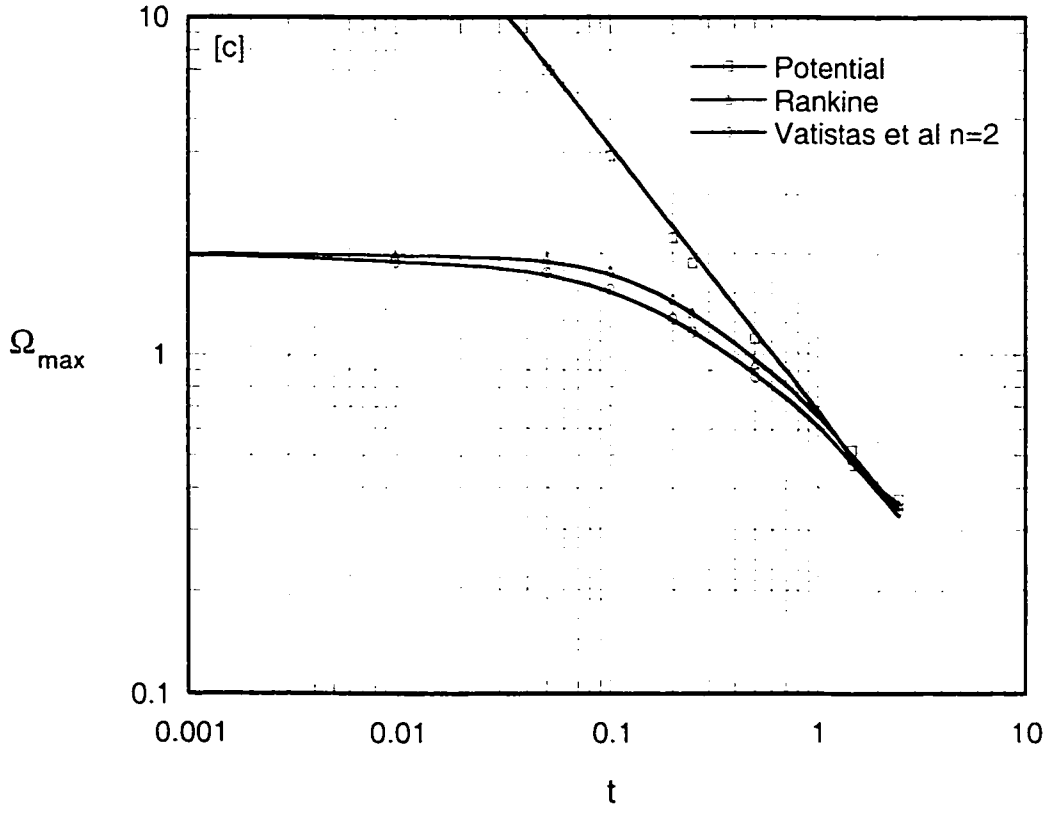
[c]
Potential
Rankine
Vatistas et al n=2
10
1
0.1
Ω_{max}
0.001
0.01
0.1
1
10
t

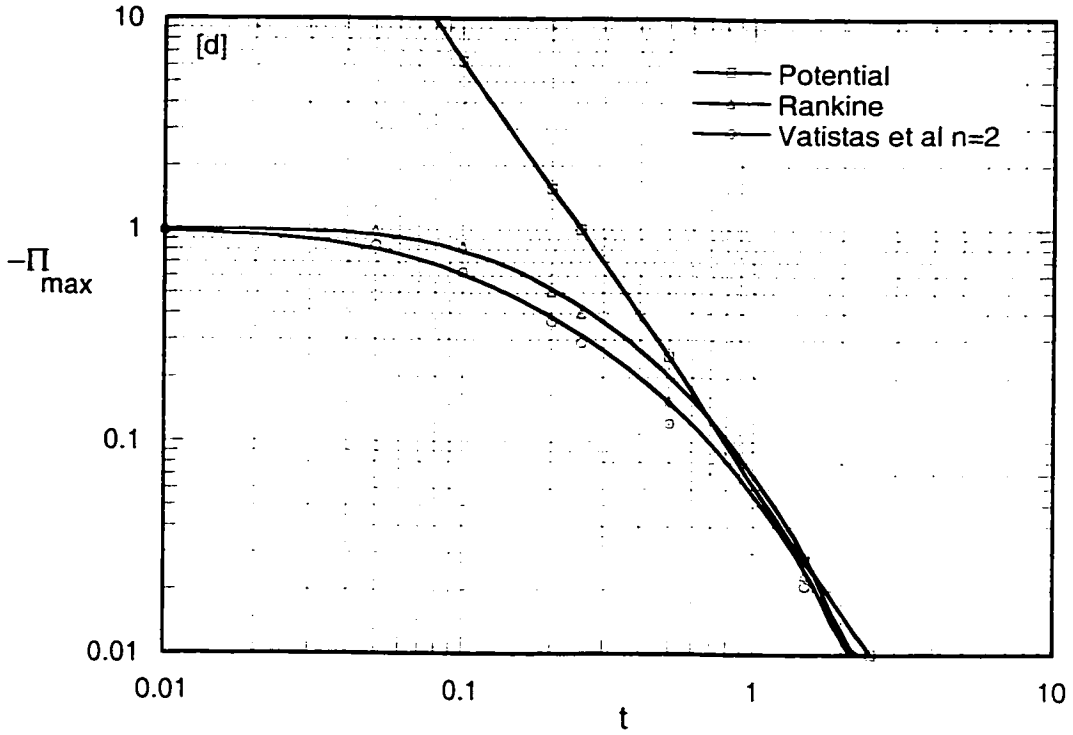

Fig.4-14 Maximum vortex core radius, velocity, vorticity and pressure Versus time on basis of various vortex models at β=0.01.

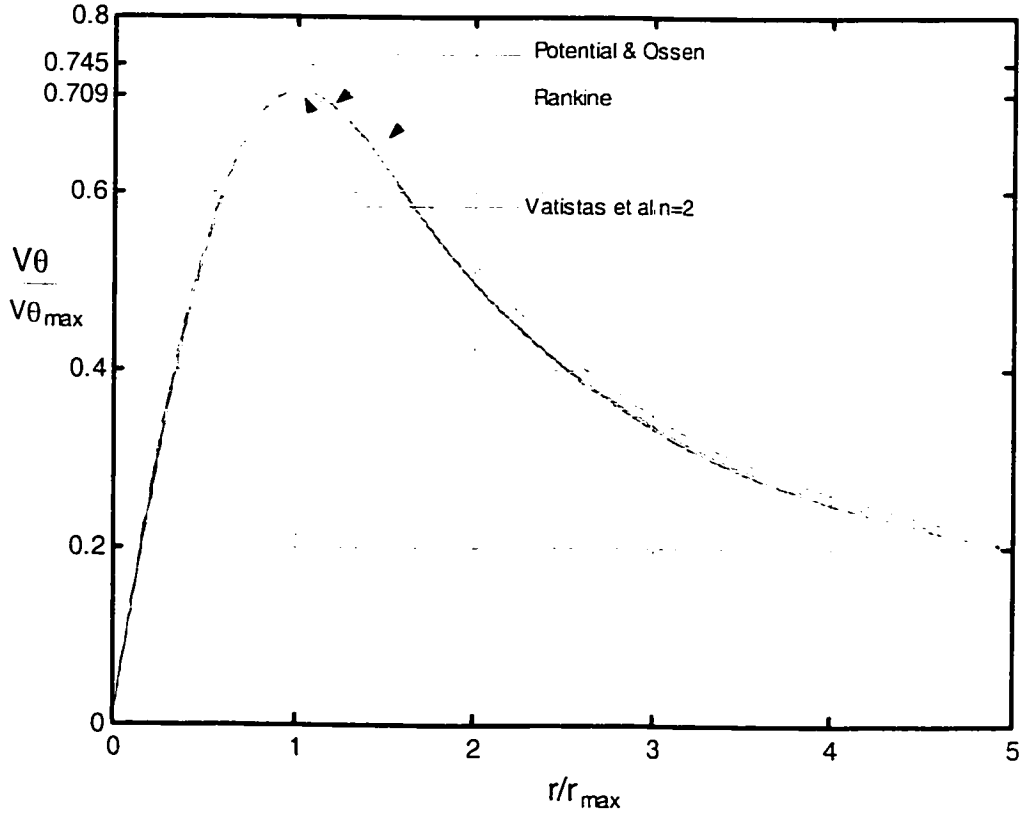

Fig.4-15 Swirl velocity decay will fall into one curve for a various vortex model Compared with Oseen-Hamel model. [Unconfined Vortex]

Table [4-2] Maximum viscous vortex core radius growth on basis of various vortex models. Using curve-fitting approach. [Unconfined Vortex]

Vortex	Potential	Rankine	Vatistas	Lamb Ossen
$\bar{r}_m =$	$2.3413(\bar{t}_c)^{0.464}$	$2.5696(\bar{t}_c)^{0.4078}$	$2.4312(\bar{t}_c)^{0.4377}$	$2.2418(\bar{t}_c)^{0.5}$
a	2.3413	2.5696	2.4312	2.2418
b	0.464	0.4078	0.4377	0.5

Table [4-3] Maximum tangential velocity growth on basis of various vortex models. Using curve-fitting approach. [Unconfined Vortex]

Vortex	Potential	Rankine	Vatistas et al n=2	Ossen-Hamel
$V_{\theta)\max}$	$\frac{0.3191}{(\bar{t}_c)^{0.5}}$	$\frac{0.3074}{(\bar{t}_c)^{0.2822}}$	$\frac{0.2918}{(\bar{t}_c)^{0.2381}}$	$\frac{0.3191}{(\bar{t}_c)^{0.5}}$
c	0.3191	0.3074	0.2918	0.3191
d	0.5	0.2822	0.2381	0.5

Chapter 5

Conclusions

A novel analytical method was developed to mathematically simulate the decay of a strong, concentrated vortex. The governing diffusion type equation was solved using separation of variables via Fourier-Bessel expansions for the tangential velocity. Three initial velocity shapes; the potential, Rankine's, and the n = 2 vortex were explored. The last has been shown not suffer from any theoretical contradictions. All the relevant fluid properties were indeed continuous and bounded, and all their derivatives preserve the same mathematical qualities as well. The methodology was kept general so as to accommodate the formulation of any initial steady-state vortex profile.

Although there were found no appreciable differences among the three near the center of rotation and far away, they do produce substantial disparities in the mixed-vortex region in the neighborhood of the core. Finally, it is shown that the time history profiles of the velocity, and thus the pressure, exhibit a distinct self-similarity characteristic. The last made possible the collapse of the various time history distributions into a single curve that is solely a function of the space coordinate, while the time dependence of the phenomenon enters parametrically.

This work is a natural evolution from steady state family of algebraic vortex equations proposed by Vatistas et al[38] over a decade ago, towards the formulation concerning the time reduction of an isolated, strong vortex. Besides the applicability of the subject matter in many areas of science and technology, the completion of the work was triggered by the remark made by Rossow [28] that: "the use of the previous algebraic equations for determination of a decay rate for the vortex is not clear".

The methodology is kept general enough to accommodate the other members of the Vatistas vortex family model, or any of the known vortex formulations such as Burgers, Taylor's, Scully's, or even two celled vortices such as Sullivan's and Vatistas [39].

List of References

[1] Akira Ogawa. Vortex Flow CRC Series on Fine Particle Science and Technology CRC Press INC., 1993.

[2] Bagai, A. and Leishman, J. G. 1993: Flow visualization of compressible vortex structures using density gradient techniques. *Exp. Fluids*, Vol. 15, pp. 431- 442.

[3] Bagai, A. and . Leishman, J. G. 1998: Adaptive grid sequencing and interpolation schemes for helicopter rotor wake analyses. *AIAA J.*, Vol. 36, No. 9, September, pp. 1593-1602.

[4] Burgers, J.M., 1948. A Mathematical Model Illustrating the Theory of Turbulence". Adv. In. App. Mech., Vol.1, pp.171-199.

[5] Coton, F.N., Copland, C. M., and Galbraith, A. D. 1998: An experimental study of the idealized vortex system on a novel rotor blade tip. *Journal of the* American Helicopter Society, August/September, pp. 385-392

[6] E. Ozger, I. Schell, and D.Jacob. "On the Structure and Attenuation of an Aircraft Wake," Aircraft.Vol.38, No5, September-October 2001,PP.878-887

[7] F.Holzapfel, T.Gerz and R.Baumann. "The Turbulent Decay of Wake Vortices In The Stably Stratified Atmosphere" AIAA-2000-0754.

[8] Faler, J.H., and S. Leibovich, 1977: Disturbed states of vortex flow and vortex breakdown. *Physics Fluids*, Vol. 20, pp. 1385-1400.

[9] Gupta, A.K., Lilley, D.G and Syred, N., Swirl Flow Abacus Press: Tunbridge Wells, 1984.

[10] Han, Y.Q., Leishman, J.G., and Coyone, A.J. 1997: Measurements of the velocity and turbulence structure of a rotor tip vortex. *AIAA J.*, Vol. 35, (3), March, pp. 477- 485.

[11] Henri Moet "The Effects of the Atmospheric Turbulence on Wake Vortices" CERFACS, Toulouse, 2002,France.

[12] Jacquin. L. and Pantano, C. 2002: On the persistence of trailing vortices. JFM, Vol. 471, pp.159-168.

[13] J.Gordon Leishman, 1998: Measurements of the periodic wake of a hovering rotor. *Exp. Fluids*, Vol. 125, pp. 252-361.

[14] J. Gordon. Leishman, Mahendra j. Bhagwat " Generalized Viscous vortex model for application to free-vortex wake and aero acoustics calculations" The 58th Annual Forum and Technology display of the Helicopter Society International, Montreal, Canada June, 2002.

[15] K.F. Riley, M.P. Hobson and S.J. Bence Mathematical Methods for Physics and Engineering. Cambridge University Press, Cambridge, UK, 1998.

[16] Kaufmann, W. 1962: Uber die ausbreitung kreiszlindrischer wirbel in zaben flussigkeiten. *Ingenieur Archiv*, Vol. 31, No. 1, p. 1.

[17] Lam, H.C., 1993: An experimental investigation and dimensional analysis of confined vortex flows. Ph.D Thesis, Department of Mechanical Engineering, Concordia University, Montreal, Canada.

[18] Lamb, H., Hydrodynamics, 6th ed. Cambridge University Press, Cambridge, UK, 1932.

[19] Lugt, H., J. 1959 Vortex Flow In Nature and Technology John Wiley & Sons, New York.

[20] Newman, B.G. 1959: Flow in a viscous trailing vortex. Aeronautical Quarterly, Vol. X, pp. 149-162.

[21] Nilay, S. U, 2001: High-accuracy wake and vortex simulations using a hybrid Euler/discrete vortex method. Master of Science Thesis, Dept. of Aerospace Engineering, The Pennsylvania State University.

[22] Oseen, C.W., "Uber Wirbelbewegune in Einer Reiben-den Flussigkeit" Ark. J. Mat. Astrom. Fys., Vol.7,1912, PP.14-21.

[23] Prichard, W.G. 1970: Solitary waves in rotating fluids. *JFM*, Vol. 42, Part 1, pp. 61-83.

[24] Robins R.E. & Delisi D.P.1999 "Further development of a wake vortex algorithm and comparisons to data" AIAA Conf. Proc. 99-0757,12pp.

[25] Rankine, W. J. M., Manual of applied Mechanics C. Griffen Co., London.1858.

[26] Robertson, J.M. 1966: Hydrodynamics in theory and application. Engelwood Cliffs, Prentice-Hall Inc.

[27] Roschke, E.J. 1966: Experimental investigation of a confined, jet-driven vortex chamber. JPL Rep. 32-982, NASA CR-78550, 1966.

[28] Rossow Vernon J. "Lift generated vortex wakes of subsonic transport aircraft" Progress in Aerospace Science, Vol.35, 1999,PP.507-660.

[29] Scully, M.P. "Computational of helicopter rotor Wake geometry and its influence on rotor Harmonic Air-loads" Massachusetts Institute of Technology Report No.ASRLTR178-1, March 1975.

[30] Sullivan, j. p., "An Experimental Investigation of Vortex Ring and Helicopter Rotor Wakes Using a Laser Doppler Velocimeter." Massachusetts Institute of Technology Aero physics Laboratory Technical Report 183.MIT DSR No.80038, June 1973.

[31] Sarpkaya, t., "A New Model for Vortex Decay In The Atmosphere" J. Aircraft, Vol.37, 2000,PP.53-61.

[32] Sarpkaya, t., "Decay of Wake Vortices of Large Aircraft" AIAA journal. Vol.36 No9, September 1998,PP.1671-1679.

[33] Tauszig, L. 1998: Numerical detection and characterization of the blade vortex interaction using free wake analysis. Master of Science Thesis, Dept. of Aerospace Engineering, The Pennsylvania State University.

[34] Thomas Gerz, Frank Holzapfel, DLR "Aircraft Wake Vortices" The European Thematic Network on Wake Vortex April 2001.

[35] Vatistas, G.H. " Theoretical And Experimental Studies on Confined Vortex Flow" Ph D. 1984,Concordia University Quebec, Canada.

[36] Vatistas, G.H., Lin, S., and Li, P.M. 1988: "A Similar Profile for the Tangential Velocity in Vortex Chambers". *Exp. Fluids*, Vol. 6, pp. 135-137.

[37] Vatistas, G.H., 1989, "Analysis of fine particle concentrations in a confined vortex", Journal of Hydraulic Research, Vol.27, No.3, p.417-427.

[38] Vatistas, G.H., Kozel, V., and Mih, W.C., "A Simpler Model for Concentrated Vortices," Experiments in Fluid. Vol.11, 1991.pp.73-76.

[39] Vatistas, G.H., "New Model for Intense Self-similar Vortices" AIAA journal of propulsion and power, VOL.14, No.4, April 1998,pp.462-469.

[40] Vatistas, G.H., 2003: The fundamental properties of the n = 2 vortex model, submitted to Exp. Fluids, February 2003.

[41] Vladimir Kozel. "Experimental and theoretical studies on Concentrated Columnar Vortices" Ph.D.1991, Concordia University Quebec, Canada.

[42] Wunenburger, R., Andreoti, B., and Petitjeans, P. 1999: Influence of precession on velocity measurements in a strong laboratory vortex. Exp. Fluids, Vol. 27, pp. 181-188.

[43] William H. Press, Saul A. Teukolsky, William T. Vetterling and Brian P. Flannery [Numerical Recipes in C], 2nd Edition Cambridge Press, 1992.

Appendix A

Bessel Function properties and important integrals

Bessel function arsis as solution of standard differential equation

$$x^2\frac{\partial^2 y}{\partial x^2}+x\frac{\partial y}{\partial x}+(x^2-n^2)y=0 \qquad n\geq 0$$

Which is called Bessel's differential equation.

The general solution of this type is given by

$$y=C_1J_n(x)+C_2Y_n(x)$$

Mathematical Fact

- $J_n(x)$ Is called Bessel function of 1st kind and order n, which must be finite as x approaches zero.
- $Y_n(x)$ Is called Bessel function of 2nd kind and order n, which is unbounded solution as x approaches zero.

Since our solution must be bounded, so we are interesting in the solution of Bessel of 1st kind and order n.

$$J_n(x)=\frac{x^n}{2^n\Gamma(n+1)}\left(1-\frac{x^2}{2(2n+2)}+\frac{x^4}{2.4(2n+2)(2n+4)}-\cdots\cdots\cdots\right)$$
$$=\sum_{r=0}^{\infty}\frac{(-1)^r(x/2)^{n+2r}}{r!\Gamma(n+r+1)}$$

Where $\Gamma(n+1)$ is called Gamma Function, if n is positive $\Gamma(n+1)=n!$

Basic Recurrence formulas are given by:

$$J_{n+1}(x) = \frac{2n}{x} J_n(x) - J_{n-1}(x)$$

$$J_n' = \frac{1}{2}[J_{n-1}(x) - J_{n+1}(x)]$$

Fourier Analysis

Based on Fourier series analysis, we can show that if any function $f(x)$ satisfies the Dirichlet boundary conditions there will e exist a Bessel series expansion having the form

$$f(x) = \sum_{n=1}^{\infty} A_n J_n(\lambda_n x)$$

Where λ_n is the positive roots and A_n successive constants

$$A_n = \frac{2}{J_{n+1}^2(\lambda_n)} \int_0^1 x J_n(\lambda_n x) f(x) dx$$

Important Integration

1- $$I = \int J_1(\lambda_n \bar{r}) d\bar{r} = \frac{-1}{\lambda_n} J_0(\lambda_n r) + C$$

2- $$I = \int r^2 J_1(\lambda_n \bar{r}) d\bar{r} = \frac{r^2}{\lambda_n} J_2(\lambda_n r) + C$$

Hence $$J_{n+1}(\lambda_n r) = \frac{2n}{\lambda_n r} J_n(\lambda_n r) + J_{n-1}(\lambda_n r)$$

Let n = 1 $\therefore J_{21}(\lambda_n r) = \frac{2}{\lambda_n r} J_1(\lambda_n r) + J_0(\lambda_n r)$ substitute back

$$\therefore I = \frac{r^2}{\lambda_n}\left(\frac{2}{\lambda_n r} J_1(\lambda_n r) + J_0(\lambda_n r)\right) + c$$

Appendix B

Detail derivation of A_n for different Vortex Models

1.Confined Vortex

Case Study1

The tangential velocity is free to Slip at the outer diameter

Rankine's Model [Slip]

$$A_n = \frac{\int_0^1 r\bar{V}_\theta(\bar{t}=0,\bar{r})J_1(\lambda_n\bar{r})d\bar{r}}{\int_0^1 rJ_1^2(\lambda_n\bar{r})d\bar{r}} = \frac{2}{J_o^2(\lambda_n)}\int_0^1 r\bar{V}_\theta(\bar{t}=0,\bar{r})J_1(\lambda_n\bar{r})d\bar{r}$$

$$A_n = \frac{2}{J_o^2(\lambda_n)}\int_0^1 \bar{r}\begin{cases}\bar{r}[\dfrac{\beta^2-1}{\beta^2}] \\ \bar{r}-\dfrac{1}{\bar{r}}\end{cases} J_1(\lambda_n\bar{r})d\bar{r}$$

$$= \frac{2}{J_o^2(\lambda_n)}\begin{cases}\int_0^\beta \bar{r}^2[\dfrac{\beta^2-1}{\beta^2}]J_1(\lambda_n\bar{r})d\bar{r} \\ \int_\beta^1 \bar{r}^2 J_1(\lambda_n\bar{r})d\bar{r} \quad + \int_\beta^1 -J_1(\lambda_n\bar{r})d\bar{r}\end{cases}$$

$$A_n = \frac{2}{J_o^2(\lambda_n)}[I_1+I_2+I_3] \;\&\; I_1 = \int_0^\beta \bar{r}^2[\frac{\beta^2-1}{\beta^2}]J_1(\lambda_n\bar{r})d\bar{r} = [\frac{\beta^2-1}{\beta^2}]\int_0^\beta \bar{r}^2 J_1(\lambda_n\bar{r})d\bar{r}$$

Using the integration techniques Appendix A.

$$I_1 = [\frac{\beta^2 - 1}{\beta^2}]\left(\frac{-\beta^2}{\lambda_n} J_o(\lambda_n \beta) + \frac{2\beta}{\lambda_n^2} J_1(\lambda_n \beta)\right)$$

$$= [\frac{\beta^2 - 1}{\beta^2}]\frac{\beta^2}{\lambda_n}\left(\frac{2}{\lambda_n \beta} J_1(\lambda_n \beta) - J_o(\lambda_n \beta)\right) \text{since, } J_2(\lambda_n \beta) = \left(\frac{2}{\beta \lambda_n}\right) J_1(\lambda_n \beta) - J_o(\beta \lambda_n)$$

$$= \frac{\beta^2 - 1}{\lambda_n}\left(\frac{2}{\lambda_n \beta} J_1(\lambda_n \beta) - J_o(\lambda_n \beta)\right)$$

$I_1 = \frac{\beta^2 - 1}{\lambda_n} J_2(\lambda_n \beta)$, Similarly

$$I_2 = \int_{\beta}^{1} \bar{r}^2 J_1(\lambda_n \bar{r}) d\bar{r} \quad = \frac{2}{\lambda_n^2} J_1(\lambda_n) - \frac{J_o(\lambda_n)}{\lambda_n} - \frac{\beta^2}{\lambda_n} J_2(\lambda_n \beta), J_1(\lambda_n) = 0$$

$$I_2 = -\frac{J_o(\lambda_n)}{\lambda_n} - \frac{\beta^2}{\lambda_n} J_2(\lambda_n \beta) \;\&\; I_3 = \int_{\beta}^{1} J_1(\lambda_n \bar{r}) d\bar{r} = \frac{J_o(\lambda_n)}{\lambda_n} - \frac{J_0(\lambda_n \beta)}{\lambda_n}$$

$$A_n = \frac{2}{J_o^2(\lambda_n)} \begin{cases} \frac{\beta^2 - 1}{\lambda_n}\left(J_2(\lambda_n \beta)\right) - \frac{J_o(\lambda_n}{\lambda_n} - \frac{\beta^2}{\lambda_n} J_2(\lambda_n \beta) \\ + \\ \frac{1}{\lambda_n}\left(-J_o(\lambda_n \beta) + J_o(\lambda_n)\right) \end{cases}$$

$$= \frac{2}{J_o^2(\lambda_n)}\left(\frac{-1}{\lambda_n} J_2(\lambda_n \beta) - \frac{1}{\lambda_n} J_o(\lambda_n \beta)\right), J_2(\lambda_n \beta) + J_o(\beta \lambda_n) = \left(\frac{2}{\beta \lambda_n}\right) J_1(\lambda_n \beta)$$

$$A_n = \frac{-4 J_1(\lambda_n \beta)}{\beta \lambda_n^2 J_o^2(\lambda_n)}$$

Vatistas's Model [Slip]

$$A_n = \frac{\int_0^1 r \bar{V}_\theta(\bar{t} = 0, \bar{r}) J_1(\lambda_n \bar{r}) d\bar{r}}{\int_0^1 r J_1^2(\lambda_n \bar{r}) d\bar{r}} = \frac{2}{J_o^2(\lambda_n)} \int_0^1 r \bar{V}_\theta(\bar{t} = 0, \bar{r}) J_1(\lambda_n \bar{r}) d\bar{r}$$

$$A_n = \frac{2}{J_o^2(\lambda_n)} \int_0^1 \bar{r} \frac{1}{\left(\beta^{2l} + 1\right)^{\frac{1}{l}}}\left(\bar{r} - \bar{r}\left(\frac{\beta^{2l} + 1}{\beta^{2l} + \bar{r}^{-2l}}\right)^{\frac{1}{l}}\right) J_1(\lambda_n \bar{r}) d\bar{r}$$

$$= \frac{2}{J_o^2(\lambda_n)} \int_0^1 \left(\frac{\bar{r}^2}{\left(\beta^{2l}+1\right)^{\frac{1}{l}}} - \frac{\bar{r}^2}{\left(\beta^{2l}+\bar{r}^{-2l}\right)^{\frac{1}{l}}} \right) J_1(\lambda_n \bar{r}) d\bar{r}$$

Integration techniques Appendix (A)

$$A_n = \frac{2}{J_o^2(\lambda_n)} \left\{ \int_0^1 \frac{\bar{r}^2}{\left(\beta^{2l}+1\right)^{\frac{1}{l}}} J_1(\lambda_n \bar{r}) d\bar{r} + \int_0^1 \frac{\bar{r}^2}{\left(\beta^{2l}+\bar{r}^{-2l}\right)^{\frac{1}{l}}} J_1(\lambda_n \bar{r}) d\bar{r} \right.$$

$$A_n = \frac{-2}{\lambda_n J_o(\lambda_n)} \frac{1}{\left(\beta^{2l}+1\right)^{\frac{1}{l}}} - \frac{2}{J_o^2(\lambda_n)} \int_0^1 \frac{\bar{r}^2}{\left(\beta^{2l}+\bar{r}^{-2l}\right)^{\frac{1}{l}}} J_1(\lambda_n \bar{r}) d\bar{r}$$

$$A_n = \frac{-2}{J^2{}_o(\lambda_n)} \left(\frac{J_o(\lambda_n)}{\lambda_n} \frac{1}{\left(\beta^{2l}+1\right)^{\frac{1}{l}}} + H \right)$$

Where, $H = \left(\int_0^1 \left(\frac{\bar{r}^{2l}}{\beta^{2l}+\bar{r}^{-2l}} \right)^{\frac{1}{l}} J_1(\lambda_n \bar{r}) d\bar{r} \right)$, found by numerical integrations

Case Study 2

The tangential velocity isn't allowed to slip at the outer diameter.

Potential Model [Non Slip]

$$A_n = \frac{2}{J_o^2(\lambda_n)} \int_0^1 r \bar{V}_\theta(\bar{t}=0,\bar{r}) J_1(\lambda_n \bar{r}) d\bar{r} = \frac{2}{J_o^2(\lambda_n)} \int_0^1 \bar{r} \left(\frac{1}{\bar{r}} \right) J_1(\lambda_n \bar{r}) d\bar{r} = \frac{2}{J_o^2(\lambda_n)} \int_0^1 J_1(\lambda_n \bar{r}) d\bar{r}$$

$$A_n = \frac{-2}{J_o^2(\lambda_n)} \left(J_o(\lambda_n) - 1 \right)$$

Rankine's Model [Non- Slip]

$$A_n = \frac{\int_0^1 r\bar{V}_\theta(\bar{t}=0,\bar{r})J_1(\lambda_n\bar{r})d\bar{r}}{\int_0^1 rJ_1^2(\lambda_n\bar{r})d\bar{r}} = \frac{2}{J_o^2(\lambda_n)}\int_0^1 r\bar{V}_\theta(\bar{t}=0,\bar{r})J_1(\lambda_n\bar{r})d\bar{r}$$

$$A = \frac{2}{J_o^2(\lambda_n)}\begin{cases}\int_0^\beta r\bar{V}_\theta(\bar{t}=0,\bar{r})J_1(\lambda_n\bar{r})d\bar{r} & 0\le\bar{r}\le\beta \\ + & \\ \int_\beta^1 r\bar{V}_\theta(\bar{t}=0,\bar{r})J_1(\lambda_n\bar{r})d\bar{r} & \beta<\bar{r}\le 1\end{cases}$$

$$A = \frac{2}{J_o^2(\lambda_n)}\begin{cases}\int_0^\beta \frac{\bar{r}^2}{\beta^2}J_1(\lambda_n\bar{r})d\bar{r} & 0\le\bar{r}\le\beta \\ + & \\ \int_\beta^1 J_1(\lambda_n\bar{r})d\bar{r} & \beta<\bar{r}\le 1\end{cases}$$

$$A_n = \frac{2}{J_o^2(\lambda_n)}\begin{cases}\frac{1}{\beta^2}\left(\frac{2\beta}{\lambda_n^2}J_1(\lambda_n\beta)-\frac{\beta^2}{\lambda_n}J_o(\lambda_n\beta)\right) \\ + \\ \frac{1}{\lambda_n}\left(J_o(\lambda_n\beta)-J_o(\lambda_n)\right)\end{cases}$$

$$A_n = \frac{2}{\lambda_n J_o(\lambda_n)}\left(\frac{2J_1(\lambda_n\beta)}{\beta\lambda_n J_o(\lambda_n)}-1\right)$$

Vatistas's Model [Non Slip]

$$A_n = \frac{\int_0^1 r\bar{V}_\theta(\bar{t}=0,\bar{r})J_1(\lambda_n\bar{r})d\bar{r}}{\int_0^1 rJ_1^2(\lambda_n\bar{r})d\bar{r}} = \frac{2}{J_o^2(\lambda_n)}\int_0^1 r\bar{V}_\theta(\bar{t}=0,\bar{r})J_1(\lambda_n\bar{r})d\bar{r}$$

$$A_n = \frac{2}{J_o^2(\lambda_n)} \int_0^1 \bar{r} \frac{\bar{r}}{\left(\beta^{2l} + \bar{r}^{-2l}\right)^{\frac{1}{l}}} J_1(\lambda_n \bar{r}) d\bar{r}$$

$$A_n = \frac{2H}{J^2{}_o(\lambda_n)}$$

$H = \int_0^1 \frac{\bar{r}^{-2}}{\left(\beta^{2l} + \bar{r}^{-2l}\right)^{\frac{1}{l}}} J_1(\lambda_n \bar{r}) d\bar{r}$, Can be found using numerical integration methods.

2.Unconfined Vortex Analysis

Boundary Conditions

Refer to the unconfined line vortex presented in figure [4.2], provided that the vortex induced swirl velocity must satisfies these boundary conditions.

1. Tangential velocity is null at the vortex center i.e. at $\bar{r} = 0$ therefore, $\bar{V}_\theta = 0$.
2. Tangential velocity tends to zero as the vortex outer radius tends to infinity i.e. at $\bar{r} = \infty$, therefore $\bar{r}\bar{V}_\theta = 1$.

i.e. $\bar{V}_\theta = 0$, Theoretically we can't let $\bar{r}$ tends to ∞ but it is possible to assume that $\bar{r}$ can reach maximum possible values which is $\frac{1}{\beta}$ consequently $\bar{V}_\theta$ will tends to minimum values which is β i.e.

$$\because Lim_{\bar{r} \to \frac{1}{\beta}} \left(\bar{r}\bar{V}_\theta\right) = 1 \ \therefore at \quad \bar{r} = \frac{1}{\beta} \to \bar{V}_\theta = \beta ,$$

Solution Model

Back to the general swirl velocity equation $\frac{\partial[\bar{V}_\theta]}{\partial \bar{t}} = [\frac{\partial^2 \bar{V}_\theta}{\partial \bar{r}^2} + \frac{1}{\bar{r}} \frac{\partial \bar{V}_\theta}{\partial \bar{r}} - \frac{\bar{V}_\theta}{\bar{r}^2}]$, using the separation of variables technique.

Let $\bar{V}_\theta(\bar{t},\bar{r}) = T(\bar{t})R(\bar{r})$

$T(\bar{t})$ Indicates only a Function of time. $R(\bar{r})$ Indicates only a function of the vortex radius.

$T(t) = Ae^{-[m^2\bar{t}]}$ and $R(\bar{r}) = BJ_1(m\bar{r})$

$\bar{V}_\theta(\bar{t},\bar{r}) = Ae^{-[m^2\bar{t}]}BJ_1(m\bar{r})$, Let $A_n = AB$

$\bar{V}_\theta(\bar{t},\bar{r}) = A_n e^{-[m^2\bar{t}]}J_1(m\bar{r})$ Where A_n =Constant

Determining the constants requires applying the set of boundary conditions illustrated above. The first boundary condition is automatically satisfied, while the second boundary conditions leads to a complicated equation.

$$\beta = A_n e^{-[m^2\bar{t}]}J_1(\frac{m}{\beta})$$

this equation is complicated; we cannot solve it explicitly to find the constant. Therefore, we have to resort to a technical mathematical transformation without losing the problem generality.

Let $\bar{V}_\theta(\bar{t},\bar{r}) = \beta^2\bar{r} - \bar{V}_\theta(\bar{t},\bar{r})$. Differentiate (3.25) with respect to $\bar{t}$, $\bar{r}$

$$\left.\begin{aligned}
&\frac{\partial \bar{V}_\theta(\bar{t},\bar{r})}{\partial \bar{t}} = -\frac{\partial \bar{V}_\theta(\bar{t},\bar{r})}{\partial \bar{t}} \\
&\frac{1}{\bar{r}}\frac{\partial \bar{V}_\theta(\bar{t},\bar{r})}{\partial \bar{r}} = \frac{\beta^2}{\bar{r}} - \frac{1}{\bar{r}}\frac{\partial \bar{V}_\theta(\bar{t},\bar{r})}{\partial \bar{r}} \\
&\frac{\partial^2 \bar{V}_\theta(\bar{t},\bar{r})}{\partial \bar{r}^2} = -\frac{\partial^2 \bar{V}_\theta(\bar{t},\bar{r})}{\partial \bar{r}^2} \\
&\frac{-\bar{V}_\theta(\bar{t},\bar{r})}{\bar{r}^2} = -\frac{\beta^2}{\bar{r}} + \frac{\bar{V}_\theta(\bar{t},\bar{r})}{\bar{r}^2}
\end{aligned}\right\}$$

Therefore, $\frac{\partial \bar{V}_\theta}{\partial \bar{t}} = [\frac{\partial^2 \bar{V}_\theta}{\partial \bar{r}^2} + \frac{1}{\bar{r}}\frac{\partial \bar{V}_\theta}{\partial \bar{r}} - \frac{\bar{V}_\theta}{\bar{r}^2}]$

Solution of this equation can be solved in terms of Bessel function.

$\bar{V}_\theta(\bar{t},\bar{r}) = A_n e^{-[m^2 \bar{t}]} J_1(m\bar{r})$ The original boundary conditions must be rewritten again relative to the transformed model equation. Boundary conditions for the transformed equation are initially given as: for $\bar{t} \geq 0$

1. $\bar{r} = 0 \rightarrow \bar{V}_\theta = 0 \qquad \rightarrow V_\theta = 0$
2. $\bar{r} = \frac{1}{\beta} \rightarrow \bar{V}_\theta = \beta \qquad \rightarrow V_\theta = 0$

By applying the 2nd boundary condition to the model equation

$0 = J_1(\frac{m}{\beta})$, Let $\lambda_n = \frac{m}{\beta}$, λ_n is the zeros of the Bessel function J_1, which is

$$\lambda_n = \pi[n + 0.25 - \frac{0.151985}{(4n+1)} + \frac{0.015399}{(4n+1)^3} - \frac{0.245275}{(4n+1)^5} \cdots\cdots\cdots], n = 1.2.3 \cdots\cdots \infty$$

Consequently, the velocity be attained by summation of enough terms.

$$\bar{V}_\theta(\bar{t},\bar{r}) = \sum_{n=1}^{\infty} A_n e^{-[\beta^2 \lambda_n^2 \bar{t}]} J_1(\beta\lambda_n \bar{r}), \quad A_n = \frac{\int_0^{1/\beta} r\bar{V}_\theta(\bar{t}=0,\bar{r}) J_1(\beta\lambda_n \bar{r}) d\bar{r}}{\int_0^{1/\beta} r J_1^2(\beta\lambda_n \bar{r}) d\bar{r}}$$

Therefore the tangential velocity is $\bar{V}_\theta(\bar{t},\bar{r}) = \beta^2 \bar{r} - \sum_{n=1}^{\infty} A_n e^{-[\beta^2 \lambda_n^2 \bar{t}]} J_1(\beta\lambda_n \bar{r})$

The Potential Model

$$A_n = \frac{2\beta^2}{J_o^2(\lambda_n)} \int_0^{1/\beta} r\bar{V}_\theta(\bar{t}=0,\bar{r}) J_1(\beta\lambda_n \bar{r}) d\bar{r}$$

$$A_n = \frac{2\beta^2}{J_o^2(\lambda_n)} \int_0^{1/\beta} (\beta^2 \bar{r}^{-2} - 1) J_1(\beta\lambda_n \bar{r}) d\bar{r} \quad \text{and} \quad \int_0^{1/\beta} J_1(\beta\lambda_n \bar{r}) d\bar{r} = \frac{-1}{\beta\lambda_n}[J_o(\lambda_n) - 1]$$

$$\int_0^{1/\beta} \beta^2 \bar{r}^{-2} J_1(\beta\lambda_n \bar{r}) d\bar{r} = \beta^2 [-\frac{1}{\beta^3 \lambda_n} J_o(\lambda_n) + \frac{2}{\beta^3 \lambda_n^2} J_1(\lambda_n)]$$

$$A_n = \frac{2\beta^2}{J_o^2(\lambda_n)} \left(\beta^2 [-\frac{1}{\beta^3 \lambda_n} J_o(\lambda_n) + \frac{2}{\beta^3 \lambda_n^2} J_1(\lambda_n)] + \frac{1}{\beta\lambda_n}[J_o(\lambda_n) - 1] \right) \& \because J_1(\lambda_n) = 0$$

$$A_n = \frac{-2\beta}{\lambda_n J_o^2(\lambda_n)}$$

Rankine's Model

$$A_n = \frac{\int_0^{1/\beta} r \bar{V}_\theta(\bar{t} = 0, \bar{r}) J_1(\beta\lambda_n \bar{r}) d\bar{r}}{\int_0^{1/\beta} r J_1^2(\lambda_n \bar{r}) d\bar{r}} = \frac{2\beta^2}{J_o^2(\lambda_n)} \int_0^{1/\beta} r \bar{V}_\theta(\bar{t} = 0, \bar{r}) J_1(\beta\lambda_n \bar{r}) d\bar{r}$$

$$A_n = \frac{2\beta^2}{J_o^2(\lambda_n)} \begin{cases} \int_0^1 [\beta^2 - 1] \bar{r}^{-2} J_1(\lambda_n \beta \bar{r}) d\bar{r} \\ \int_1^{1/\beta} [\beta^2 \bar{r}^{-2} - 1] J_1(\lambda_n \beta \bar{r}) d\bar{r} \end{cases}$$

$$= \frac{2\beta^2}{J_o^2(\lambda_n)} \begin{cases} \int_0^1 [\beta^2 - 1] \bar{r}^{-2} J_1(\lambda_n \beta \bar{r}) d\bar{r} \\ + \\ \int_1^{1/\beta} \beta^2 \bar{r}^{-2} J_1(\lambda_n \beta \bar{r}) d\bar{r} - \int_1^{1/\beta} J_1(\lambda_n \beta \bar{r}) d\bar{r} \end{cases} \qquad \text{so } A_n = \frac{2\beta^2}{J_o^2(\lambda_n)} [I_1 + I_2 + I_3]$$

Where, $I_1 = \int_0^1 \bar{r}^{-2} [\beta^2 - 1] J_1(\beta\lambda_n \bar{r}) d\bar{r} = [\beta^2 - 1] \int_0^1 \bar{r}^{-2} J_1(\beta\lambda_n \bar{r}) d\bar{r}$

$$I_1 = [\beta^2 - 1] \left(\frac{-1}{\beta\lambda_n} J_o(\lambda_n \beta) + \frac{2}{\beta^2 \lambda_n^2} J_1(\lambda_n \beta) \right)$$

$$I_2 = \beta^2 \int_1^{1/\beta} \bar{r}^{-2} J_1(\beta\lambda_n \bar{r}) d\bar{r}$$

$$= \frac{\beta^2}{\beta^3 \lambda_n^2}\left(-\lambda_n J_o(\lambda_n) + 2J_1(\lambda_n) + \lambda_n \beta^2 J_o(\lambda_n\beta) - 2\beta J_1(\lambda_n\beta)\right) \&\ \because J_1(\lambda_n) = 0$$

$$I_2 = \frac{\beta^2}{\beta^3 \lambda_n^2}\left(-\lambda_n J_o(\lambda_n) + \lambda_n \beta^2 J_o(\lambda_n\beta) - 2\beta J_1(\lambda_n\beta)\right)$$

$$I_3 = \int_1^{1/\beta} -J_1(\beta\lambda_n \bar{r}) d\bar{r}, \; I_3 = \frac{J_o(\lambda_n)}{\lambda_n \beta} - \frac{J_0(\lambda_n\beta)}{\lambda_n \beta}$$ By using I_1 I_2 I_3 substitute back

$$A_n = \frac{-4J_1(\lambda_n\beta)}{\lambda_n^2 J_o^2(\lambda_n)}$$

Vatistas's Model

$$\because A_n = \frac{2\beta^2}{J_o^2(\lambda_n)} \int_0^{1/\beta} r \bar{V}_\theta(\bar{t} = 0, \bar{r}) J_1(\beta\lambda_n \bar{r}) d\bar{r}$$

$$= \frac{2\beta^2}{J_o^2(\lambda_n)} \int_0^{1/\beta} \left(\frac{\beta^2}{\left(1 + \beta^4\right)^{\frac{1}{l}}} \bar{r}^{-2} - \frac{\bar{r}^{-2}}{\left(1 + \bar{r}^{-4}\right)^{\frac{1}{l}}} \right) J_1(\beta\lambda_n \bar{r}) d\bar{r}$$

$$A_n = \frac{2\beta^2}{J_o^2(\lambda_n)} \left\{ \int_0^{1/\beta} \beta^2 \bar{r}^{-2} J_1(\beta\lambda_n \bar{r}) d\bar{r} - \int_0^{1/\beta} \frac{\bar{r}^{-2}}{\left(1 + \bar{r}^{-2l}\right)^{\frac{1}{l}}} J_1(\beta\lambda_n \bar{r}) d\bar{r} \right.$$

$$A_n = \frac{2\beta^2}{J_o^2(\lambda_n)} \left(\frac{\beta^2}{\lambda_n \beta^3} \left(-J_o(\lambda_n) + \frac{2}{\lambda_n} J_1(\lambda_n) \right) - \int_0^{1/\beta} \frac{\bar{r}^{-2}}{\left(1 + \bar{r}^{-2l}\right)^{\frac{1}{l}}} J_1(\beta\lambda_n \bar{r}) d\bar{r} \right), \; J_1(\lambda_n) = 0$$

$$A_n = \frac{2\beta^2}{J_o^2(\lambda_n)} \left(\frac{1}{\lambda_n \beta \left(1 + \beta^4\right)^{\frac{1}{l}}} \left(-J_o(\lambda_n)\right) - H \right)$$

where, $H = \int_0^{1/\beta} \left(\frac{\bar{r}^{-2l}}{1 + \bar{r}^{-2l}} \right)^{\frac{1}{l}} J_1(\beta\lambda_n \bar{r}) d\bar{r}$, H Can be found using numerical integration.